GEOTECHNICAL PRACTICE PUBLICATION NO. 9

Rocky Mountain Geo-Conference 2014

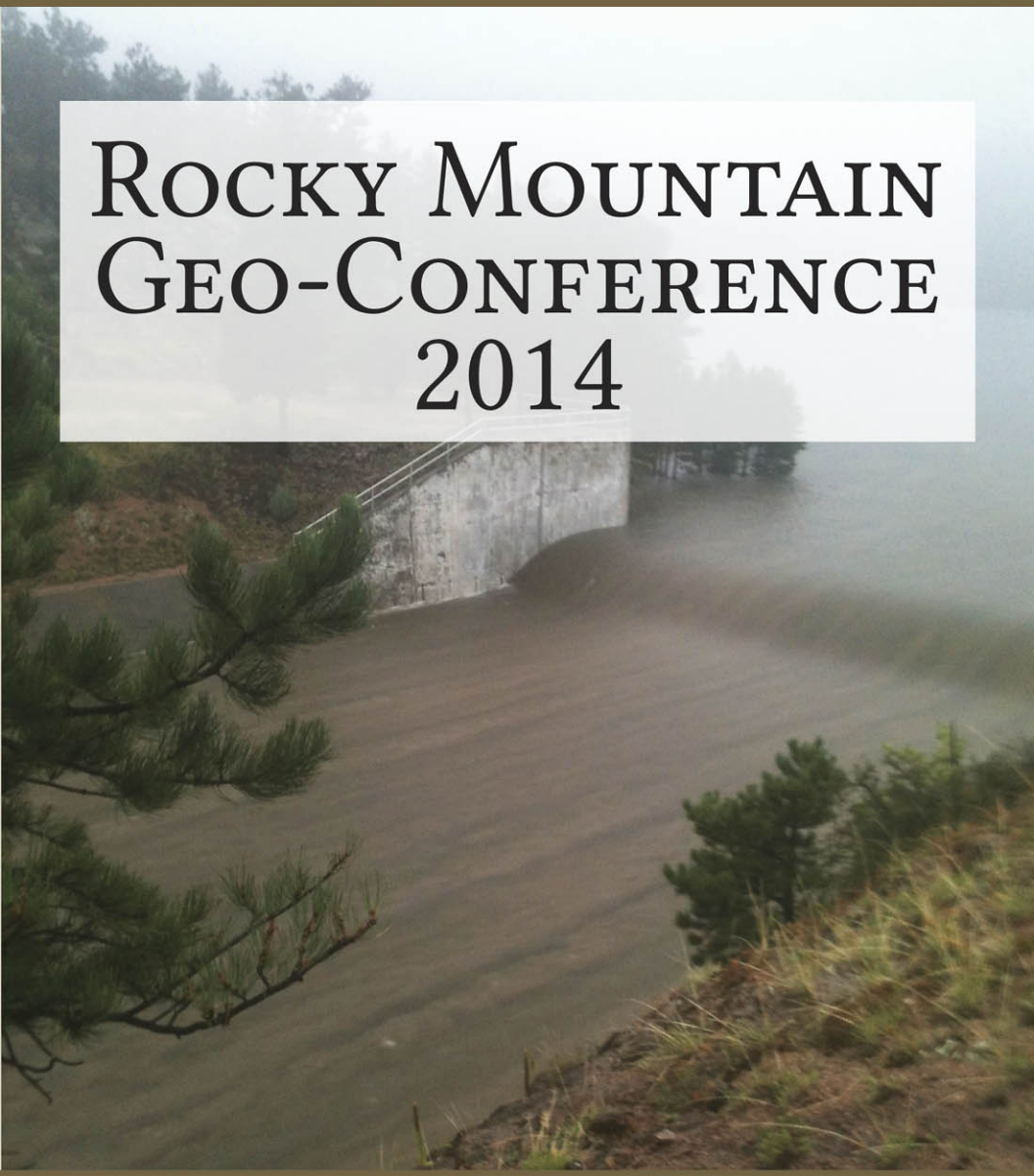

Edited by
Jere A. Strickland, P.E.
Richard L. Wiltshire, P.E.
Christoph M. Goss, Ph.D., P.E.

ASCE
G-I ASCE GEO-INSTITUTE

GEOTECHNICAL PRACTICE PUBLICATION NO. 9

ROCKY MOUNTAIN GEO-CONFERENCE 2014

PROCEEDINGS OF THE 2014 ROCKY MOUNTAIN GEO-CONFERENCE

November 7, 2014
Lakewood, Colorado

SPONSORED BY
The Geo-Institute of the American Society of Civil Engineers

Geo-Institute Chapter of the Colorado Section of the American Society of Civil Engineers

Rocky Mountain Section of the Association of Environmental and Engineering Geologists

Colorado Association of Geotechnical Engineers

EDITED BY
Jere A. Strickland, P.E.
Richard L. Wiltshire, P.E.
Christoph M. Goss, Ph.D., P.E.

Published by the American Society of Civil Engineers

Library of Congress Cataloging-in-Publication Data

2014 Rocky Mountain Geo-Conference (2014 : Lakewood, Colo.)
Rocky Mountain Geo-Conference 2014 : proceedings of the 2014 Rocky Mountain Geo-Conference, November 7, 2014, Lakewood, Colorado / sponsored by the Geo-Institute of the American Society of Civil Engineers [and 3 others] ; edited by Jere A. Strickland, P.E., Richard L. Wiltshire, P.E., Christoph M. Goss, Ph.D., P.E.
pages cm. -- (Geotechnical practice publication ; no. 9)
ISBN 978-0-7844-1380-7 (paper : alk. paper) 1. Engineering geology--Colorado--Congresses. I. Strickland, Jere, editor. II. Wiltshire, Richard L., editor. III. Goss, Christoph M., editor. IV. American Society of Civil Engineers. Geo-Institute, sponsoring body. V. Title.
TA705.3.C6B534 2014
624.1'5109788--dc23

2014033267

Published by American Society of Civil Engineers
1801 Alexander Bell Drive
Reston, Virginia, 20191-4382
www.asce.org/bookstore | ascelibrary.org

Errata: Errata, if any, can be found at http://dx.doi.org/10.1061/ 9780784413807.

ISBN 978-0-7844-1380-7 (paper)
Manufactured in the United States of America.

Front and Back Cover Photo Credit: Bill McCormick

Preface

As geo-professionals, we are called to provide solutions for the many challenges that our earth presents in the areas we choose to work, play and live. From nature's geological features to our world's aging infrastructure, we are presented with the challenge of developing in areas and in ways that many thought were unbuildable or un-attainable. Yet, through the use of new technologies, modeling methods and visual mapping, geo-professionals have answered these many challenges by providing viable solutions. This book provides examples of how some in our profession have overcome these types of challenges in mining applications, tunneling, geological anomalies, alternative energy resources and infrastructure. This will highlight, again, how the geo-professional community provides solutions to the most challenging applications.

Since 1984, the Geotechnical Institute Chapter of Colorado (formally known as the ASCE Colorado Section's Geotechnical Group) in collaboration with the Rocky Mountain Section of the Association of Environmental and Engineering Geologists and the Colorado Association of Geotechnical Engineers, has organized a biennial series of geotechnical seminars on a wide variety of themes that have been attended by as many as 270 civil/geotechnical engineers, geologists, and other geo-professionals. The geotechnical seminars have been held at area universities or hotels and have offered the opportunity for sharing ideas and experiences among Colorado's diverse geo-disciplines. Since 2004, ASCE's Geo-Institute has published the papers of these seminars in Geotechnical Practice Publications, allowing the experiences to be shared with a worldwide audience.

The Geo-Influence Steering Committee convened in August 2013 and held monthly meetings to plan for the 2014 Rocky Mountain Geo-Conference. The Steering Committee members included Christoph Goss (Conference Chair), Sam Adettiwar, Dustin Bennetts, Mark Brooks, Laura Campbell, Robin Dornfest, Darin Duran, Julia Frazier, Evan Friedman, Joseph Kerrigan, Joels Malama, Bill McCarron, Minal Parekh, Becky Roland, Jere Strickland, Lindsay Tita, Mark Vessely, Chris Wienecke, Richard Wiltshire, and John Worthen.

Jere Strickland, Richard Wiltshire, and Christoph Goss

Acknowledgments

The GeoChallenges Steering Committee wishes to take this opportunity to thank all of the authors and reviewers of our papers, which are herein presented as Geotechnical Practice Publication No. 9. The authors have spent many hours in preparing and finalizing their papers, which will be presented at the 2014 Rocky Mountain Geo-Conference on November 7, 2014. These papers have been reviewed by a volunteer group of Denver area geo-professionals who put in their valuable time and helped make these papers even better. The Geo-Institute's Committee on Technical Publications completed its review of our papers in a very timely manner and their adherence to our aggressive publication schedule is greatly appreciated. We would also like to acknowledge the assistance of Donna Dickert of ASCE's Publications Division for putting this publication together.

Contents

Author List

Dam Performance along Left Hand Creek during the Front Range Flood of 2013

Richard J. Tocher[1], P.E, M. ASCE and L. Clint Brown[2], P.E.

[1]Principal, Engineering Analytics, Inc. 1860 Blake Street, Ste 200, Denver, CO 80202 rtocher@enganalytics.com
[2]Project Manager, Engineering Analytics, Inc., 1600 Specht Point Road, Ste 209, Fort Collins, CO 80525 cbrown@enganalytics.com

ABSTRACT: Severe flooding on the Front Range of Colorado in September 2013 tested many dams including several dams on and adjacent to the Left Hand Creek drainage north of Boulder, Colorado. A tropical-like storm drove moisture up against the foothills dropping 200 mm (8 in) to more than 350 mm (14 in) of precipitation in a 24-hour period based on a number of weather stations within the watershed. The precipitation resulted in flash flooding in Left Hand Creek. A dam west of the main precipitation event experienced no damage. A diversion dam near the mouth of Left Hand Canyon was completely destroyed by the storm event due to scour. An off-channel valley reservoir dam experienced damage to both the service and emergency spillways. The experiences along Left Hand Creek demonstrate the need for geotechnical and structural design of dams for extreme events especially in mountain environments where uncertain flood events can occur due to unusual weather patterns.

INTRODUCTION

Left Hand Creek is 55 km (34 miles) long from its headwaters on Niwot Ridge at an elevation of over 3660 m (12,000 ft) to its confluence with St. Vrain Creek as shown on Fig. 1. The creek descends from the mountains in a steep canyon, known as Left Hand Canyon. It emerges from the foothills north of Boulder, Colorado and crosses the Colorado Piedmont, passing north of Niwot and joining St. Vrain Creek on the south side of Longmont. The basin covers 186 km^2 (72 sq miles) and discharges into the St. Vrain Creek in Longmont at an elevation of 1500 m (4924 ft).

GEOLOGIC SETTING

Pre-Cambrian metamorphic and granitic rocks dominate the geology of the mountainous portions of the watershed, including intrusive stocks and dikes. Glacial deposits occur near the upper watershed alongside and west of Highway 72. These are

mostly glacial moraine material rather than glacial outwash, and can reach up to 15 m (50 ft) thick in some locations. The crystalline rocks within the watershed contain

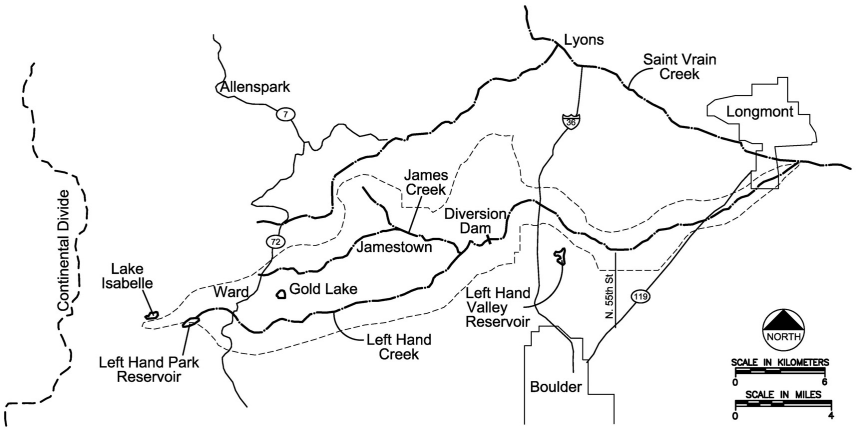

FIG. 1. Left Hand Creek Watershed

several minerals in extractable quantities, including gold, fluorite, lead, silver, uranium, tungsten, and copper. These minerals were deposited with intrusions of molten igneous rocks during periods of mountain uplift. Soils in the watershed are fairly thin.

The Left Hand Creek watershed covers portions of two distinct physiographic regions: the Southern Rocky Mountain province and the Colorado Piedmont section of the Great Plains province. Foothills separate these distinct topographical features. Glaciation, stream erosion and deposition, wind erosion, and atmospheric weathering formed and continue to alter the watershed topography. The watershed features gentle slopes concentrated near the upper reaches of the watershed and steep canyon reaches near the watershed mouth. Although some glacial deposits are present near the upper watershed, the canyons in the middle and lower portions of the watershed have a V-shaped morphology, formed by water flow rather than glacial ice.

SEPTEMBER 2013 FLOOD EVENT

The Front Range of Colorado experienced an unusually moist and persistent weather pattern from September 9 through 15, 2013. The storm dropped all time record precipitation in the area north of Boulder, Colorado with some areas receiving over 400 mm (16 in) of rain. The event was caused by a near stationary low pressure system over eastern Nevada that pulled tropical moisture from the Pacific Ocean and the Gulf of Mexico. An upslope condition developed along the foothills creating the large rainfall. Most of the rainfall occurred over 36 hours between September 11 and 13. The event was similar to a storm in 1938 that also occurred in September. The peak rainfall intensities were lower than previous storms but the intensity of the storm was about 5 mm (0.2 in) per hour from September 11 through 13 with a peak

intensity of 28 mm (1.1 in) per hour. There were sufficient rain gages in the watershed (NOAA, 2013) to construct total event precipitation contours as shown in Fig. 2. About 40 percent of the basin received over 355 mm (14 in) of precipitation from the event.

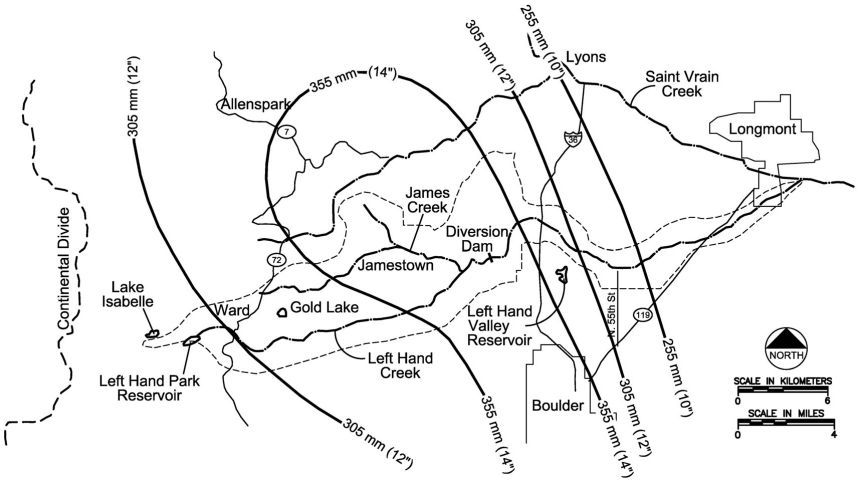

FIG. 2. Total Basin Precipitation

Once the floodwaters receded, Left Hand Ditch Company engineers found that Left Hand Creek had to be re-channeled to its original course over 1.6 km (1 mile) in an area of critical diversion structures and head gates. Some sections of the company's systems were completely destroyed. When applying for emergency loans from the Colorado Water Conservation Board, the company estimated the cost to repair the damage would be $3.2 million. Without critical repairs to the company's infrastructure, a significant portion of irrigated farm land in Boulder County and the company's five reservoirs would have been unusable for the following irrigation season. One of those reservoirs provides water for residential use in the Left Hand Water District.

The U.S. Geological Survey (1988) study of peak flows in the creeks surrounding Left Hand Creek generated a series of empirical correlations for flood levels based on elevation and drainage basin area below an elevation of 2440 m (8000 ft). These correlations were used to calculate exceedance probabilities for Left Hand Creek at the Allen's Lake diversion dam, North 55th Street, and the confluence with the St. Vrain Creek as shown in Fig. 3. The results show a 100-year recurrence flow of 120 m^3/s (4300 cfs) at the diversion structure. This estimated flow was not able to be verified by field measurements during the flood event.

Damage along Left Hand Creek and its tributary James Creek was massive. Photographs 1 and 2 show the degree and damage sustained.

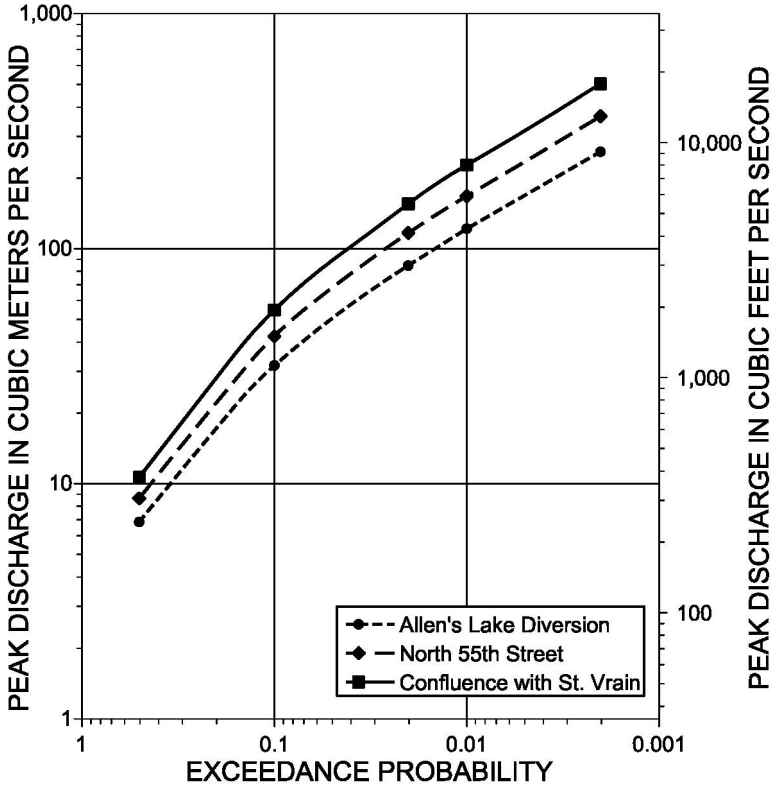

FIG. 3. Flood Recurrence along Left Hand Creek

LEFT HAND CREEK DAMS

There are five dams and reservoirs in and adjacent to the watershed that are owned and operated by Left Hand Ditch Company Lake Isabelle, Gold Lake, Allen's Lake Diversion Dam, Left Hand Valley Reservoir and Left Hand Park Reservoir. Relevant features of three of these facilities are shown in Table 1.

Lake Isabelle Dam

Construction of the Lake Isabelle reservoir was authorized through an easement issued by the U.S. Department of Interior (DOI) in the 1920's to R.D. George. Mr. George worked on the tunnel and dam until the construction was accepted by the DOI in 1935. Mr. George then conveyed the rights and appurtenances of Lake Isabelle to

Photograph 1. Damage along James Creek

Photograph 2. Damage on Lower Left Hand Creek

the Left Hand Ditch Company (LDC) in 1936. LDC has owned, operated and maintained Lake Isabelle since that time. Administration of this easement has shifted to the U.S. Forest Service.

In 1977, LDC performed major maintenance on the control building, gate valve and tunnel. A 610-mm (24-in) diameter steel pipe was added to the outlet and intake and the ladder and platforms were replaced. The control building was reconstructed and covered with native rock to disguise the building. In 2013, LDC completed additional improvements to the outlet works by replacing the valves.

Table 1. Selected Left Hand Watershed and Adjacent Dams

Dam Type	Lake Isabelle Dam – Natural Moraine	Allen's Lake Diversion Dam – Concrete Gravity	Left Hand Valley North Dam – Homogeneous Earthfill
Height	11.6 m (38 ft)	1.8 m (6 ft)	17.7 m (58 ft)
Length	122 m (400 ft)	14.9 m (49 ft)	116 m (380 ft)
Spillway Capacity	(Natural channel) 11 m^3/s (400 cfs)	Service 17 m^3/s (600 cfs)	Service 71 m^3/s (2500 cfs)
		Emergency 113 m^3/s (4000 cfs)	Emergency 351 m^3/s (12,400 cfs)
Original Construction	1935	1930's	1952
Reconstructed	1977	2014	1997 (RCC spillway added)
Reconstructed	2013	---	---

The Indian Peaks Wilderness was designated in 1978, nearly 43 years after construction of the dam and tunnel for Lake Isabelle was accepted. LDC has a pre-existing right to use, operate and maintain the Lake Isabelle dam and tunnel.

Lake Isabelle was west of the main precipitation event during the 2013 flood. The lake level rose by less than 0.3 m (1 ft) and no damage occurred to the facility.

Left Hand Creek Diversion Dam (Allen's Lake Diversion)

The diversion dam was originally constructed in the 1930's to allow diversion of water from Left Hand Creek to Allen's Lake. The original construction was undocumented, but included a run of the river spillway section, sand trap and a 914-mm (36-in) gate for water diversion. The dam was completely destroyed by September 13. The channel was scoured up to a depth of 1.8 m (6 ft) and bedrock was exposed in about 20 percent of the dam alignment.

The dam required complete replacement. Colorado water law allows head gates to be moved upstream because of changes in the channel. The remains of the original structure were removed and the new structure placed slightly upstream of the original structure. The water right remained unaffected, since it did not impact another water right. The new structure has a spillway capacity of 130 m^3/s (4600 cfs).and includes a cutoff extending down 1.8 to 3.6 m (6 to 12 feet) to bedrock across the entire channel. Photographs 3 and 4 show the new diversion dam under construction.

Left Hand Valley Reservoir

Left Hand Valley Reservoir was originally constructed in the 1952 as an off-channel reservoir along Left Hand Creek to store approximately 740,000 m^3 (600 acre-ft). The reservoir required north and south compacted earth dams to retain the

Photograph 3. Foundation Cutoff for the Dam

Photograph 4. Diversion Dam Reconstruction

reservoir. The spillways at the reservoir included a cut channel in bedrock (service spillway) constructed in 1952 and a roller compacted concrete (RCC) stepped channel constructed over an existing earth embankment (emergency spillway) in 1997.

The roller compacted concrete spillway has a capacity of 351 m^3/s (12,400 cfs). The service and emergency spillways are shown in Photographs 5 and 6.

Photograph 5. Erosion in Service Spillway

Photograph 6. Damage in Emergency Spillway

During the flood event both the service right abutment natural channel spillway and the emergency RCC spillway flowed for a combined flow of about 57 m^3/s (2000 cfs). The cut bedrock channel eroded down to competent bedrock and performed well. Minor repairs were required to make the spillway serviceable for the future. The RCC spillway experienced significant damage with 150 mm to 200 mm (6 in to 8 in) of flow depth at the crest of the structure. The damage consisted of wide spread raveling of the RCC surface and rounding of up to 100 mm (4 in) from the edge of the steps. The spillway surface was subsequently found to be satisfactory for continued service.

Left Hand Creek Downstream of the Left Hand Valley Reservoir

Left Hand Creek runs for about 19 km (12 miles) from its exit of Left Hand Canyon at Highway 36 east to its confluence with St. Vrain Creek in Longmont. The creek destroyed several houses and bridges as it exited the canyon carrying debris and boulders up to 1 m (3 ft) in diameter. The creek cut through Highway 36 and severed utility lines. As the flood extended east the channel is less constrained and the flood flows exceeded the channel capacity. New channels were created and numerous fields were covered with sediment and debris.

CONCLUSIONS

The experiences along Left Hand Creek demonstrate the need for geotechnical and structural design of dams for extreme events especially in mountain environments where uncertain flood events can occur due to unusual weather patterns or persistent climate change.

REFERENCES

Jarrett, R.D. and Costa, J.E. (1988) “Evaluation of Flood Hydrology in the Colorado Front Range using Precipitation, Stream flow and Paleoflood Data for the Big Thompson River Basin,” *USGS Water Resources Investigation Report 87-4117*.

NOAA (2103) “Boulder Area Flood of September, 2013: Climate and Weather Information,” *www.esrl_noaa.gov/psd/boulder/flood 2013*.

GIS Modeling to Assess Economic Risk from Post-Fire Debris-Flows

Kevin McCoy[1], Paul Santi P.G.[2], Daniel Kaffine[3], and Vitaliy Krasko[4]

[1]Graduate Research Assistant, Department of Geology and Geological Engineering, Colorado School of Mines, Berthoud Hall, 1516 Illinois Street, Golden, CO 80401; kemccoy@mines.edu
[2]Department Head and Professor of Geological Engineering, Department of Geology and Geological Engineering, Colorado School of Mines, Berthoud Hall, 1516 Illinois Street, Golden, CO 80401; psanti@mines.edu
[3]Associate Professor, Department of Economics, University of Colorado at Boulder, Economics Building Room 212, 256 UCB, Boulder, CO 80309-0256; Daniel.kaffine@colorado.edu
[4]Graduate Research Assistant, Division of Economics and Business, Colorado School of Mines, Engineering Hall, 816 15th Street, Golden, CO 80401; vkrasko@mymail.mines.edu

ABSTRACT: Post-fire debris-flows are a serious hazard in the western United States. Potential impacts of these events include loss of human life, destruction of structures, and degradation of habitat and water quality. While loss of human life is the most important concern in a geohazard assessment, potential loss of life is extremely difficult to quantify and is beyond the scope of this paper. This paper focuses instead on the analysis of economic risk from post-fire debris-flows in support of cost-optimized post-fire debris flow hazard management strategies. Common approaches to evaluating post-fire debris-flow hazards provide either qualitative estimates of inundation zones, or no inundation estimates at all. Quantitative estimates of debris-flow damage and economic risk support the selection of natural hazard management strategies following a fire via optimization approaches. The first step in this process is an analysis of damage cost estimates and related probabilities. Debris-flow hazards and associated damage costs for individual drainages can be analyzed in ArcGIS utilizing existing models and readily available GIS data. Preliminary case study results suggest that this process can be used to identify the most economically concerning drainages. These results can guide allocation of emergency management funds and optimization of debris-flow management strategies following a wildfire. This paper discusses where to acquire geologic and social input data, and how to operate the GIS models in support of the post-fire debris-flow economic risk assessment. A case study from southern California is provided to illustrate the methods.

INTRODUCTION

Debris-flows generated by rainfall in recently burned drainage basins (basins) are a serious hazard in the western United States. According to Cannon and Gartner

(2005), debris-flows pose a distinct hazard within the spectrum of post-fire hydrologic response (ranging from floods through debris-flows) due to their unique destructive power. Potential impacts of these events include loss of human life, destruction of structures, and degradation of habitat and water quality. Of particular concern is the fact that debris-flows in burned areas can occur with little warning in response to relatively frequent, low-recurrence interval (less than 2 year) storms (Cannon et al., 2008). These events often occur in basins that would have otherwise been unlikely to generate debris-flows before the fire. Further, as Cannon and DeGraff (2009) point out, increases in wildfire occurrence associated with factors such as climate change combined with increased population density in the wildland-urban interface will likely lead to increased occurrences of debris-flows in populated areas. It is therefore evident that increasing mitigation efforts will be required following wildfires to protect life, structures, infrastructure, and natural systems.

Post-fire debris-flow hazard assessments (e.g. Cannon et al., 2010a, Tillery et al., 2011) are commonly performed after a fire to help guide natural hazards management. The scope of these hazard assessments is often limited to estimating probability and volume of potential debris-flows. Some assessments may include modeling of debris-flow runouts, but the analysis is usually limited to production of hazard zone maps. These hazard assessments are an important component of post-fire debris-flow hazard management, but they are not the final step. Lee and Jones (2004) point out that the focus of risk assessment "should not be on the what (e.g. probability, volume, or runout), but on the so what" (e.g. fatalities or damages). Napper (2006) states that for post-fire hazard management projects selecting the appropriate treatment technology requires the practitioner to consider the effectiveness and cost of treatment, as well as the nature of downstream values-at-risk. With this in mind, methods for estimating cost (Napper, 2006) and effectiveness of treatment (Napper, 2006, Robichaud et al., 2010) have been prepared by the United States Forest Service. However, identifying and assessing downstream values-at-risk is a complicated task. Calkin et al. (2007) describes a framework for assessing post-fire values-at-risk. This framework is based on a combination of mass based sediment yield calculations described by Robichaud et al. (2007) and professional judgment. These calculations are based on probability of occurrence of a given mass-based magnitude of soil erosion. While the framework indicates that debris-flow hazards may exist, it does not specify how to identify features affected by debris-flows or assign values to them.

The purpose of the work described in this paper is to develop a consistent method for identifying and assigning economic values to features potentially affected by post-fire debris-flows as part of a larger post-fire risk management strategy. While human life is the primary concern in any geohazard assessment, estimating exposure and vulnerability of humans to post-fire debris-flows is extremely difficult. Discussion of specific hazards and/or risk to human life from post-fire debris-flows is beyond the scope of this paper. Previously existing post-fire hazard assessment calculations and debris-flow runout models have been combined with easily obtainable feature data in a geographic information system (GIS) to model expected damages and economic risk from individual burned basins following a fire. The basic process involves 1) estimating probability, volume, and runout of a potential post-fire debris-flow, 2)

identifying and valuing the elements at-risk, and 3) calculating economic risk. This paper provides an overview of the process, describes where to obtain the necessary inputs for common post-fire debris-flow hazard models, and describes methods of estimating damage costs. A case study is presented for a series of burned basins in southern California.

POST-FIRE DEBRIS-FLOW HAZARD MODELING

The process described in this paper utilizes existing methods to estimate probability, volume, and runout of post-fire debris-flows. The following sections briefly discuss each method, followed by a description of data extraction methods and risk calculations. Information on where to obtain relevant data is provided as appropriate in each respective section.

Probability and Volume Modeling

Overview

The first step in the process is to evaluate the debris-flow probability (P) and volume (V) for a given expected rainfall scenario (or range of scenarios). Methods of estimating P and V for post-fire debris-flows in southern California and the intermountain western United States have been described by Rupert et al. (2008), Gartner et al. (2008), and Cannon et al. (2010b). These methods are generally based on regression of local geologic, hydrologic, and burn severity characteristics of specific burned basins. Following Cannon et al. (2010b), equations to estimate P and V for any general burned area can be expressed in the following forms:

$$P = \frac{e^x}{1+e^x} \quad (1)$$

$$x = \beta_0 + \beta_1 x_1 + \beta_2 x_2 + \cdots + \beta_i x_i \quad (2)$$

Where: P is the modeled probability of debris-flow occurrence, β_i are regression coefficients, x_i are independent variables (e.g. geologic, hydrologic, and burn characteristics), and i is the number of variables used in the P model.

The volume is estimated by:

$$ln(V) = \alpha_0 + \alpha_1 y_1 + \alpha_2 y_2 + \cdots + \alpha_j y_j \quad (3)$$

Where: ln(V) is the natural logarithm of debris-flow volume, α_j are regression coefficients, y_j are independent variables (e.g. geologic, hydrologic, and burn characteristics), and j is the number of variables used in the V model. V is calculated by exponentiation of Eq. 3 using the base e (approximately 2.71828).

Eq. 1 through Eq. 3 show the general form of the equations. Because of differences in physical and hydrologic characteristics both within and between regions, the coefficients (β_i and α_j), and the independent variables (x_i and y_j), may vary between

regional models. The use of a given set of P and V equations is generally limited to the region for which a particular model was derived. Cannon et al. (2010b) describe several models for P based on data from 388 burned basins, for use in the intermountain western United States. Cannon et al. (2010b) and Gartner et al. (2008) describe a single model for V based on data from 53 burned basins in Colorado, Utah, and California, that is applicable to both the intermountain west and southern California. Models may be revised or superseded as additional data is obtained (e.g. USGS, 2014c). Additionally, new models may be developed to more effectively model unique site conditions.

Acquiring Data for P and V Models

P and V models often rely on geomorphic data extracted from digital elevation models (DEMs). DEM data for the United States from the National Elevation Dataset (NED) (Gesch et al., 2002) is available for download from the National Map webpage (USGS, 2014b). Horizontal resolution of the NED dataset varies from approximately 30 meters (m) to approximately 3 m by location (USGS, 2014a). Coverage for 3 m data is currently limited to relatively few regions. Vertical accuracy of the dataset is nominally +/- 2.44 m, but also may vary by location (USGS, 2014a). These data are useful when other elevation data are not available. However, for modeling purposes (especially runout modeling), higher resolution (sub meter) terrain data is preferred when available. Higher resolution terrain data usually must be acquired from a private source or project specific survey. Several of the commonly used models require geoprocessing to derive specific geomorphic characteristics. Gartner et al. (2011) describes the processes for some of the inputs to a southern California model. Additional guidance for deriving geomorphic characteristics in a GIS can be found at the website (G4G 2014).

Soil characteristics used by some common P and V models are available for download from the Natural Resource Conservation Service (NRCS) web soil survey (Soil Survey Staff 2014). The file structure of the NRCS data is complex. The soil data viewer extension (Soil Survey Staff, 2014) available for ArcGIS (ESRI, 2010) significantly simplifies the data extraction process. As described in the help files for the tool, a version of Microsoft® Access or its corresponding runtime package is required to prepare the data for use in ArcGIS. Without this program, the soil data viewer extension will not be able to import the tabulated soil data and will therefore not function.

Rainfall intensity/duration characteristics are another common feature of debris-flow hazard models. Cannon et al. (2008) described conditions that led to post-fire debris-flows in southwestern Colorado and southern California. Staley et al. (2013) discuss recently revised methods for estimating intensity/duration thresholds in southern California. Rainfall intensity and depth recurrence interval data can be downloaded from the National Oceanic and Atmospheric Administration (NOAA) online precipitation frequency data server (NOAA, 2013). Single precipitation intensity/depth values for a specific recurrence interval storm may be selected for a region, or a GIS grid of expected intensity distribution may be downloaded for more precise estimation.

The final feature necessary for estimating P and V of post-fire debris-flows is burn severity data. Burn severity data are either generated from satellite imagery, or by burned area emergency response (BAER) personnel on the ground (Parsons et al., 2010). Satellite burn severity data are readily available online. The BAER imagery support data download site (Forest Service, 2013) now provides soil burn severity data following fires. Users should be aware that older data or preliminary data from this website, such as the burned area reflectance classification (BARC) that was available prior to 2012, reflect vegetation burn severity and not necessarily soil burn severity. Soil burn severity data include both the loss of vegetation, and impacts to soil characteristics (e.g. reduced infiltration rates of burned soils). Additionally, because preliminary data are usually collected shortly after a fire, they may capture clouds or residual smoke which affects the digital image interpretation. Field verification of BARC imagery is used to address these issues. As discussed by Parsons et al. (2010), satellite burn severity data must be field verified and edited to generate soil burn severity data (which may be more useful for debris flow calculations). This process may result in changes to the reported burn severity classifications. Field verification may be performed by BAER teams. Parsons et al. (2010) provides a description of field methods to map burn severity on the ground, and to ground truth BARC data immediately following a fire.

An alternative source of burn severity data is the monitoring trends in burn severity (MTBS) website (MTBS, 2014). Similar to the preliminary BARC data, MTBS data reflects vegetation burn severity, not soil burn severity. MTBS data is typically collected approximately 1-year following a fire in order to observe the site near the maximum vegetation growth season (MTBS, 2014, Parsons et al., 2010). Because these data are collected on a less critical time scale, image quality and interpretation is often better than that used for the BARC data. Drawbacks of these data for debris-flow hazard and risk assessments are that the data do not reflect soil impacts (e.g. reduced infiltration rates), and the data are usually not available for at least a year following the fire.

A range of models for predicting P and V have been developed by various investigators. A particular regression model may have been derived using a specific type of burn severity data (i.e. BARC, soil burn severity, or MTBS). Experience running models with different data sources suggests that while differences between these different sources may be subtle in some cases, they can be dramatic in others. It is therefore important to know the source of the burn severity data used for analysis, and what data were used to derive the specific model that will be used to predict P and V. For emergency debris-flow hazard analysis, soil burn severity data obtained from the responsible local or federal agency or field verification of the downloaded BARC data are usually the best option, but in some cases preliminary BARC data must be used. For longer term studies, MTBS data may be more appropriate if those data were used to derive the model. In some cases, it is not clear which burn severity data source was used to derive the model, or that data source may not be available. If this is the case, the user should be aware that there could be unquantified error in the P and V calculations.

Model Uncertainty and Alternative Methods

The methods of calculating P and V discussed in the preceding section (Eq. 1 through Eq. 3) have been widely used by the United States Geological Survey (USGS) to evaluate post-fire debris-flow hazards. Cannon et al. (2010b) and Gartner et al. (2008) indicate that their V model is valid to within an order of magnitude of the predicted debris-flow V. These methods are most commonly used to evaluate hazards to within an order of magnitude by calculating P and V for a specific rainfall scenario, generalizing expected Vs and Ps into relative hazard classes, and identifying the relative hazard along a portion of a mountain front through combined P and V classes. Examples of this process can be seen in Cannon et al. (2010a) and Tillery et al. (2011). One reason for this generalized approach is the uncertainty inherent in the models, especially modeled Vs.

An alternative to modeling any single value is to calculate multiple V estimates within reasonable bounds using either the standard error of the regression model at a selected confidence interval as was done in the case study described herein, or by using a single order of magnitude as a bound for the range as described by Magirl et al. (2010). For extremely large storms, or unfavorable basin conditions, modeled Vs may exceed reasonable expectations. Reasonable upper bounds can be selected from historically observed post-fire debris-flow activity using a database such as that compiled by Santi and Morandi (2013). Using a database, a range of reasonably expected volumes can be calculated for a given scenario.

Even though a range of likely Vs can be predicted, a limitation of many existing V models is an inability to predict P of a specific V occurring. As Lee and Jones (2004) discuss, P of a given V or runout occurring is a necessary input for a true landslide risk assessment. Donovan (2014) recently developed a probabilistic method for estimating V along channel lengths. Donovan (2014) indicates that the probabilistic model also provides improved accuracy over the previously discussed V models. This model may prove useful for future post-fire debris-flow risk calculations. The model was not used for the work described in this paper because it was developed after the case study analysis was completed.

Runout Modeling

Runout modeling is the next step following estimation of P and V for post-fire debris-flow risk assessment. Rickenmann (2005) discusses a broad range of methods for evaluating landslide runout, some of which may be useful for post-fire debris-flow modeling. One relatively simple model to evaluate debris-flow runout is the GIS based computer program LAHARZ (Iverson et al., 1998, Schilling, 1998). As described by Rickenmann (2005), the program utilizes a pair of semi-empirical relationships between planimetric and cross-sectional areas inundated by a lahar or debris-flow to model through GIS the expected runout and footprint of the flow.

The LAHARZ program was initially developed by the USGS to model lahars in volcanic terrain. It has subsequently been modified to model non-volcanic debris-flows and rock avalanches (Griswold and Iverson, 2008), and post-fire flows (Bernard, 2007). Magirl et al. (2010) describe use of the program to analyze large

debris-flows in Arizona and Witt et al. (2012) describe use of the program for hazard assessment in North Carolina. Berti and Simoni (2007) describe development of a computer code that is conceptually similar to LAHARZ, but features more control in unconfined channel reaches and the ability to batch model a range of planimetric and cross-sectional areas to account for uncertainty in the inundation area regression models.

Alternative methods that are sometimes used for modeling debris-flow runouts include FLO-2D (e.g. Jakob et al., 2013) and Flow-R (e.g. Horton et al., 2013). These programs have the ability to model more complex flow relationships than the simple space filling model of LAHARZ. However, caution should be exercised when using more complex flow models. As Magirl et al. (2010) point out, some of the key parameters necessary to operate more complex flow models may be difficult to estimate, and may vary over space and time during a debris-flow.

POST-FIRE DEBRIS-FLOW ECONOMIC RISK MODELING

As described by Lee and Jones (2004), risk is concerned with the likelihood and scale of adverse consequences that result from the interaction of hazard and vulnerability. The preceding sections discuss methods to analyze post-fire debris-flow hazard. The subsequent sections discuss using these models to estimate economic risk from post-fire debris-flows. It is important to note that these methods are currently restricted to direct economic risk (expected loss of market and non-market valued items). This process does not currently account for risk to life and health, or for indirect economic losses (e.g. cost associated with rerouting freeway traffic).

Identifying and Valuing Elements at-Risk in GIS

ArcGIS was used to organize, compile, and extract economic impact data. Cost data can be derived from various sources published in various years. Historic cost data can be adjusted to a specified year for comparison using the Consumer Price Index (CPI) (BLS, 2013). The following paragraphs describe data sources, assumptions for damage estimates, and data extraction methods for identifying and valuing elements at-risk.

In the United States, major linear features (e.g. roads, railroads, streams) can be located using TIGER/Line® shapefiles, available for download from the United States Census geographic data center (Census, 2012). TIGER/Line® files are available for many major cities and counties in the United States. TIGER/Line® files include unique identifiers for different linear features (e.g. types of infrastructure and natural features) which allows for rapid sorting and identification of specific feature types. Infrastructure (road and railroad) damages per unit length of linear feature associated with a given debris flow inundation volume are estimated based using construction cost guides such as the R.S. Means Heavy Construction Cost Data guide (R.S. Means Company, 1999), and some assumptions of feature width and debris-flow depth. Non-market valued items (e.g. stream damage) are more difficult to estimate. For this study, damage to streams was estimated per unit length based on the value of lost ecosystem services following Holmes et al. (2004). Where available, residences can

be located in ArcGIS using parcel maps. Alternatively, if parcel maps are not available, residences can be located by digitizing features from aerial imagery. A circular buffer around the parcel centroid or digitized point approximates the extent of the structure. Damage is estimated as a fraction of total home value. Total home value may be estimated from Census data, or from real estate websites such as Zillow®.

When the debris-flow runout and elements at-risk are simultaneously plotted in ArcGIS, the intersect tool is used to identify features (e.g. structures, infrastructure, and streams) that intersect the runout footprint. Lengths of linear features (roads, railroads, and streams) that fall within the footprint of a given modeled debris-flow runout are extracted. If the modeled runout intersects any part of a residence buffer, the buffer is extracted. Due to possibility of splitting single features into multiple features during the intersect process, the dissolve tool is used to clean up extracted parcels so that no parcel is counted more than once. For a single modeled runout event, the quantity of residences, and lengths of roads are summed and multiplied by their respective unit values. These values are then summed to estimate the total damage cost associated with a debris-flow of given V issuing from a given basin.

Economic Risk Calculation

Lee and Jones (2004) state that if the probabilities of a specific magnitude landslide event occurring in a given time are known, specific risk can be calculated as follows:

$$R_s = P(H_k) * \sum_k (E * U * E_x) \quad (4)$$

Where: R_s is the specific risk associated with a slide of magnitude H, $P(H_k)$ is the probability of the slide of magnitude H occurring in a given time period, E is the total value of all threatened items (elements at-risk), U is the vulnerability (proportion of E reduced by event), and E_x is the exposure (proportion of total value likely to be present at the time of the event), k indicates summation of all elements affected by the event.

If it the vulnerability (U) is integrated into the damage estimate and exposure is assumed to be complete (E_x = 1), Eq. 4 can be re-written for a given basin and estimated V as:

$$R_v = (P_A * D) \quad (5)$$

$$P_A = (P * P_{storm}) \quad (6)$$

Where: R_v is the specific risk associated the basin for the modeled volume scenario expressed in units of cost, P_A is the total annual probability of a debris-flow occurring, D is the total modeled damage (cost), P is the probability of a debris-flow occurring given the occurrence of the modeled storm, and P_{storm} is the annual probability of the storm occurring (0.5 for a 2-year recurrence storm).

CASE STUDY: ECONOMIC RISK FROM POST-FIRE DEBRIS-FLOWS

By walking through the steps in an example case study for a single rainfall scenario at a wildfire impacted site, the following sections describe the methods used to identify elements at-risk from post-fire debris-flows, assign values to the elements, and calculate modeled risk for a given rainfall scenario from a given burned watershed.

Overview

The Jesusita fire burned a series of basins north of the city of Santa Barbara, California in 2009 (Cannon et al., 2010a). Fig. 1 shows the location of the study area.

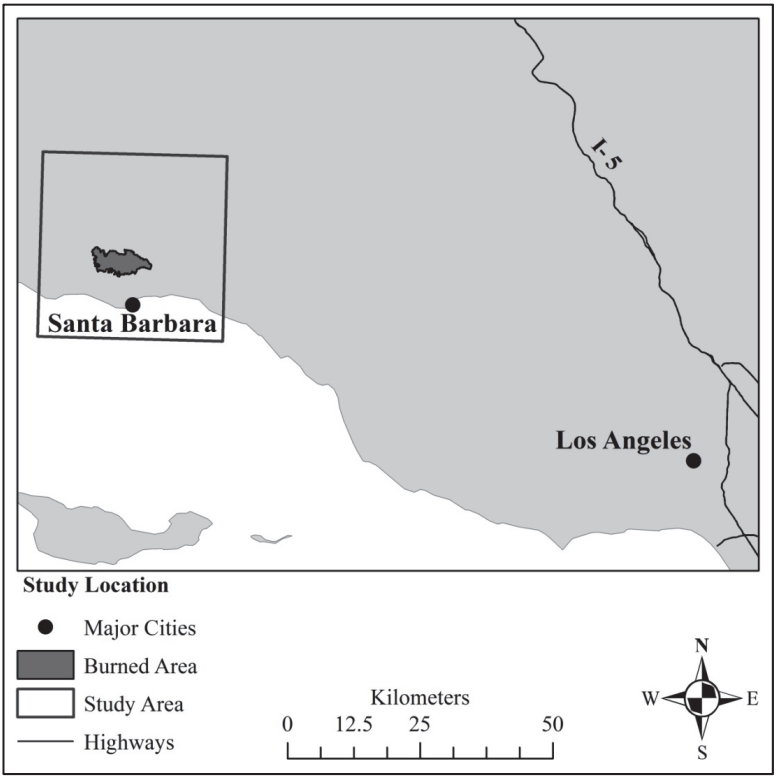

FIG. 1. Study location.

The box on Fig. 1 outlines the general region of the study area. The dark gray polygon within the box shows the approximate extent of the fire as downloaded from the GeoMac historic fire perimeter data repository (GeoMAC, 2013). Fig. 2 shows the key study area features.

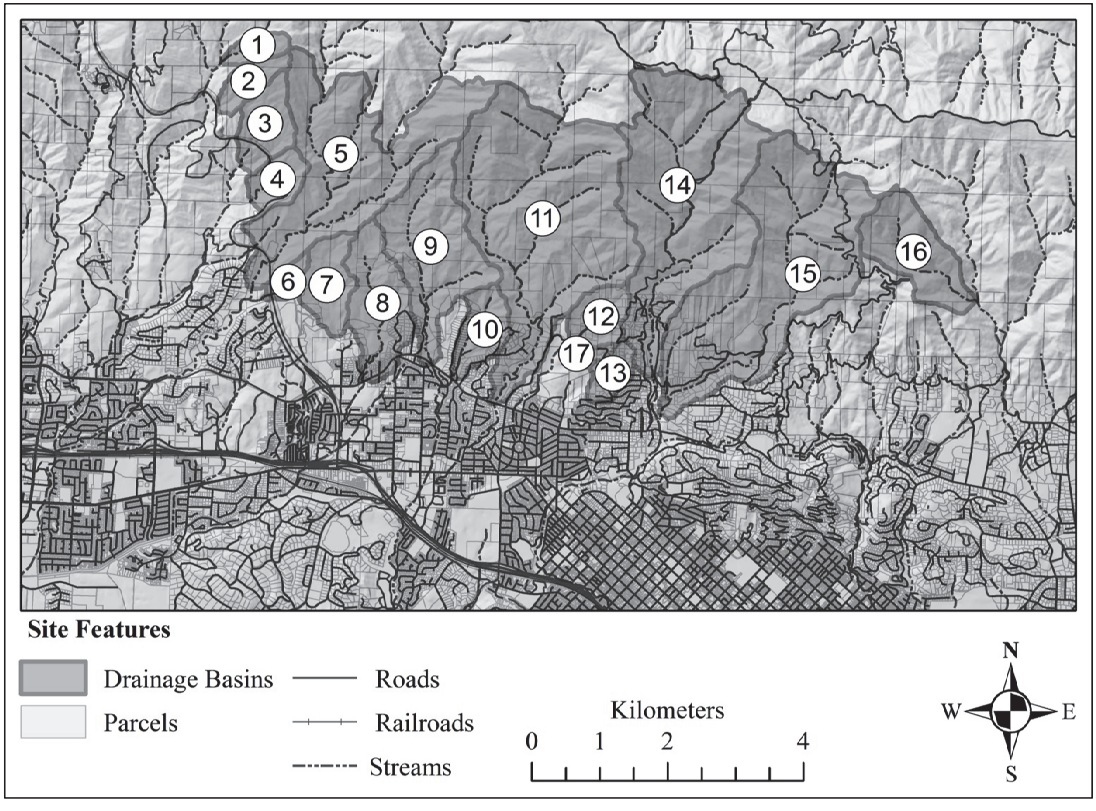

FIG. 2. Overview map of study area features.

Post-Fire Debris-Flow Hazard Modeling

P, V, and runout were modeled for a single 2-year recurrence, 15-minute rainfall scenario downloaded from NOAA (2013). A single rainfall intensity value was used for the entire range front. A 10 m resolution digital elevation model was downloaded from the national map (USGS, 2014b). Burn severity data (BARC) was downloaded from the BAER imagery support catalog (Forest Service, 2013). All GIS files were projected to North American Datum of 1983 (NAD 1983) Universal Transverse Mercator Zone 11N. Raster files were resampled to 10 m resolution and snapped to the DEM using the ArcGIS snap raster command. Seventeen basins were delineated using the hydrology tools in the ArcGIS spatial analyst toolbox. It is common practice to delineate the upper and lower extents of each basin from the lower fire perimeter to the upslope drainage basin divide. For this case study, the upper and lower extents of each basin were delineated by the fire perimeter unless the fire extended entirely to the upslope drainage basin divide. This change was done to maintain consistency with a previous debris flow hazard assessment of the site performed by the USGS (Gartner, 03/01/2013 personal communication).

P was estimated for each basin using Eq. 1 with a model developed for southern California where Eq. 2 is function of: elevation range across the basin (m), percent of basin burned at moderate and high severity with slopes steeper than 50 percent, percent of basin burned at high severity, standard deviation of basin slope, storm duration (hours), and total storm rainfall (mm) (Cannon, 10/11/2012 personal communication).

V (m^3) was estimated using Eq. 3 with the model presented in Cannon et al. (2010b). Uncertainty in V was estimated using a 95 percent confidence interval (CI). Assuming a normal distribution of the regressed data, approximate upper and lower bounds for a 95percent CI can be estimated by respectively adding and subtracting twice the residual standard error of the regression to the modeled value. Cannon et al. (2010b) reported a residual standard error of 0.90; it is assumed that the natural logarithmic transformation of their data yielded an approximately normal distribution. Therefore, lower and upper bounds for the 95 percent CI of the model used in this study were estimated using:

$$ln(V_{95L}) = [\, ln(V) \, - \, 1.8] \tag{7}$$

$$ln(V_{95U}) = \, [ln(V) + \, 1.8] \tag{8}$$

Where: $\ln(V_{95L})$ and $\ln(V_{95U})$ are the upper and lower bounds, respectively, of a 95 percent CI about the modeled natural logarithm of V. Estimates of the bounds are found by exponentiation of Eq. 7 and Eq. 8 using the base e.

Model inputs were extracted in ArcGIS. P and V calculations (including 95percent CI on V) were performed in a spreadsheet using Eq. 1 – Eq. 3 and Eq. 7 – Eq. 8. Modeled Vs were restricted to a maximum of 500,000 m^3 based on the upper limit of ranges of post-fire debris-flows reported by (Santi and Morandi, 2013). Basins 12 and 17 were excluded from runout modeling because they empty directly into a reservoir. Quantification of debris-flow impacts to reservoirs is important, but can be difficult

due to conditions that are specific to each reservoir. Analysis of debris-flow impacts to reservoirs is beyond the scope of this paper. Debris-flow runouts for V_{95U}, V, and V_{95L} were analyzed with a version of the LAHARZ program calibrated for post-fire debris-flows (Bernard, 2007). Onset of deposition of post-fire debris-flows depends on complex processes and is difficult to predict (Bernard, 2007, Brock, 2007). For this model, onset of debris-flow deposition was assumed to occur approximately at the edge of the burned area. These points generally coincide with decreases in channel slope. Actual onset of deposition may vary depending on local conditions. While this may affect modeling results, analysis of varying onset of deposition is beyond the scope of this paper.

Fig. 3 shows the results of the LAHARZ runout modeling. Three debris-flow runout shapes are plotted for each basin on Fig. 3. The largest (black) shape represents runout of the upper bound of the 95 percent CI (V_{95U}). These are very large events and are generally unlikely to occur. The middle (gray) shape represents runout of the modeled V. The smallest (white) shape represents the lower bound of the 95 percent CI (V_{95L}). In many cases, this feature barely extends beyond the debris-flow initiation point. It can also be seen in Fig. 3 that modeled debris-flows from multiple basins meet where streams combine. The implication of this is that elements at-risk in these areas are potentially subject to debris-flow hazards from multiple basins.

Identifying and Valuing Elements at-Risk in GIS

Potential elements at-risk for the Jesusita site are shown on Fig. 2. Cost data were derived from various sources published in various years and were subsequently adjusted to 2012 United States Dollars (USD) using the CPI.

Linear features were located using TIGER/Line® shapefiles. All types of road features were grouped together into the category “roads”. Railroad features were retained as the category “railroads”. Natural streams were grouped together into the category “streams”. Infrastructure (road and railroad) damages were estimated based on 1999 R.S. Means Heavy Construction Cost Data guide (R.S. Means Company, 1999), updated for inflation to 2012 USD. Road damage was estimated as cost per linear meter of road ($81.86/m) assuming $8.19/$m^3$ for soil removal, an average 10 m wide roadway, and an average 1 m thick debris deposit. Railroad damage was estimated as cost per linear meter of railroad ($143.38/m) assuming $61.52/m of track to repair, and $81.86/m of soil removal. Stream value was estimated as cost per linear meter of stream ($3.28/m) based on the value of lost ecosystem services following Holmes et al. (2004).

Residences were located in ArcGIS using parcel maps downloaded from the county of Santa Barbara website (County of Santa Barbara, 2011). Centroids of each parcel were plotted in ArcGIS, and a 20 m radius buffer was generated around this point to estimate the structure location and size. Analyzed parcels were limited to those listed in the Assessor’s parcel file as single family homes and apartments, on the ground floor. Basements, upper floors, mobile homes, and non-residential structures are included in the dataset, but were excluded from analysis to avoid counting a residence more than once. Median home values were determined by neighborhood from a pre-

existing ESRI map (based on 2010 census data). The median home value was applied to each parcel centroid (and associated buffer) falling within a given neighborhood.

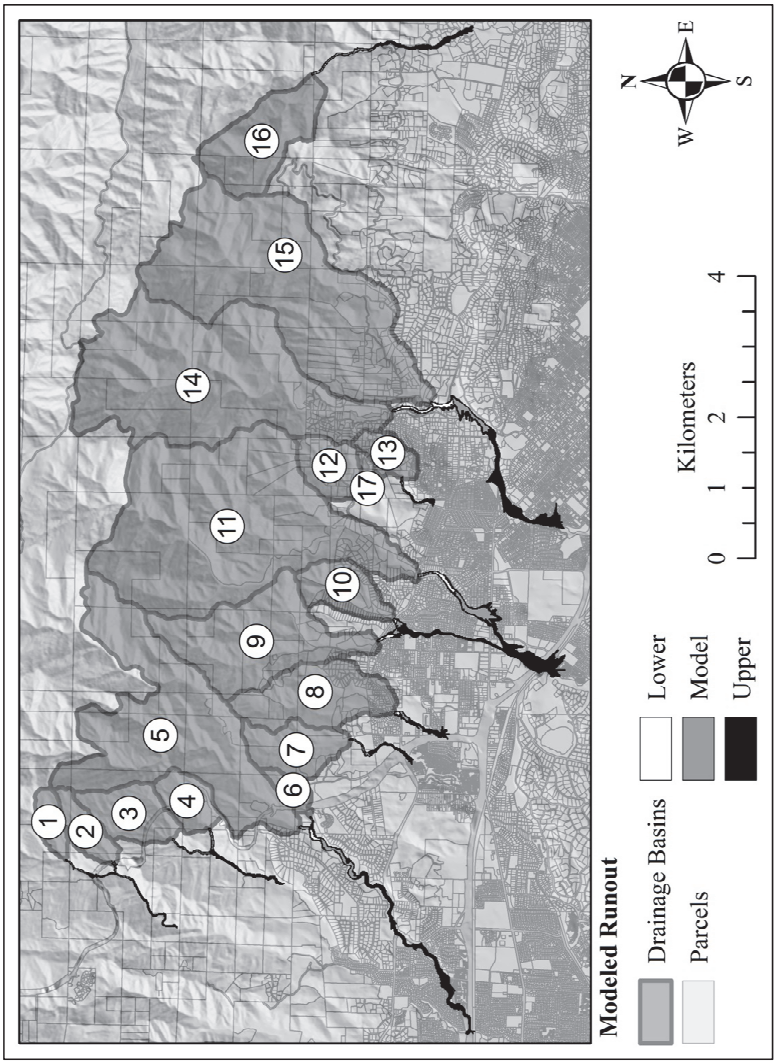

FIG. 3. Debris-flow runouts modeled with LAHARZ.

Average damages were assumed to be approximately 30 percent of the estimated home value. This method was selected over more precise methods (e.g. explicit values of each home) because of the ability for rapid implementation.

Fig. 4 shows features intersected by three modeled debris-flow runouts from Basin 11.

Economic Risk Calculation

For the linear elements at-risk described in the preceding section, it was assumed that the vulnerability and exposure were both 1 (i.e. 100 percent of the elements at-risk were damaged to their full estimated value). Assessing vulnerability and exposure of residences is difficult because there are not easily obtainable statistics related to economic impacts to homeowners from post-fire debris-flows. For this study, the vulnerability of homes to post-fire debris-flow damage was accounted for by multiplying the median home value by 30 percent. Since values of the individual elements at-risk were already summed for a given basin, risk calculations were performed using Eq. 5 and Eq. 6. Uncertainty in the economic risk is estimated by calculating R_v for three values of D associated with V_{95U}, V, and V_{95L}, respectively, assuming that P applies to any flow within the 95 percent CI. By repeating the risk calculation for the upper and lower bounds, a risk range was generated.

Results of Economic Risk Modeling

Damage Estimate Results

Damage estimates for modeled debris-flows from each basin (including upper and lower bounds on the 95 percent CI) for the modeled 2-year, 15-minute storm are presented in Table 1. This table includes modeled V, as well as extracted values for each category of element at-risk (residences, roads, railroads, and streams). Vs and damage costs have been reported to the nearest whole number. However, based on uncertainty of the V model as discussed in Cannon et al. (2010b) and Gartner et al. (2008), modeled results are only accurate to an order of magnitude. This uncertainty was accounted for by utilizing the 95 percent CIs around the modeled values.

A comparison of the upper 95 percent CI bound of Basin 2 with the same feature from Basin 7 highlights one of the most striking observations made in this study. The modeled volumes for these two basins are not significantly different, but the estimated damages for Basin 7 are significantly larger than those for Basin 2. The majority of the difference is accounted for by the inclusion of several homes in the upper 95 percent CI bound of Basin 7. This observation illustrates the important relationship between development density in the wildland-urban interface and expected damages from post-fire debris-flows.

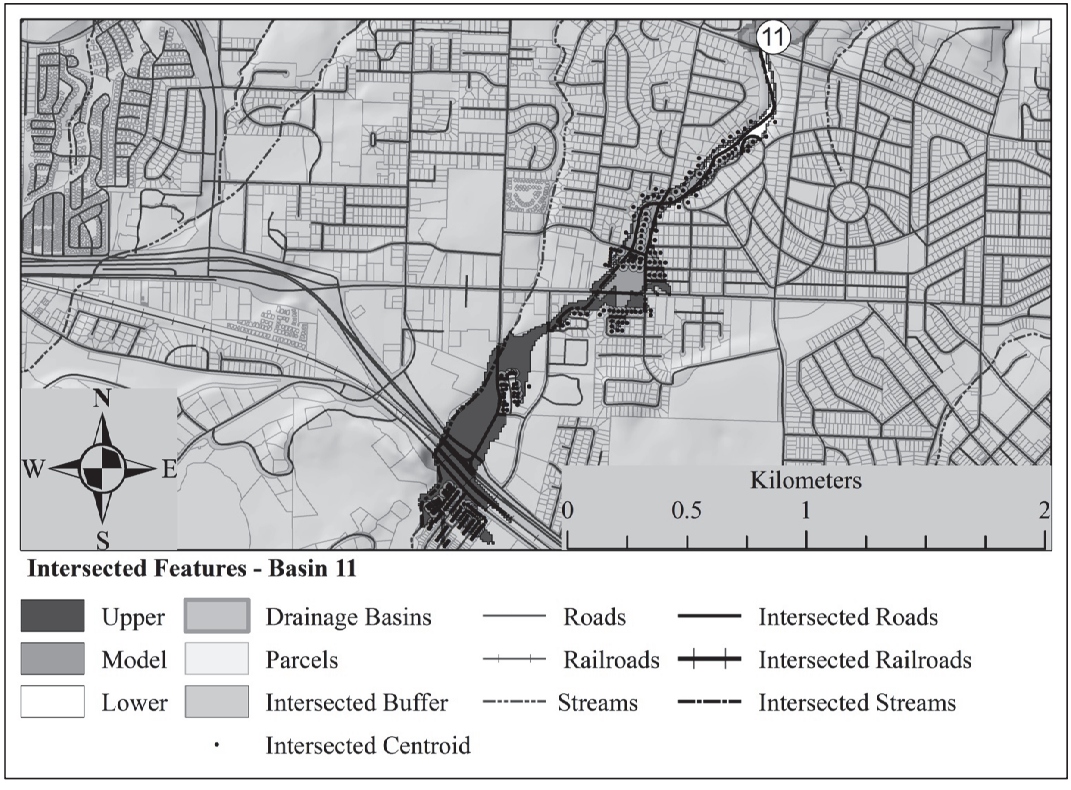

FIG. 4. Features intersected by modeled debris-flow runout from Basin 11.

Risk Estimate Results

The damage results discussed in the preceding section were input into Eq. 5 and Eq. 6 to estimate economic risk for each basin. Results (including 95 percent CI) for the modeled 2-year, 15-minute storm are presented in Table 2. The results of these economic risk analyses can be used to evaluate the relative economic feasibility of a set of proposed mitigation options. Cost-optimized treatment strategies can be analyzed using these results and estimates of expected cost and effectiveness (at reducing P, V, or both) of various post-fire debris-flow prevention and protection technologies (e.g. Napper, 2006, and Robichaud at al., 2010). The table also includes a ranking of basins (based on modeled risk, not including 95 percent CI bounds) from highest to lowest economic risk (1 to 14). This ranking system could be used by emergency management personnel following a fire to direct resources and spending.

CONCLUSIONS

A method was developed that utilizes previously existing post-fire hazard assessment calculations and debris-flow runout models combined with easily obtainable feature data in a GIS to model expected damages and economic risk from individual burned basins following a fire. Preliminary case study results suggest that this process can identify the drainage basins posing the greatest economic risk. These results can guide allocation of emergency management funds and optimization of debris-flow management strategies following a wildfire. The process is modular; a variety of probability, volume, and runout models can be used depending on data availability, project needs, and skills of the analyst.

Some limitations should be kept in mind when performing post-fire debris-flow risk assessment using the process described in this paper. The process was specifically developed to address economic risk associated with post-fire debris-flows; it has not been designed to address other concerns (e.g. fatalities, flooding, or long-term erosion and sedimentation). The quality of the estimates is tied to the methods used to calculate probability and volume, the methods used to model runout, and the assumptions used to identify and value the elements at-risk. Due to the uncertainty in the volume model used in this analysis, damage estimates generated by this modeling are generally only accurate for order of magnitude assessments.

ACKNOWLEDGEMENTS

Funding for work described in this paper was provided by the Joint Fire Science Program, National Interagency Fire Center, Project 12-2-01-35. The authors would like to thank Joe Gartner, Dennis Staley, Sue Cannon, and John Michael of the United States Geological Survey for valuable input and guidance in the use of the debris-flow probability, volume, and runout models. Finally, the authors thank Dr. Steffen Rebennack and Timo Lohmann from the Division of Economics and Business at Colorado School of Mines, and the anonymous reviewers for their comments, which improved this document.

Table 1. Damage Cost Estimates for 2-year, 15-minute Storm Scenario

Basin ID	Debris Volume (m^3)		Residences (USD)	Roads (USD)	Railroads (USD)	Streams (USD)	Total Estimated Damage (USD)
1	V_{95L}	684	$0	$0	$0	$303	$303
	V	4,143	$0	$0	$0	$1,311	$1,311
	V_{95U}	25,068	$0	$5,560	$0	$3,831	$9,391
2	V_{95L}	942	$0	$2,456	$0	$0	$2,456
	V	5,699	$0	$5,940	$0	$840	$6,781
	V_{95U}	34,482	$0	$6,759	$0	$4,644	$11,403
3	V_{95L}	1,636	$0	$0	$0	$533	$533
	V	9,902	$0	$0	$0	$2,077	$2,077
	V_{95U}	59,903	$582,472	$32,749	$0	$6,158	$621,379
4	V_{95L}	935	$0	$0	$0	$176	$176
	V	5,661	$0	$0	$0	$210	$210
	V_{95U}	34,252	$291,236	$9,936	$0	$2,801	$303,973
5	V_{95L}	10,558	$0	$0	$0	$1,490	$1,490
	V	63,873	$0	$0	$0	$4,564	$4,564
	V_{95U}	386,414	$19,738,306	$105,881	$1,434	$14,359	$19,859,980
6	V_{95L}	114	$0	$0	$0	$71	$71
	V	690	$0	$0	$0	$250	$250
	V_{95U}	4,178	$0	$0	$0	$686	$686
7	V_{95L}	1,022	$0	$0	$0	$0	$0
	V	6,186	$0	$0	$0	$0	$0
	V_{95U}	37,428	$2,784,106	$20,518	$0	$0	$2,804,624
8	V_{95L}	1,420	$0	$3,874	$0	$187	$4,061
	V	8,591	$0	$6,235	$0	$784	$7,019
	V_{95U}	51,975	$7,397,451	$21,216	$0	$2,787	$7,421,454
9	V_{95L}	5,060	$0	$3,075	$0	$805	$3,880
	V	30,615	$0	$15,778	$0	$1,975	$17,753
	V_{95U}	185,211	$19,529,205	$71,102	$0	$7,911	$19,608,219
10	V_{95L}	1,077	$0	$2,041	$0	$189	$2,230
	V	6,517	$0	$12,106	$0	$594	$12,700
	V_{95U}	39,426	$3,412,383	$27,516	$0	$2,238	$3,442,138
11	V_{95L}	18,578	$0	$10,701	$0	$2,008	$12,709
	V	112,390	$0	$67,199	$0	$4,209	$71,408
	V_{95U}	500,000	$49,128,536	$300,196	$59,743	$8,504	$49,496,979
13	V_{95L}	540	$0	$0	$0	$0	$0
	V	3,268	$0	$0	$0	$0	$0
	V_{95U}	19,773	$1,238,225	$1,518	$0	$0	$1,239,743
14	V_{95L}	15,219	$0	$15,171	$0	$2,150	$17,321
	V	92,075	$0	$25,035	$0	$4,822	$29,856
	V_{95U}	500,000	$32,598,497	$161,630	$0	$11,648	$32,771,775
15	V_{95L}	13,227	$0	$5,030	$0	$1,066	$6,096
	V	80,024	$0	$8,929	$0	$3,469	$12,398
	V_{95U}	484,117	$5,572,340	$171,787	$0	$10,150	$5,754,276
16	V_{95L}	3,311	$0	$0	$0	$948	$948
	V	20,034	$0	$0	$0	$3,502	$3,502
	V_{95U}	121,201	$2,211,118	$35,534	$0	$8,510	$2,255,163

Table 2. Debris Flow Hazard and Economic Risk Modeling Results

Basin ID	P_{storm}	P_{flow}	Modeled Volume (m^3)	95% CI Volume (m^3)	Modeled Damage (USD)	95% CI Damage	Modeled Risk (USD)	95% CI Risk (USD)	Risk Rank
1	0.50	0.13	4,143	684 - 25,068	$1,311	$303 - $9,391	$86	$20 - $622	11
2	0.50	0.19	5,699	942 - 34,482	$6,781	$2,456 - $11,402	$641	$232 - $1,078	7
3	0.50	0.12	9,902	1636 - 59,903	$2,077	$532 - $621,378	$127	$32 - $38,186	10
4	0.50	0.08	5,661	935 - 34,252	$210	$175 - $303,972	$8	$6 - $11,779	12
5	0.50	0.45	63,873	10,558 - 386,414	$4,564	$1,489 - $19,859,980	$1,018	$332 - $4,432,377	6
6	0.50	0.04	690	114 - 4,178	$250	$70 - $685	$5	$1 - $15	13
7	0.50	0.06	6,186	1,022 - 37,428	$0	$0 - $2,804,624	$0	$0 - $84,029	14
8	0.50	0.06	8,591	1,420 - 51,975	$7,019	$4,061 - $7,421,454	$222	$128 - $235,072	9
9	0.50	0.35	30,615	5,060 - 185,211	$17,753	$3,880 - $19,608,218	$3,142	$686 - $3,470,319	4
10	0.50	0.07	6,517	1,077 - 39,426	$12,700	$2,230 - $3,442,137	$471	$82 - $127,767	8
11	0.50	0.55	112,390	18,578 - 500,000	$71,408	$12,708 - $49,496,979	$19,724	$3,510 - $13,672,203	1
13	0.50	0.05	3,268	540 - 19,773	$0	$0 - $1,239,743	$0	$0 - $31,638	14
14	0.50	0.66	92,075	15,219 - 500,000	$29,856	$17,320 - $32,771,775	$9,813	$5,693 - $10,771,749	2
15	0.50	0.56	80,024	13,227 - 484,117	$12,398	$6,095 - $5,754,276	$3,446	$1,694 - $1,599,711	3
16	0.50	0.61	20,034	3,311 - 121,201	$3,502	$947 - $2,255,162	$1,076	$291 - $693,207	5

REFERENCES

Bernard, D. R. (2007). "Estimation of inundation areas of post-wildfire debris-flows." MS, Colorado School of Mines, Golden, CO.

Berti, M., and Simoni, A. (2007). "Prediction of debris-flow inundation areas using empirical mobility relationships." *Geomorphology*, 90(1–2), 144-161.

Brock, R.J. (2007). "Controlling factors for the onset of deposition of wildfire-related debris flows." MS, Colorado School of Mines, Golden, CO.

BLS (2013). "Consumer price index." *Bureau of Labor Statistics*, <http://www.bls.gov/cpi/>. (June 13, 2013).

Calkin, D. E., Hyde, K. D., Robichaud, P. R., Jones, J. G., Ashmun, L. E., and Loeffler, D. (2007). "Assessing post-fire values-at-risk with a new calculation tool. Gen. Tech. Rep. RMRS-GTR-205.", U.S. Department of Agriculture, Forest Service, Rocky Mountain Research Station, Fort Collins, CO.

Cannon, S. H., and Gartner, J. E. (2005). "Wildfire-related debris-flow from a hazards perspective." *Debris-flow hazards and related phenomena*, M. Jakob, and O. Hungr, eds., Springer Berlin Heidelberg, 363-385.

Cannon, S. H., Gartner, J. E., Wilson, R. C., Bowers, J. C., and Laber, J. L. (2008). "Storm rainfall conditions for floods and debris-flows from recently burned areas in southwestern Colorado and southern California." *Geomorphology*, 96(3–4), 250-269.

Cannon, S. H., and DeGraff, J. (2009). "The increasing wildfire and post-fire debris-flow threat in western USA, and implications for consequences of climate change." *Landslides – disaster risk reduction*, K. Sassa, and P. Canuti, eds., Springer Berlin Heidelberg, 177-190.

Cannon, S. H., Gartner, J. E., Rupert, M. G., and Michael, J. A. (2010a). "Emergency assessments of postfire debris-flow hazards for the 2009 la brea, jesusita, guiberson, morris, sheep, oak glen, pendleton, and cottonwood fires in southern California." *Open-File Report 2010-1186*, U.S. Department of the Interior, U.S. Geological Survey, Reston, Virginia.

Cannon, S. H., Gartner, J. E., Rupert, M. G., Michael, J. A., Rea, A. H., and Parrett, C. (2010b). "Predicting the probability and volume of postwildfire debris-flows in the intermountain western united states." *Geological Society of America Bulletin*, 122(1-2), 127-144.

Census (2012). "Topologically integrated geographic encoding and referencing (TIGER®)." *United States Census Bureau*, <http://www.census.gov/geo/maps-data/data/tiger.html>. (February 18, 2013).

County of Santa Barbara (2011). "County GIS spatial catalog, boundaries, tax assessment parcels (without owner names), file: Parcel_layers2011_0210." <http://www.countyofsb.org/gis/default.aspx?id=2802>. (February 6, 2013).

Donovan, I. P. (2014). "A probabilistic approach to post-wildfire debris-flow volume modeling." MS, Colorado School of Mines, Golden, Colorado.

ESRI (2010). "Arcgis." ESRI, Redlands, California.

Forest Service (2013). "Baer imagery support data download." <http://activefiremaps.fs.fed.us/baer/download.php>. (June 6, 2013).

G4G (2014). "GIS 4 geomorphology." <http://gis4geomorphology.com/>. (April 29, 2014).

Gartner, J. E., Cannon, S. H., Santi, P. M., and Dewolfe, V. G. (2008). "Empirical models to predict the volumes of debris-flows generated by recently burned basins in the western U.S." *Geomorphology*, 96(3–4), 339-354.

Gartner, J. E., Cannon, S. H., and Santi, P. M. (2011). "Implementation of post-fire debris-flow hazard assessments along drainage networks, southern California, U.S.A." *Proc., 5th International Conference on Debris-Flow Hazards Mitigation: Mechanics, Prediction and Assessment*, Italian Journal of Engineering Geology and Environment - Book, 855 - 863.

GeoMAC (2013). "Geosciences and environmental change science center (GECSC) outgoing datasets." <http://rmgsc.cr.usgs.gov/outgoing/GeoMAC/historic_fire_data/>. (April 30, 2014).

Gesch, D., Oimoen, M., Greenlee, S., Nelson, C., Steuck, M., and Tyler, D. (2002). "The national elevation dataset." *Photogrammetric Engineering and Remote Sensing*, 68(1), 5-11.

Griswold, J. P., and Iverson, R. M. (2008). "Mobility statistics and automated hazard mapping for debris-flows and rock avalanches." *Scientific Investigations Report 2007–5276*, U.S. Department of the Interior, U.S. Geological Survey, Reston, Virginia.

Holmes, T. P., Bergstrom, J. C., Huszar, E., Kask, S. B., and Orr Iii, F. (2004). "Contingent valuation, net marginal benefits, and the scale of riparian ecosystem restoration." *Ecological Economics*, 49(1), 19-30.

Horton, P., Jaboyedoff, M., Rudaz, B., and Zimmermann, M. (2013). "Flow-R, a model for susceptibility mapping of debris-flows and other gravitational hazards at a regional scale." *Nat. Hazards Earth Syst. Sci.*, 13(4), 869-885.

Iverson, R. M., Schilling, S. P., and Vallance, J. W. (1998). "Objective delineation of lahar-inundation hazard zones." *Geological Society of America Bulletin*, 110(8), 972-984.

Jakob, M., Holm, K., Weatherly, H., Liu, S., and Ripley, N. (2013). "Debris flood risk assessment for Mosquito Creek, British Columbia, Canada." *Natural Hazards*, 65(3), 1653 - 1681.

Lee, E. M., and Jones, D. K. C. (2004). *Landslide risk assessment*, Thomas Telford Publishing, London.

Magirl, C. S., Griffiths, P. G., and Webb, R. H. (2010). "Analyzing debris-flows with the statistically calibrated empirical model LAHARZ in southeastern Arizona, USA." *Geomorphology*, 119(1–2), 111-124.

MTBS (2014). "Monitoring trends in burn severity (MTBS)." <http://www.mtbs.gov/index.html>. (April 30, 2014).

Napper, C. (2006). "Burned area emergency response treatments catalog (BAERCAT)." USDA Forest Service, National Technology and Development Program, Watershed, Soil, Air Management, San Dimas Technology & Development Center, San Dimas, California.

NOAA (2013). "Precipitation frequency data server." *National Oceanographic and Atmospheric Administration: Hydrometeorological Design Studies Center*, <http://dipper.nws.noaa.gov/hdsc/pfds/>. (June 4, 2013).

Parsons, A., Robichaud, P. R., Lewis, S. A., Napper, C., and Clark, J. T. (2010). "Field guide for mapping post-fire soil burn severity. General technical report RMRS-GTR-243." U.S. Department of Agriculture, Forest Service, Rocky Mountain Research Station, Fort Collins, CO.

R.S. Means Company (1999). *Heavy construction cost data*, Kingston, MA.

Rickenmann, D. (2005). "Runout prediction methods." *Debris-flow hazards and related phenomena*, M. Jakob, and O. Hungr, eds., Springer Berlin Heidelberg, 305-324.

Robichaud, P. R., Elliot, W. J., Pierson, F. B., Hall, D. E., Moffet, C. A., and Ashmun, L. E. (2007). "Erosion risk management tool (ERMiT) user manual (version 2006.01.18). General technical report RMRS-GTR-188." U.S. Department of Agriculture, Forest Service, Rocky Mountain Research Station, Fort Collins, CO.

Robichaud, P. R., Ashmin, L. E., and Simms, B. D. (2010). "Post-fire treatment effectiveness for hillslope stabilization. Gen. Tech. Rep. RMRS-GTR-240.", U.S. Department of Agriculture, Forest Service, Rocky Mountain Research Station, Fort Collins, CO.

Rupert, M. G., Cannon, S. H., Gartner, J. E., Michael, J. A., and Helsel, D. R. (2008). "Using logistic retression to predict the probability of debris-flows in areas burned by wildfires, southern California, 2003-2006." *Open-File Report 2008-1370*, U.S. Department of the Interior, U.S. Geological Survey, Reston, Virginia.

Santi, P., and Morandi, L. (2013). "Comparison of debris-flow volumes from burned and unburned areas." *Landslides*, 10(6), 757-769.

Schilling, S. P. (1998). "LAHARZ: GIS programs for automated mapping of lahar-inundation hazard zones." *Open-File Report 98-638*, U.S. Department of the Interior, U.S. Geological Survey, Vancouver, Washington.

Soil Survey Staff "U.S. General soil map (STATSGO2)." *Natural Resources Conservation Service, United States Department of Agriculture*, <http:// sdmdataaccess.nrcs.usda.gov/>. (April 29, 2014).

Soil Survey Staff (2014). "Soil data viewer." <http://www.nrcs.usda.gov/ wps/portal/nrcs/detailfull/soils/home/?cid=nrcs142p2_053620>. (April 30, 2014).

Staley, D. M., Kean, J. W., Cannon, S. H., Schmidt, K. M., and Laber, J. L. (2013). "Objective definition of rainfall intensity-duration thresholds for the initiation of post-fire debris-flows in southern California." *Landslides*, 10(5), 547-562.

Tillery, A. C., Darr, M. J., Cannon, S. H., and Michael, J. A. (2011). "Postwildfire debris-flow hazard assessment for the area burned by the 2011 track fire, northeastern new mexico adn southeastern Colorado." United States Geological Survey.

USGS (2014a). "National elevation dataset frequently asked questions." <http:// ned.usgs.gov/faq.html>. (April 30, 2014).

USGS (2014b). "The national map." <http://nationalmap.gov/index.html>. (2014, April 30).

USGS (2014c). "Scientific background." *Landslide Hazards Program Postfire Debris-flow*, <http://landslides.usgs.gov/current/postfire_debrisflow/background.php>. (April 30, 2014).

Witt, A. C., Gillon, K. A., Wooten, R. M., Douglas, T. J., Bauer, J. B., and Fuemmeler, S. J. (2012). "Determining potential debris-flow inundation zones for an emergency response using LAHARZ: The ghost town debris-flow, Maggie Valley, N.C., USA." *Landslides and engineered slopes: Protecting society through improved understanding*, E. Eberhardt, C. Froese, A. K. Turner, and S. Leroueil, eds., CRC Press/Balkema.

Rio Grande Dam – Seepage Reduction Design and Construction

Derek H. Foster[1], M. ASCE, P.E., Dan Bole,[2] and Ted W. Deere[3]

[1]Project Manager, Deere & Ault Consultants, Inc., 600 South Airport Road, Suite A-205, Longmont, CO 80503; phone (303) 651-1468; derek.foster@deereault.com
[2]Project Manager, Hayward Baker, Inc., 11575 Wadsworth Blvd. Broomfield, CO 80020; phone (303) 469-1136; dpbole@haywardbaker.com
[3]Project Engineer, Deere & Ault Consultants, Inc., 600 South Airport Road, Suite A-205, Longmont, CO 80503; phone (303) 651-1468; ted.deere@deereault.com

ABSTRACT:

Rio Grande Dam was constructed over 100 years ago near the headwaters of the Rio Grande in the San Juan mountains of southwest Colorado. The reservoir is impounded by an earthfill and rockfill dam built in a challenging geologic environment. The left abutment consists of a large heterogeneous rock slide deposit, while the right abutment is made up of fractured volcanic rock. Historically, the reservoir has experienced high seepage through both abutments and the dam foundation. A rehabilitation project was designed in 2012 and constructed in 2013 with the goal of reducing the seepage through the abutments and the foundation of the dam. A clay slope liner and clay blanket were constructed on the upstream face of the left abutment over the rock slide deposit to decrease seepage. A grout program was developed, utilizing real-time computer aided grout delivery monitoring, to construct a grout curtain into the fractured volcanic rock of the dam foundation and right abutment with the intent of infilling fractures to reduce seepage. Preliminary data, to date, indicate the rehabilitation project appears to have successfully reduced seepage through the dam foundation and the abutments by more than 50 percent of the historical average.

INTRODUCTION

Rio Grande Dam and Reservoir are located near the headwaters of the Rio Grande in central Hinsdale County in the San Juan Mountains of southwestern Colorado at an elevation of approximately 2,880 m (9,450 ft) as shown on Fig. 1. It is approximately 32 km (20 miles) west-southwest of the town of Creede and about 32 km (20 miles) south of Lake City. The total maximum reservoir storage at gage height 27.7 m (91 ft) is approximately 2,357,000 m^3 (54,100 acre-ft).

FIG. 1. Location Map

The reservoir is impounded by an earthfill and rockfill dam constructed in a difficult geologic environment with a maximum height of 33.8 m (111 ft) and a crest length of approximately 167.6 m (550 ft). The right abutment consists of highly-fractured volcanic rock, while a very non-uniform rock slide deposit makes up the left abutment. Alluvial deposits may or may not be present, overlaying massive volcanic rock, underneath the rockfill central portion of the dam in the valley bottom.

The reservoir has generally been operated at an annual average gage height of 12.2 m to 15.2 m (40 ft to 50 ft), depending on the precipitation in the basin. In the last 15 years of record, the dam has stored water above gage height 24.4 m (80 ft) in only four of these years and at gage height 27.7 m (91 ft) (full pool) only once. In each of these cases, the reservoir was only able to store water near the full capacity

for only a few weeks before the water was released due to water right constraints. When full the seepage out of the reservoir through all sources was estimated to be over 158 L/s (2500 gal/min).

Historically, the dam has experienced excessive seepage rates at high reservoir stages (above gage height 12.2 m (40 ft)). The purpose of this rehabilitation project was to evaluate the existing condition of the dam and look for ways to reduce the seepage. As shown on Fig. 2, the result of the geotechnical investigations and subsequent rehabilitation design was to construct a clay slope liner and clay blanket on the upstream left abutment and a grout curtain in the dam foundation extending to the right abutment with a clay blanket cover. The clay blankets, consisting of a two foot thick layer of compacted clay, were constructed on both the left and right abutments to increase the seepage path at the dam. This combination was expected to reduce the seepage and should allow the reservoir to safely operate at higher levels for longer periods of time and better enable water storage at higher stages that can be carried over from one water year to the next. The seepage reduction project was construction in the summer of 2013. The primary contractor was MCMS, Inc who, along with employees of the Owner, San Luis Valley Irrigation District (SLVID), performed all of the construction with the exception of the grouting which was performed by Hayward Baker, Inc. (HBI).

BACKGROUND AND HISTORY

The Rio Grande Dam was designed by Engineer J.C. Ulrich of Denver beginning in 1905. San Luis Valley Irrigation District (SLVID), the Owner and operator of the dam since the original construction, has maintained excellent files of the original dam construction. From the information available in these files, a very complete background of the history of the dam and reservoir was available to the project team.

In 1905, Ulrich had originally planned to construct a 41 m (135 ft) high masonry dam at the site but quickly changed his plans after recognizing the challenging geological conditions during the excavation of a 34 m (110 ft) long exploration tunnel into the left abutment. Ulrich found a heterogeneous mass of loose rock, sand, and clay, which was contrary to the bedrock in the right abutment. He decided to design a 29 m (95 ft) high zoned earthfill and rockfill dam.

The dam was constructed with 2/3 (by volume) earthfill on the upstream side of the dam and 1/3 rockfill on the downstream side of the dam. The upstream zone was constructed as compacted earthfill with staggered puddle trenches constructed within the earthfill. Puddle trenches consisted of clay fill placed in basins that were flooded with water. This construction method is not used in modern dam construction due to the development of roller compaction equipment. Dumped rockfill, placed in 76 cm (30 in) maximum lifts, was used to construct the downstream zone. A cross-section of the dam through the maximum section showing the two primary embankment zones is shown on Fig. 3.

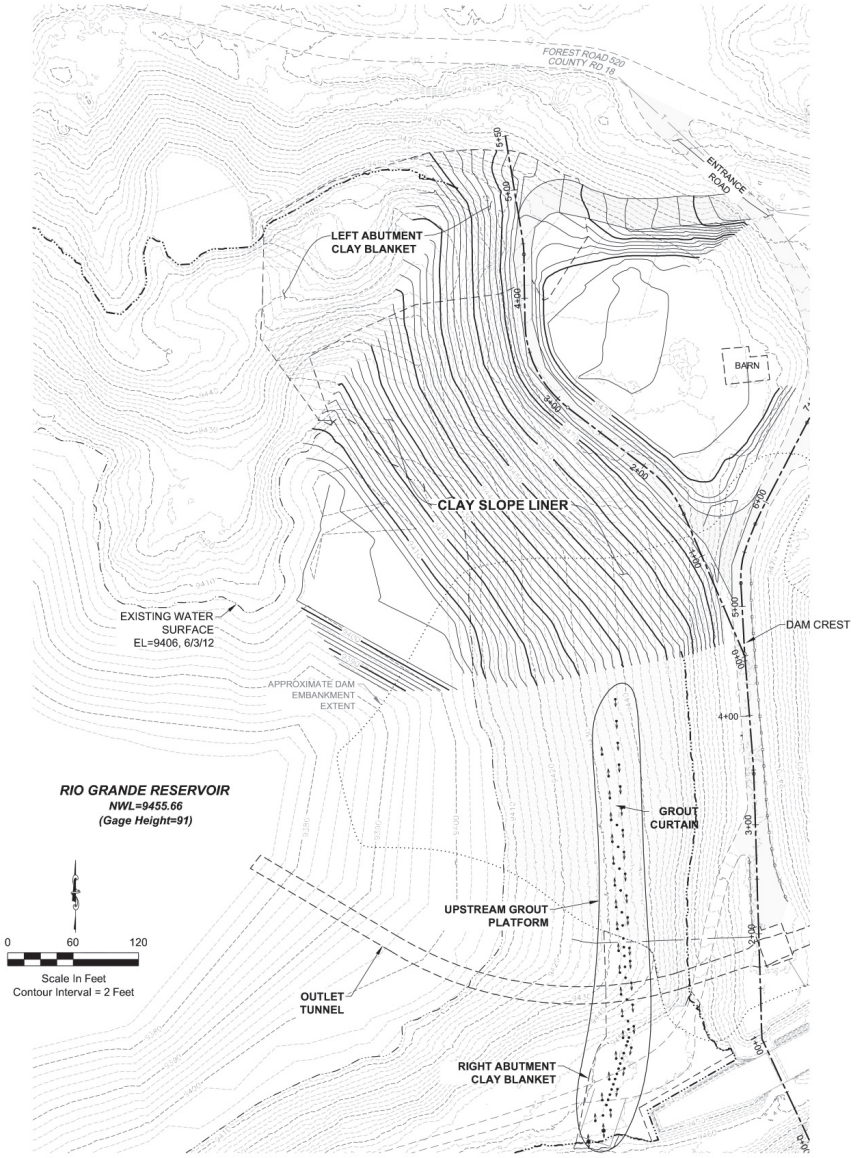

FIG. 2. Plan View of Rio Grande Dam Seepage Reduction Project

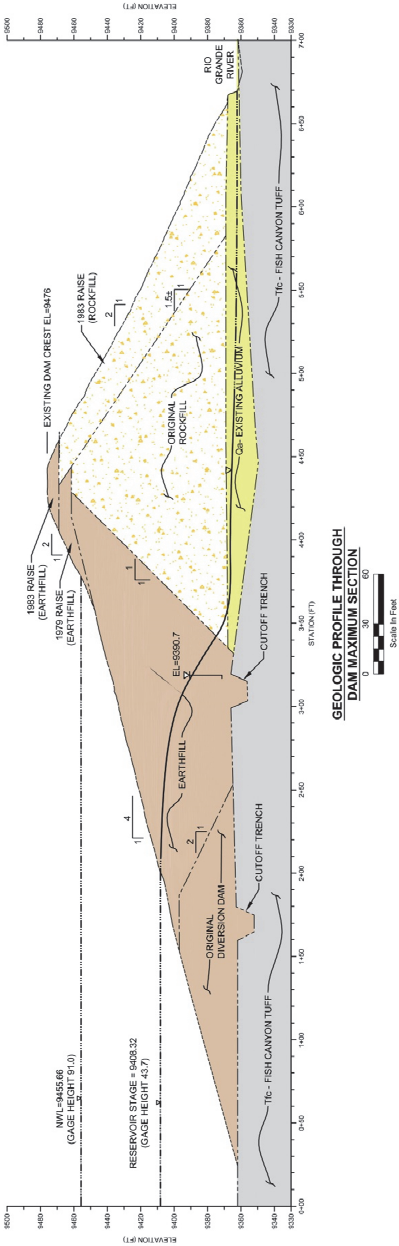

FIG. 3. Dam Cross-Section

Construction of the diversion/outlet tunnel began in 1908. The Photograph 1 below shows a view of the site in 1911 looking westward into the reservoir basin. The light colored rock pile at the upstream tunnel portal can be seen on the left side of the photograph.

Photograph 1. View west from dam location looking into reservoir area

Original Dam Design and Construction

The engineer, Ulrich, demonstrated in his specification (Ulrich,1910b) that he had an appreciation for many modern day dam engineering construction requirements. The specifications called for "*The entire surface that will underlie the structure must be thoroughly cleared off of all vegetable matter of every description, and all roots and stumps must be removed from the site…to the entire satisfaction of the Engineer*."

The earthfill construction schedule fell behind the rockfill work due to Ulrich's demand that the specifications be strictly followed. Cold weather placement was not allowed for the earthfill while the rockfill placement continued in the winter. Two 3 m (10 ft) deep cutoff trenches were constructed on the upstream side (Fig. 2) and puddled with "select earthfill." The design required that the existing alluvium was removed from under the earthfill section of the dam and left in place for the rockfill portion. The earthfill was to be "*entirely free of vegetable matter, and containing not too large a proportion of sand or loose rock*." Ulrich allowed a maximum particle size of "*1 cubic foot*" and a maximum percentage "*of loose rock of 25% ... provided further…that the loose rock is evenly intermixed with the earth*." In order to meet this

specification, borrow material was screened through wooden grizzlies and rocks were hand separated from the fill. The rockfill specifications allowed rock sizes that ranged from "*one-fourth cubic foot to one cubic yard, or more. It will be required that the rock of different sizes be distributed*."

The earthfill placement was not to exceed two-foot-thick lifts and was compacted by horses and loaded wagons. Over 50 teams of horses or mules were used during the construction. Photograph 2 shows construction of the Rio Grande Dam with horses and loaded wagons. Parallel embankments along the crest line were built up to 1.8 m (6 ft) high with compacted soil and material in between was puddled with water. The puddle trenches or basins were staggered going upward, resulting in a honeycombed pattern. Thus, the puddled sections were allowed to drain and consolidate. Ulrich called this method of construction "the embankment and basin method".

Photograph 2. Earthfill construction, June 2, 1912

The concept of filter compatibility was not directly considered by Ulrich due to lack of knowledge at the time. A transition filter zone, which would be specified in modern dam engineering, was not installed to prevent seepage channels and piping through the embankment.

Only one specific problem has ever been documented to occur with the embankment. Ulrich discusses (Ulrich, 1914) an abrupt settlement feature that appeared somewhere on the upstream face in 1914, the third season of operations. This could have been caused by embankment piping or settlement of puddled trench fill.

In summary, the historical data point to a reasonably well-built earthfill and rockfill dam given its era of design and construction. This was confirmed by the geotechnical investigations, for this seepage reduction project, that found a well-graded clayey earthfill embankment with an average of 35 percent fines, liquid limit of 38, plasticity index of 13 and blow count values of 20. The Atterberg limits testing plots directly on the "A"-Line indicating low to moderate plasticity, classifying the average soil in between a lean clay (CL) and silt (ML) according to the Unified Soil Classification System (USCS). The large phreatic head loss across the earthfill embankment zone, as shown in FIG. 2**,** shows the effectiveness of a well-built dam.

The dam was raised on two occasions, 1979 and 1983, both times to increase freeboard. The raises are also shown on Fig. 2. The 1983 raise included flattening the downstream rockfill slope to 2:1 (horizontal to vertical) and raising the crest to gage height 34 m (111 ft). Toe drains were installed beneath the rockfill material placed on the downstream slope as part of the raise.

Abutment Seepage History

Upon the first filling of the reservoir in 1912, seepage issues were immediately apparent through both the left and right abutments. Seepage exiting the left abutment rock slide deposits is shown in the 1913 photograph, Photograph 3. Seepage in the right abutment bedrock was documented by Atwood (1918) and is shown in the Photograph 4.

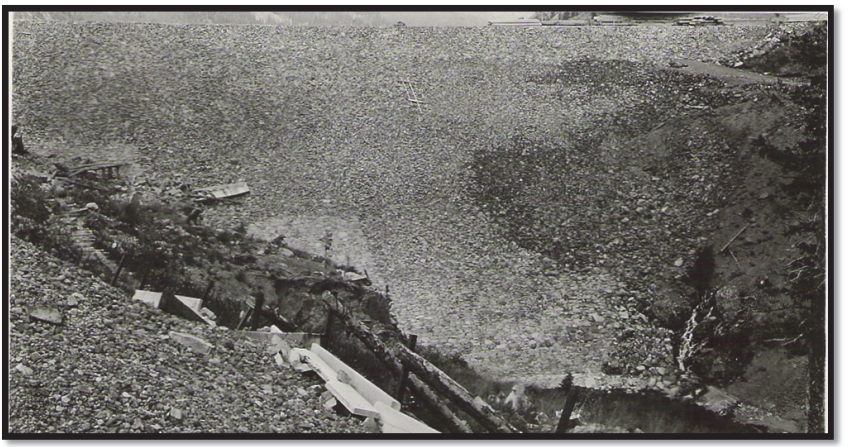

Photograph 3. 1913 seepage exiting left abutment rock slide deposits (right side of photo)

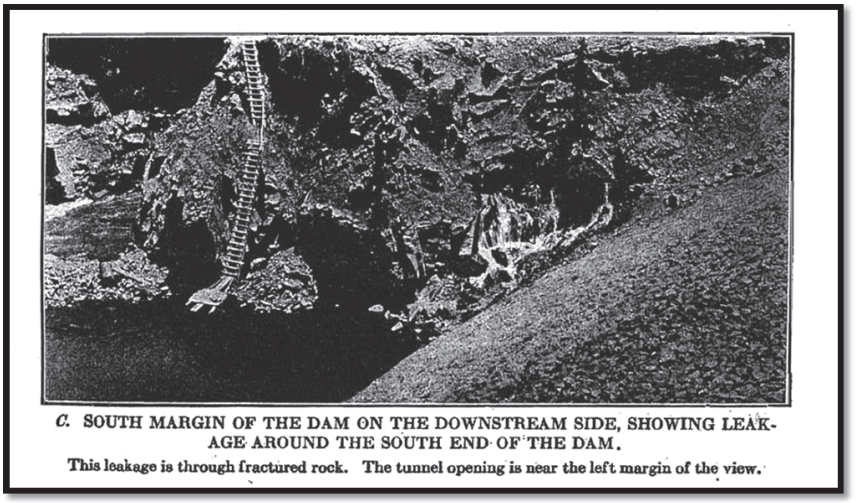

C. SOUTH MARGIN OF THE DAM ON THE DOWNSTREAM SIDE, SHOWING LEAKAGE AROUND THE SOUTH END OF THE DAM.
This leakage is through fractured rock. The tunnel opening is near the left margin of the view.

Photograph 4. 1918 seepage exiting right abutment tuff bedrock

Thomas Grieve of the Colorado State Engineer's Office (Grieve, 1932) in his report to M.C. Hinderlider, State Engineer, discusses seepage he observed while up at the dam and reservoir in June and July of 1932. With the reservoir full, he observed "*10 major leaks around the dam. Seven of those appear on the north side of the river and three on the south side… one on the north side which appears to equal in volume all of the rest on that side… These leaks ran clear at all times*."

The biggest mitigation project for seepage was the 1993 repairs overseen by Harza. Horizontal drains and a rockfill buttress were constructed on the downstream left abutment. Excellent monitoring of seepage flows and piezometer levels have been recorded by the dam caretaker since 1993. The monitoring performed by the dam caretaker consists of water levers measurements for 8 standpipe piezometers and water flow measurements of the toe drains, horizontal drain and estimated seepage from the toe of the dam. Monitored seepage rates from 1993 to 2012 through the reservoir are shown in Fig. 4. When the reservoir is full, seepage flows from the horizontal drains exceed 95 L/sec (1,500 gal/min) and an additional 63 L/sec (1,000 gal/min) seeps from the toe of the dam and toe drains for a total of 158 L/sec (2,500 gal/min) total measured flow from all sources.

The purpose of the this project was to reduce the abutment and dam foundation seepage by constructing a clay slope liner and clay blanket on the upstream left abutment and a double-row grout curtain in the dam foundation extending to the right abutment (beneath the embankment). The right abutment was also covered with a clay blanket layer of soil after the grout program was completed as shown on Fig. 2.

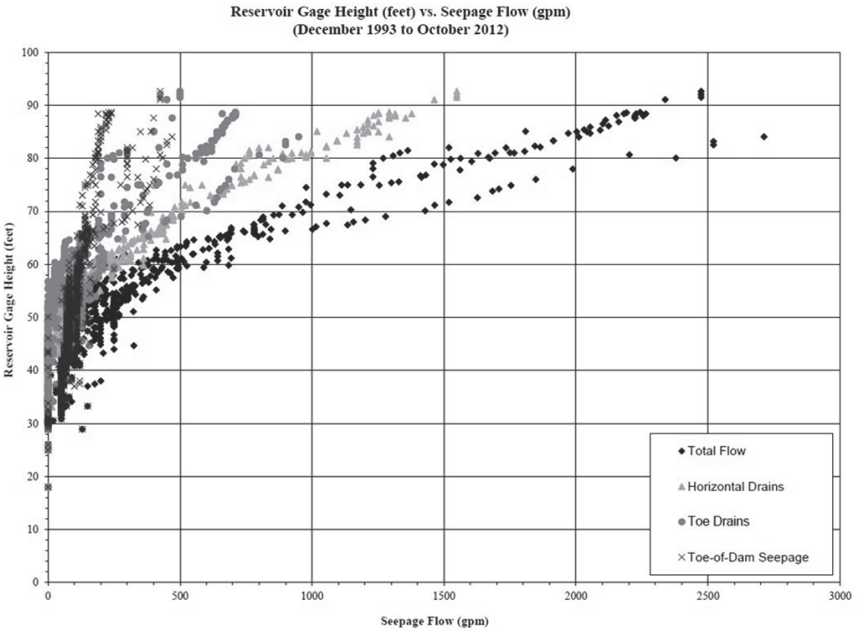

FIG.4. Reservoir Gage Height Compared to Seepage Source Flows

DAM SITE GEOLOGY

Geologic History

Rio Grande Reservoir is located in the San Juan volcanic field within the southern Rocky Mountains physiographic province of Colorado. The general bedrock geology in the region consists of multiple layers of volcanic rocks that erupted from nearby calderas during the Tertiary Period approximately 22 to 28 million years ago (Kirkham, 2007). Most of the volcanic rocks at the reservoir site are silicic ash-flow tuffs. Following sudden and voluminous calderic eruptions, expansive voids would form beneath the surface of the caldera creating instability, typically causing the caldera to collapse. Collapsed calderas form highly irregular topographic surfaces within the surrounding volcanic region. Between eruptions, the paleo-topography was subjected to erosion, enhancing the irregularity of the topography onto which subsequent volcanic rocks were deposited. As a result, the geometry of the various volcanic deposits is also very irregular, often exhibiting significant changes in thickness within short distances.

The dominant geologic processes in the San Juan mountains transitioned from volcanic processes to geomorphic processes with glaciation beginning about 2 million years ago and volcanic activity ending approximately 1 million years ago. During periods of glacial advance, glaciers scoured unconsolidated deposits and weak

weathered bedrock forming the valleys and incorporating the debris into the ice, or pushing it aside and depositing lateral moraines. During interglacial periods, receding glaciers would also deposit the debris as end moraines or till, leaving U-shaped valleys with broad floors and steep walls. This geometry is prone to slope failures as fractures in the rock open up due to stress relief as the glacial ice retreats, fill with water, and become subject to freeze-thaw cycles. Today, the region is in an interglacial period, where mass-movement geomorphic processes superimposed on the glacial valleys dominate the landscape.

Rio Grande Reservoir currently occupies one of these glacial valleys that has been subjected to several glacial episodes and has experienced numerous landslides along the steep valley walls, especially since the last glacial retreat about 10,000 years ago.

Site Geology

There are three primary geologic units in and around Rio Grande Dam that affected the evaluation and design process for this project. They are:

1. Tfc - Fish Canyon Tuff Bedrock
2. Qrs - Rock Slide Deposits
3. Qa - Alluvium

A geologic profile along the centerline of the dam FIG. 5, shows the differing geologic units across the abutment more specifically the left abutment rock slide deposit and right abutment bedrock, the Fish Canyon Tuff.

Right Abutment and Foundation Bedrock

The Tertiary-aged Fish Canyon Tuff makes up the right abutment and dam foundation underneath the unconsolidated deposits. The near surface bedrock crops out on the right abutment above the spillway and then gently slopes towards the valley before forming a cliff about 15 m (50 ft) high downstream of the outlet tunnel portal. The tuff deposits formed from a very large volcanic eruption about 27.6 million years ago during the Oligocene Epoch from the La Garita Caldera (Kirkham, 2007).

The rock is a medium to coarse-grained crystal-rich ash-flow tuff that is fairly massive to depth, but locally fractured, jointed, and weathered, especially near the surface and along the steeper valley slopes. The fractures and joints are mainly the result of stress relief following the last glacial retreat. The non-welded to densely-welded tuff is classified as low to moderate strength rock with an average unconfined compressive strength of about 41,400 kPa (6,000 lb/in^2) and a density of about 2,100 kg/m^3 (130 lb/ft^3).

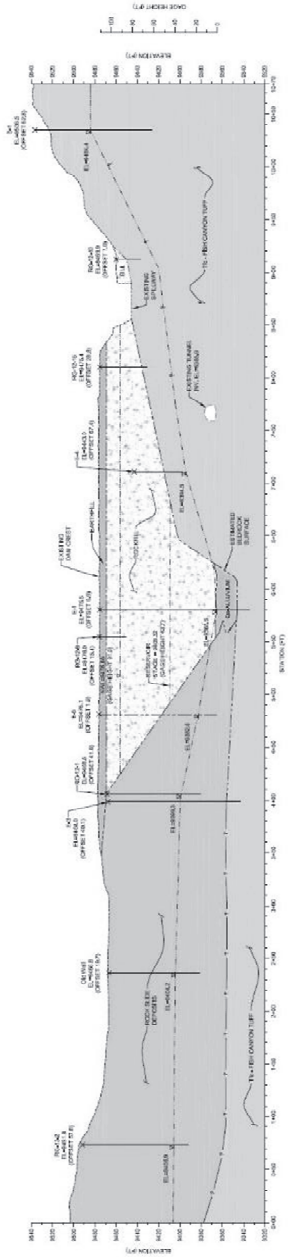

FIG. 5. Geologic Profile of the Dam (looking downstream)

Left Abutment Rock Slide Deposits

The left abutment is made up of Pleistocene-aged rock slide deposits (Qrs) approximately 46 m (150 ft) thick. The rock slide deposit is a heterogeneous deposit of boulders and tabular rock rafts up to 18 m (60 ft) long in a matrix of clayey, gravelly sand. The rock slide deposits were derived from the Huerto Formation (Thu) and the Crystal Lake Tuff (Tcl), which forms the prominent cliffs north of the dam and reservoir site, shown in photograph 6. The Huerto Formation consists primarily of aphanitic andesite and dacite overlying a volcaniclastic sedimentary deposit reminiscent of lahars. The Crystal Lake Tuff is a non-welded to densely-welded crystal-poor rhyolitic ash-flow tuff that erupted from the Silverton caldera approximately 27.5 million years ago (Kirkham, 2007).

The rock slide likely occurred as a rapid failure of an over-steepened north valley wall after the last glacier receded up the valley. The rock rafts in the deposit are relatively intact bus-sized pieces of rock that "rafted" or surfed on the top of the rock slide during slide movement. The deposit probably created a natural dam across the valley, forming an upstream lake after the landslide blocked the river. The broad and flat natural valley upstream of the rock slide shown in Photograph 1**,** typical of alpine lake deposits, supports this hypothesis. The bedrock underlying the rock slide deposit deposits consists of the Fish Canyon Tuff.

The clayey and gravelly sand soils within the rock slide deposits are formed from severely to completely weathered deposits of Huerto Formation and Crystal Lake Tuff rock. Local voids up to 20.3 cm (8 in) wide, 1.2 m (4 ft) long, and 2.4 m (8 ft) deep occur within the deposits. These voids could have formed for two reasons: 1) cracking and settling of rock rafts during deposition, and 2) melting of ice blocks within the deposits.

SLOPE LINER AND CLAY BLANKET DESIGN

This rehabilitation project consisted of the construction of a clay slope liner overlying the upstream left abutment rock slide deposit. The bottom of the slope liner cutoff key was excavated at elevation 2866 m (9404 ft) (Gage Height 12 m (40 ft)). Total measured seepage out of the reservoir below this elevation was determined to be minor compared to the seepage at higher gage heights. The slope liner consisted of two zones of compacted earthfill on the upstream face of the existing left abutment. Zone 1 was constructed as a 6 m (20 ft.) wide zone of clay soils that created an 2.4 mr (8 ft) thick core sandwiched between layers of Zone 2. Zone 1 was 3-inch-minus material with a percent passing the No. 200 sieve ranging between 15 and 35 percent, placed in maximum 20.3 cm (8 in) lifts. Zone 2 was 15 cm (6 in) minus material with a percent passing the No. 200 sieve between 5 and 30 percent, placed in maximum 30.5 cm (12 in) lifts,. A typical cross-section of the slope liner is shown on Fig. 6**.** Confirmation Atterberg Limit testing of the Zone 1 material was performed throughout construction of the slope liner. Zone 1 material had an average liquid limit of 48 and plasticity index of 21, classifying the materials as a CL according the USCS.

Photograph 5. Left Abutment Rock Slide Deposits
(Note tuff cliffs that mark slide scarp)

All materials for the construction of the upstream left abutment slope liner were made on site by screening borrow from the rock slide deposit. As the slope liner zones were constructed from the rock slide deposits with various coarse fractions removed, filter compatibility was naturally achieved. The existing left abutment was prepared by excavation a slope between 2.5:1 and 2:1 on the existing face. Large rafts and boulders were removed by mechanical methods and or dynamite blasting.

SEEPAGE ANALYSIS

Seepage analysis were performed during the initial evaluation and design of the Rio Grande Dam Seepage Reduction Project. Utilizing the seepage data collected by the Owner over the last 20 years, seepage analysis models were developed for the existing dam, using GeoStudio Seep /W computer software. The models were calibrated to produce results similar to the measured seepage. The seepage data showed that the seepage increased significantly when the reservoir stage is above gage height 15 m (50 ft). This is shown on Fig. 3**,** which is a plot of seepage measured (by source) versus reservoir elevation prior to the seepage reduction project.

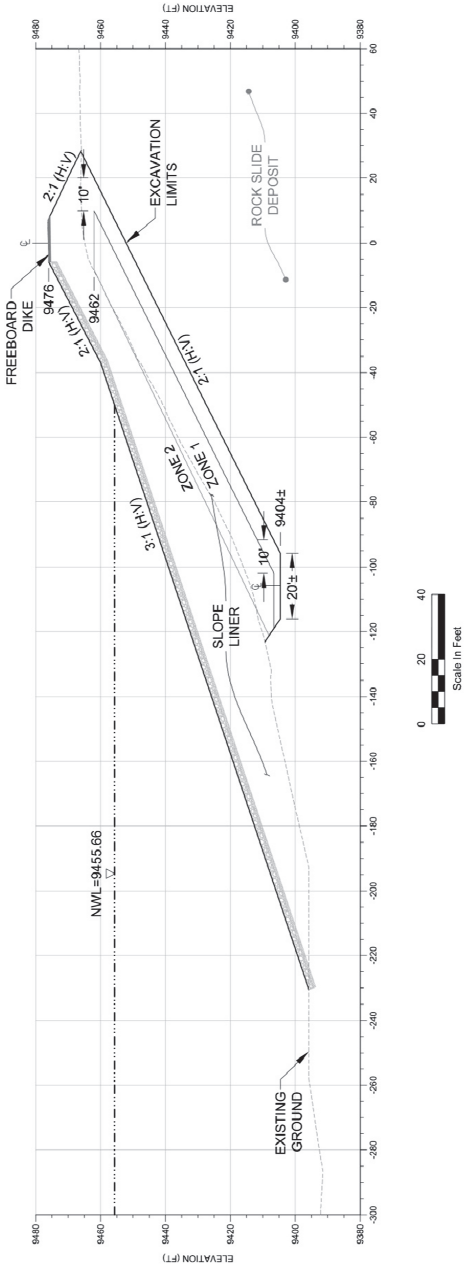

FIG. 6. Typical Slope Liner Cross Section

A cross-section of the left abutment with measured water levels and horizontal drain flows is presented on Fig. 7. Horizontal drain flows are only a trace at reservoir gage height 13 m (44 ft), but are over 95 L/sec (1,500 gal/min) above gage height 27.7 m (91 ft).

The permeability of the rock slide deposit in the field was determined to be far from homogeneous based on analysis of seepage flows and observations of excavations into the slide mass. High permeability zones occur in the rock slide deposit as clusters of large boulders or "rock rafts" with local voids.

Since seepage flows increase greatly above gage height 15 m (50 ft), the modeled rock slide deposit has very high permeability zones (1 cm/sec and 2 x 10^{-1} cm/sec) above gage height 15 m (50 ft) and lower permeability (2 x 10^{-3} cm/sec) elsewhere. This is shown on the calibrated model run shown on Fig. 8.

The effect of placement of a clay slope liner over highly permeable rock slide deposit zones was evaluated utilizing 8 different model runs. A summary of the results of the seepage analyses is shown in Table 1.

Model runs 1, 2, 5 and 6 shows the calibration of the seepage model with the measured seepage rates using a uniform landslide mass and a more permeable zone in the rock slide deposit. Model runs 3, 4, 7 and 8 show the effects on the model of adding a zoned earthfill slope liner over the rock slide deposit. While the modeling shows a significant reduction in seepage with the construction of a slope liner, it appears to overestimate the order of magnitude of seepage reduction. Case in point, model run 7 shows that seepage flows would be reduced from over 63 L/sec (1,000 gal/min) to only 0.7 L/sec (11 gal/min) (two orders of magnitude reduction) under full reservoir. Modeling of the slope, utilizing moderate permeabilities and a homogenous slide mass yielded seepage reductions of about 50 percent.

RIGHT ABUTMENT AND DAM FOUNDATION SEEPAGE REDUCTION – GROUT CURTAIN

A bedrock grout curtain was designed by Deere & Ault and constructed by Hayword Baker, Inc (HBI) to reduce seepage in the right abutment and the bedrock foundation of the dam. It was determined that the foundation bedrock was groutable based on geotechnical exploratory borings and geologic mapping of the rock in the local area. The design was also based on the joint orientations of the rock, the location of the outlet tunnel, and the existing cutoff trenches in the earthfill embankment.

Historically, when the reservoir is at high stages, a significant amount of seepage has been observed coming out of the bedrock profusely near the right abutment spillway. The majority of the seepage is located in the zone where the rock mass is most jointed above the outlet tunnel. The grout curtain was constructed in the Fish Canyon Tuff, a low to moderate strength, brittle, locally-weathered, and jointed crystal-rich ash-flow tuff. There are three primary steep joint sets; two near vertical sets are sub-perpendicular to the valley with the third set running parallel to the valley likely due to stress relief. There is shallow dipping fourth joint set associated with flow bedding.

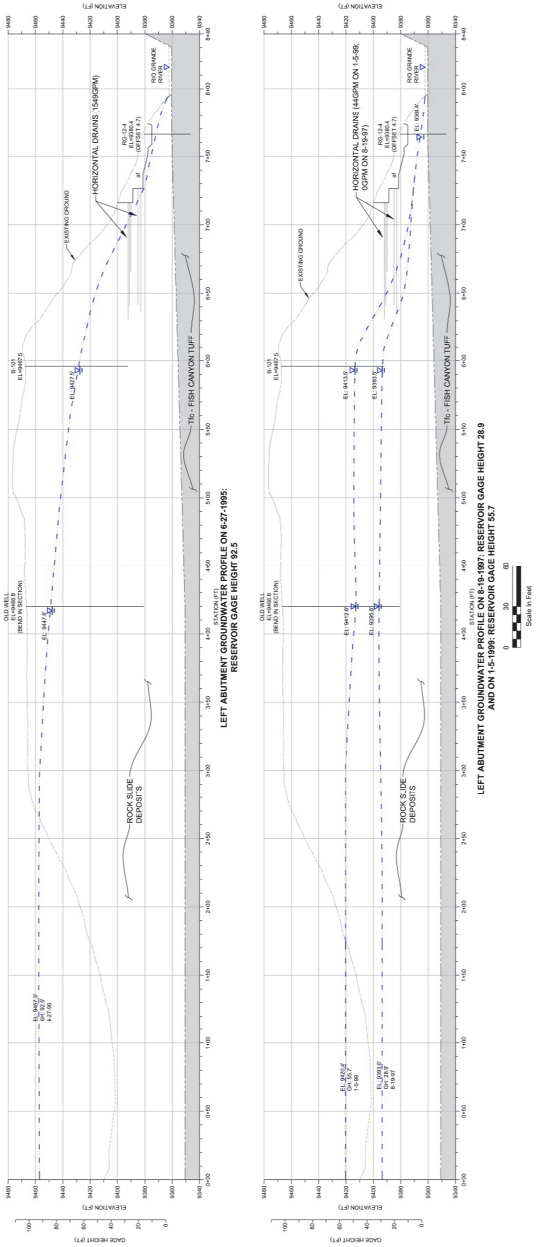

FIG. 7. Cross-Section of the Left Abutment with Water Levels

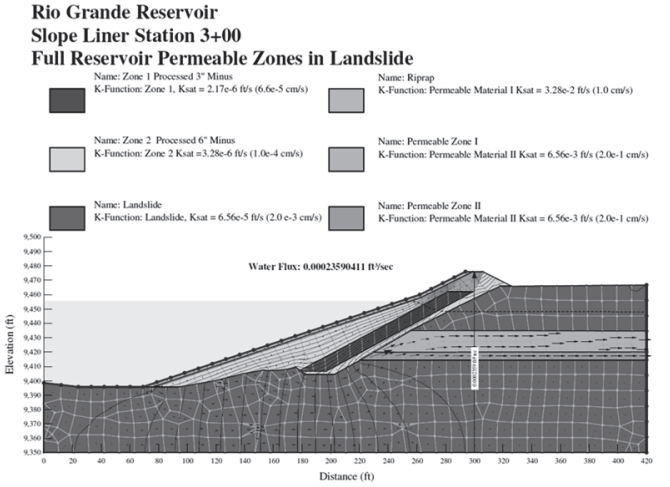

FIG. 8. Calibrated Seepage Model with Left Abutment Slope Liner

Table 1. Seepage Analysis

Rio Grande Dam and Reservoir Seepage Analysis

Run	Model	Flux ($feet^3/sec/ft$)	Flux in 100 ft Section ($feet^3/sec$)	Flux in 100 ft Section (gal/min)
1	Existing Full Reservoir Uniform Landslide	2.85E-02	2.85	1279
2	Existing Lower Reservoir Uniform Landslide	1.41E-02	1.41	633
3	Full Reservoir Uniform Landslide with Slope Liner	9.37E-03	0.94	421
4	Lower Reservoir Uniform Landslide with Slope Liner	7.38E-03	0.74	331
5	Existing Full Reservoir Permeable Zones in Landslide	2.27E-02	2.27	1021
6	Existing Lower Reservoir Permeable Zones in Landslide	1.23E-03	0.12	55
7	Full Reservoir Permeable Zones in Landslide with Slope Liner	2.36E-04	0.02	11
8	Lower Reservoir Permeable Zones in Landslide with Slope Liner	1.34E-04	0.01	6

The initial design consisted of a primary double-row grout curtain (upstream and downstream) constructed through the dam embankment and into the foundation of the dam right abutment bedrock. The two rows of grout holes were drilled so that the upstream (U-Line) and downstream (D-Line) rows were spaced 3 m (10 ft) apart and the holes in each row were staggered so that they were 6 m (20 ft) on center. When drilled, the forty-nine primary grout holes were drilled so that they were battered at a 20 degree angle (upstream to downstream, respectively). On the right abutment the grout holes were drilled in a fan that required angles ranging from 20 degrees to a maximum of 80 degrees from vertical. A plan view of the final layout of all the holes grouted for this seepage reduction project is shown on Fig. 9. The location of the grout curtain upstream of the dam crest is shown in Fig. 2.

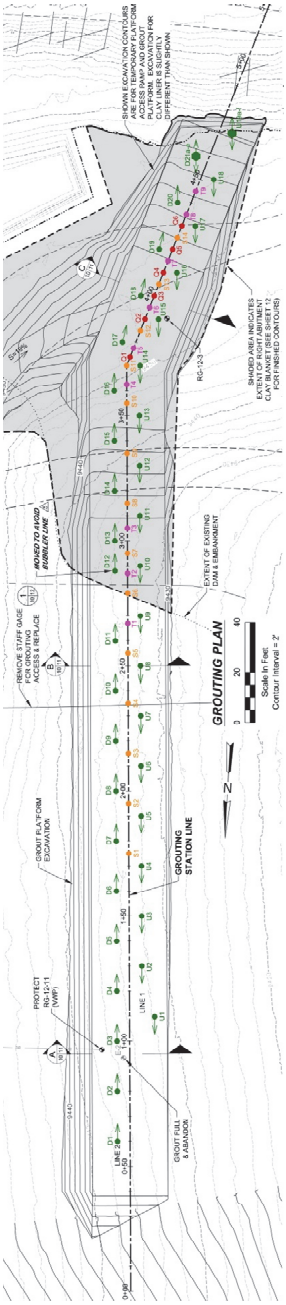

FIG. 9. Plan View of Grout Hole Layout

The grout curtain was constructed in an upstage manner due to the geology to the bedrock. Upstage grouting consists of the drilling of a hole to the full design depth and then grouting from the bottom up in predetermined stage lengths. Computer monitoring of the grouting operation was employed during the project to allow the engineer and contractor to conduct real-time monitoring of the grouting operations. The grouting specification dictated that the GIN (Grout Intensity Number) approach would be utilized for the "completion" of the grouting operations. (Lombardi and Deere, 1993) The GIN method uses one stable grout mix the entire grouting program. GIN requires a steady pumping rate where pressures gradually increase with time. By monitoring the volume injected and pressure in real time, the termination of the grouting is determined when pressure multiplied by volume reaches the selected GIN curve value. The goal of the grout curtain was to reduce the seepage through the massive volcanic bedrock that was determined to be a significant source of seepage through the dam.

The grouting program consisted of the following major components:

1. Rotary duplex drill through the dam embankment, socketed 1.5 m (5 ft) into the bedrock, and install PVC casing, a minimum of 1.5 m (5 ft) into bedrock, that provided access to rock drilling and grouting of the foundation. The PVC was grouted in place to protect the embankment from hydraulic fractures and washout.
2. Treatment of the embankment-rock interface to be completed.
3. Percussion rock drill the foundation bedrock.
4. Up-stage grout each hole utilizing the GIN Methodology
5. Monitor real-time computer-aided grouting systems to evaluate the response of the bedrock to the grouting.

The first step was the drilling and installation of a temporary casing through the embankment's upstream earthfill zone. To complete the casing installation, rotary-duplex drilling was utilized to drill down through the embankment and embed the casing a minimum of one foot into the foundation rock. Rotary-duplex drilling is a technique for advancing an outer steel casing ahead of an inner drill string that cuts inside the casing to remove the cuttings. The drilling specifications required the utilization of water during all drilling operations, as air-flush drilling was strictly prohibited. Care and caution were required to be taken during all drilling operation through the dam embankment. The rotary-duplex drilling method was selected for its ability to remove the cuttings with an internal water flush, which focuses the energy to the material inside the steel casing, thereby limited any impact on the dam embankment. A double-headed drill rig was utilized for the rotary-duplex drilling. The double head allowed for the rotating of the casing in one direction, and the spinning of the internal drill rod in the opposite direction. The ability to spin in opposite directions allows for the drilling of a straighter hole. Once the hole was advanced to the design depth 1.5 m (5 ft) into rock, the inner drill string was removed and a flush threaded, schedule 40 PVC casing was inserted inside the steel outer casing. The annulus space was grouted up with a bentonite-cement mix with a 1:1 water to cement-bentonite ratio by volume, while the steel casing was removed,

leaving only the grouted PVC casing in the embankment. The completion of the annulus grouting required two steps:

1. Grout the space between the steel casing and the PVC
2. Remove the casing and re-grout the annulus space to ensure complete coverage.

Following the installation of the temporary PVC casing in each hole, the drill tooling was swapped to allow for the drilling of the rock below the temporary PVC casing. The rock drilling specification required the use of only water flush for the removal of the drill cuttings. To meet the project requirements, the contractor utilized a water-actuated down-the-hole hammer for the completion of all percussion style rock drilling. The completion of the grouting was scheduled to be performed in an upstage manner, bottom to top progression, which requires the advancement of the grout hole to the full depth, bottom elevation, of the grout curtain. The drilling would be performed on each hole to the full depth with the exception of a few situations. If the hole continued to collapse at an elevation above the final design elevation, the hole would be stopped for grouting at the collapse depth, or if water loss (lack of water return) of greater than 50 percent was witnessed, the hole would be stopped for grouting at the depth where the water-loss occurred.

Rock drilling was completed with a Wassara W-80 water-actuated down-the-hole hammer with a 8.6 cm (3-3/8 in) diameter bit. The water hammer was selected over the traditional DTH (down-the-hole) technology due to the advantages provided with the water hammer technology. The water hammer offers a straighter hole and uses less energy than the traditional DTH technology and hits at approximately two times the frequency.

Following the installation of the primary hole casing, HBI began production rock drilling through the zone to be grouted. Observations of the primary holes indicated that a high number of water-loss issues were occurring within the first 5 m to 6 m (15 ft to 20 ft) of the rock strata. Many holes were being stopped shallow due to the lack of water return as the drilling progressed in the first 6 m (20 ft). The water loss was a result of a significantly fractured zone within the volcanic tuff. The construction team decided it was best to terminate the holes in the fractured zone when a high water loss was observed, and grouting the rock in more of a down-stage fashion instead. The stage lengths for grouting were limited to a maximum length of 5 m (15 ft). Once the stage was grouted to completion, the rock was then re-drilled to the full design elevation for continued grouting below the completed stage. The rock drilling was advanced ahead of grouting to maintain appropriate space requirements between operations, as required by project specifications.

Grouting was able to begin once the rock was drilled and the drill rig moved off of the hole. For this project, computer-aided grouting was required by specification, and real-time development of the GIN was expected to be generated by the contractor. HBI utilized the custom software i-GROUT to complete the real-time monitoring and instant GIN development. The contractor had not completed a grouting project utilizing real-time GIN development prior to the Rio Grande Dam site work, and had to customize the program to meet the specific requirements for the completion of the

grouting. The GIN value is a calculation that utilizes pressure and volume to determine when “closure" has been established. Due to the shallow grouting to be performed in the right abutment and in order to protect the embankment from hydro-fracturing during grouting, two separate maximum pressure criteria were established to limit the chance of heaving or damaging the embankment and/or the bedrock in the abutment. In addition to the use of the GIN value on this project, a maximum pressure was established for completing a grouting stage. The specifications were established listed below:

GIN value is achieved
Total bedrock grouting depths less than or equal to 9 m (30 ft), maximum pressure of 2.1 bar (30 lb/in^2)
Total bedrock grouting depths greater than 9 m (30 ft), maximum pressure of 21 kPa (300 lb/in^2)

The GIN number for this project was established as 478 bar*L/m (150 $lb/in^2*ft^3/ft$). The following equation was utilized for calculating the GIN (Deere Lombardi 1993):

$$GIN = p*V$$

GIN = constant specific energy
p = max grout pressure, bar (lb/in^2)
V= largest allowable grout volume injected at maximum pressure/length of stage, L/m (ft^3/ft)

To properly utilize the GIN grouting monitoring method, it is imperative that a stable, thick mix is utilized for grouting operations. The grout mix design was a basic water and cement mixture with the utilization of a water-reducing superplasticizier admixture. The grout mix design established for production grouting was a 1:1 water to cement ratio by volume, which is the approximate equivalent of a 0.7:1 water to cement ratio by weight. The cement was a Type-I/II and Glenium 3030NS by BASF was the superplasticizier selected for the grout mix. The grout mixing was completed with a high-shear colloidal mixer to allow for thorough mixing of the cement particles. The grout was pumped utilizing a steady-state (Moyno) pump to allow for the smooth development of the GIN envelope. The grouting operations were monitored in real-time using HBI’s i-GROUT computer system. i-GROUT is composed of a series of electronic pressure transducers and magnetic flowmeters that generate electronic signals that are converted to display the real-time grouting pressure and flow characteristics during grouting operations. The i-GROUT system by HBI offers flexibility for performing projects of all sizes. The grouting monitoring system utilized at this seepage reduction project was a smaller, more portable unit, which was a necessary requirement due to the location of the project site.

The revised grouting operations began in a downstage manner due to the fractured nature of rock indicated during the drilling operations. The ideal stage was set for 5 m (15 ft) with a maximum desired stage length of 9 m (30 ft). In the early stages of grouting, the stage length was determined by the ability of the drill to advance the

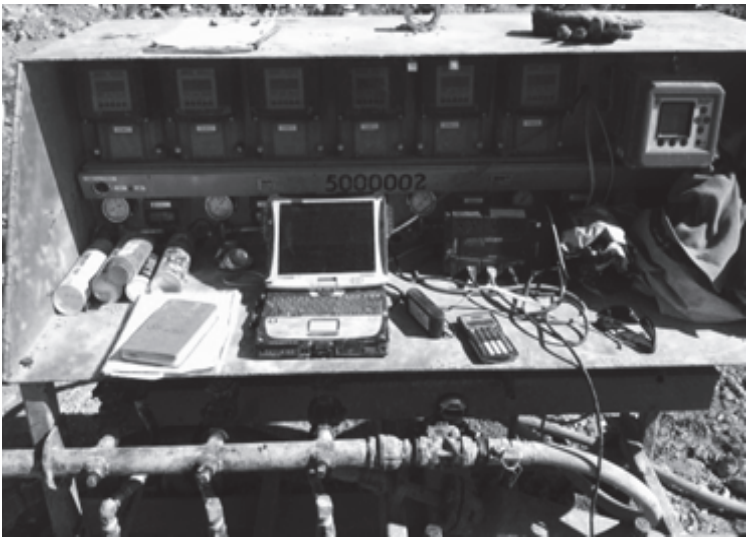

Photograph 7. Grout Field Setup

hole without losing water return at the surface. The initial stages varied in length from 1.5 m to 3 m (5 ft to 10 ft) due to the inability to advance to any greater depth in the highly-fractured rock zones. The strategy of the GIN is to achieve a low permeability grout curtain without the excessive installation of grout material. The grouting of the primary holes indicated the potential for high, or excessive, grout takes, based on the inability to generate pressure until high amounts of grout were placed. To accommodate the needs of the project and to limit the excessive installation of grout, the technique of "intermittent grouting" was employed. The intermittent grouting program for this project was set for a maximum of 0.43 m^3 (15 ft^3) of grout before terminating the stage, unless;

1. Significant back pressure is achieved
2. The flow is reduced as the pressure increases, or
3. The GIN value is reached

The treatment of the 49 primary holes required a significant intermittent grouting program. Stages were grouted until 0.43 m^3 (15 ft^3) of grout were injected, and then allowed to set for a few hours. Following the set time, the stage would be re-grouted until one of the three desired refusal criteria was achieved. In many cases, the intermittent grouting treatment would be required three and four times to achieve proper closure in the stage. A summary of the grouting stages and grout takes is shown on Fig. 10.

The grouting program was executed in accordance with all specifications and field directives, and yielded an effective result. The grouting program required the utilization of higher series grout holes (secondary, tertiary, and quaternary) to achieve

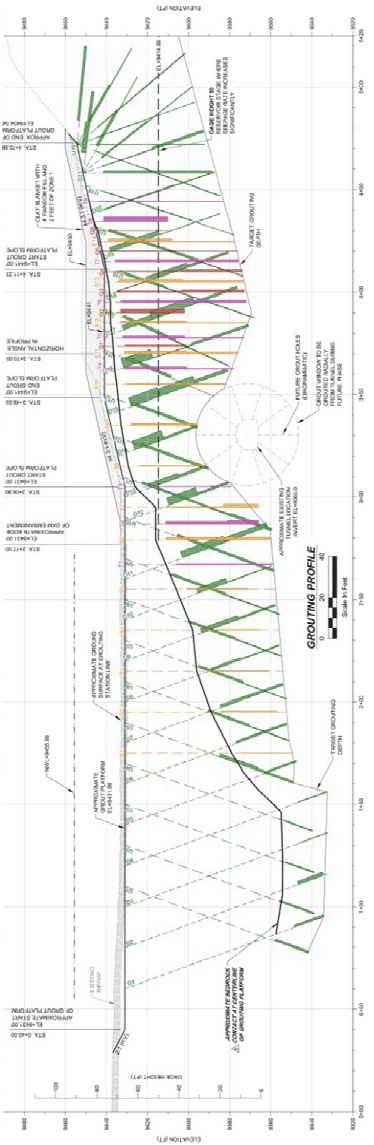

FIG. 10. Cross-Section of Grout Holes and Takes

the project goals. Hence, the final grout curtain was comprised of primary, secondary, tertiary, and quaternary sequences of grout holes. With the benefits of the real-time grouting data collection system, the higher series grout holes were able to be added with a direct and specific plan of attacking the rock zones of greatest concern. In total, approximately 518 linear m (1,700 linear ft) of primary hole drilling and 183 m (600 ft) of secondary, tertiary, and quaternary hole drilling were completed.

To evaluate the effectiveness of the grouting program, the grout takes have been evaluated based on the grout takes in cubic ft per linear foot of treated hole. The grout takes on the primary grout holes averaged 0.15 m^3/m (1.6 ft^3/ft) of hole. The secondary hole grouting averaged 0.10 m^3/m (1.02 ft^3/ft) of hole. The tertiary hole grouting was completed vertically in between the upstream and downstream lines, and observed a slight increase in the grout take per linear foot, averaging 0.11 m^3/m (1.20 ft^3/ft) of hole. However, the quaternary grout holes saw a significant reduction, 50 percent, in average grout take per linear foot compared to the primary grout holes. The quaternary grout holes averaged 0.07 m^3/m (0.80 ft^3/ft) of hole. This grout work was completed in early October 2013. Additional final grouting will be completed from within the intake tunnel and spillway area during planned future repairs. The grout holes were also completed in 100 percent upstage fashion, indicating a significant reduction of permeability in the rock from the treatment of the primary grout holes. Fig. 11 demonstrates the grout takes for each grout hole series.

In summary, the drilling methods proved to be appropriately selected for the completion of both phases of the drilling program (embankment and rock). Rotary-duplex drilling was proven to be appropriate for the installation of the temporary PVC casing while protecting the embankment. The utilization of the down-the-hole water hammer proved to be a very efficient and effective method for drilling the volcanic tuff rock beneath the base of the dam embankment. The grouting program was viewed as an overall success and was completed under budget. The grouting specifications were a significant driving force when completing the grout curtain, but sound field decisions regarding the use of intermittent grouting criteria, the locations and depths of higher series grout holes, and the varying of the grout mix to utilize super-plasticizier when needed all proved to be critical parts of the successful grouting program. HBI's computer-monitored grouting system, i-GROUT, allowed for sound and quick decisions on the grouting program and criteria, which always proves to be a significant factor on dam grouting programs.

INITIAL ANALYSIS OF SEEPAGE REDUCTION DURING FIRST RE-FILLING

Based on the seepage data collected during re-filling of Rio Grande Reservoir in the first "year" of operation after the completion of the this seepage reduction project (the winter of 2013-2014), it appears that the overall seepage through the left and right abutments and the dam foundation has been reduced by approximately 60 percent from previous seepage measurements recorded at similar reservoir gage height readings. A comparison of historical seepage flows to post-construction seepage results is shown on Fig. 12. Five times since June of 1999, the reservoir has held

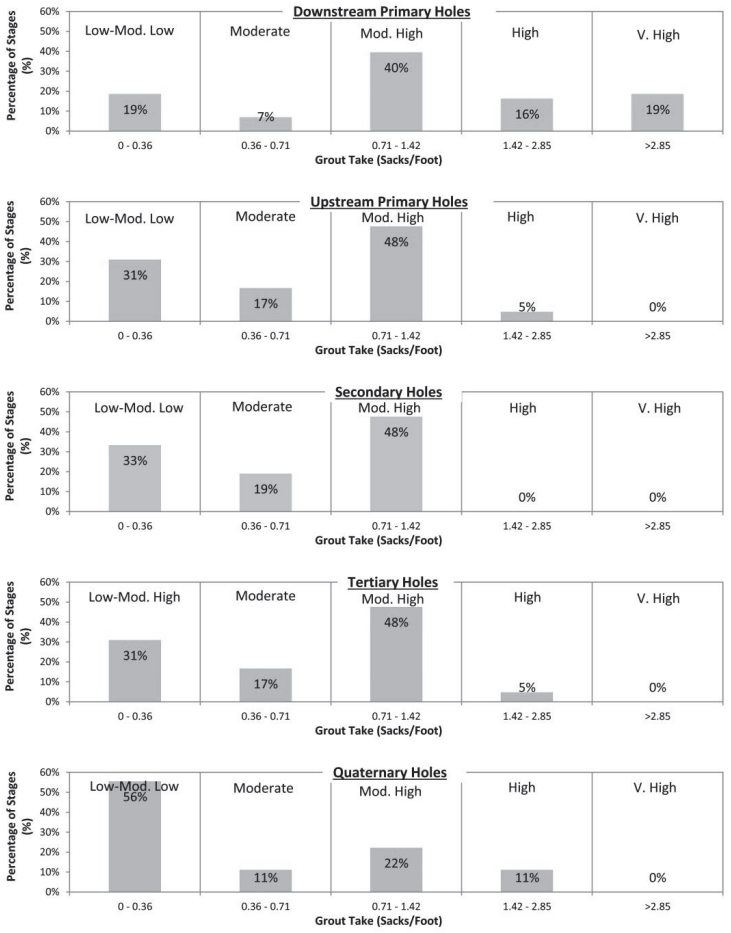

FIG. 11. Grout Take by Grout Hole Series

water at or near gage height 21 m (70 ft). During those times, the average seepage out of the reservoir was recorded to total between 51 l/s and 63 l/s (806 gal/min and 995 gal/min). The seepage out of the reservoir was recorded to total 24 l/s (385 gal/min) at gage height 21 m (70 ft) this first “year” (the winter of 2013-2014).

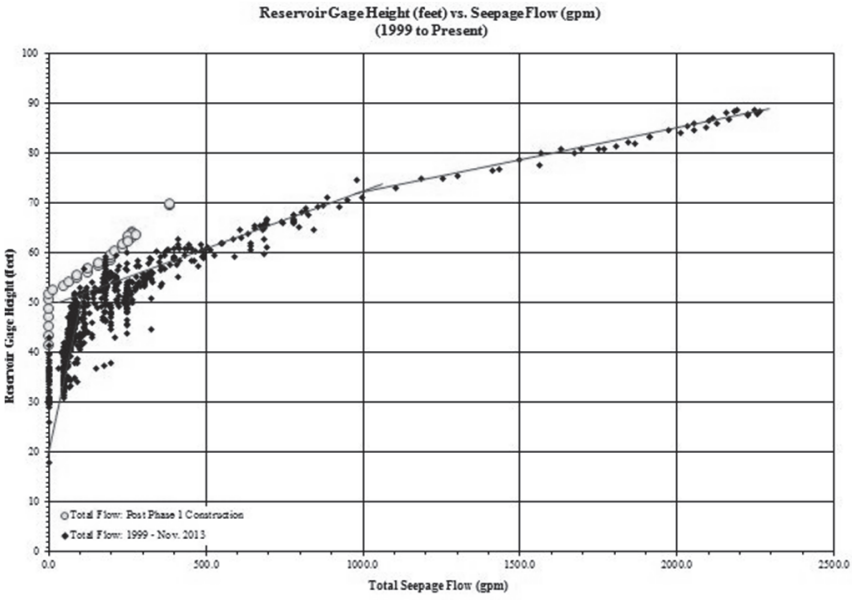

FIG. 12. Reservoir Gage Height compared to Total Seepage Post-Rehabilitation

CONCLUSIONS

Based on the limited seepage data available at this time (July 2014), it appears that the seepage reduction project as designed and constructed has successfully reduced the seepage losses out of Rio Grande Reservoir by approximately 60 percent.

REFERENCES

Atwood, W.W., 1918, "*Relation of Landslides and Glacial Deposits to Reservoir Sites in the San Juan Mountains, Colorado*," Department of the Interior, United States Geological Survey, Bulletin 685.

Colorado State Engineer's Office, 2007, *Rules and Regulations for Dam Safety and Dam Construction*.

Deere & Ault Consultants, November 2013, "*Rio Grande Dam and Reservoir Phase I Rehabilitation Final Construction Report.*"

Deere & Ault Consultants, April 2013, "*Rio Grande Dam and Reservoir Geotechnical Design Report and Phase I Rehabilitation Design*."

Deere & Ault Consultants, January 2008, "*Draft Preliminary Design Report: Rio Grande Reservoir Rehabilitation and Enlargement*."

Grieve, T., 1932, *Report on Farmers Union Reservoir, Water District #20*: Report submitted by Thomas Grieve to the State Engineer, dated July 17, 1932, San Luis Valley Irrigation District Archives, Center, Colorado.

Haywood Baker Incorporated, 2012, Promotional Materials, I-Grout Computer Aided Data Acquisition and Monitoring System.

Houlsby, A.C., 1990, "*Construction and Design of Cement Grouting*," John Wiley and Sons.

Kirkham, R.M., November 14, 2007, "*Geologic Investigation of Landslides, Rio Grande Reservoir, Hinsdale County, Colorado*." Appendix A in Deere & Ault Consultants, January 2008, "*Draft Preliminary Design Report: Rio Grande Reservoir Rehabilitation and Enlargement*."

Lombardi, G., and Deere, D.U., 1993, "*Grouting Design and Control Using the GIN Principle*," International Water Power and Dam Construction, June 1993

Ulrich, J.C., 1914, *Letter Re: Dam Settlement*: Letter to Mr. Frank G. Sylvester dated August 14, 1914, San Luis Valley Irrigation District Archives, Center, Colorado.

Ulrich, J.C., 1910a, *Rio Grande Dam & Reservoir Design Plans*: Original Design submitted to the Colorado State Engineer, Approved May 31, 1910: San Luis Valley Irrigation District Archives, Center, Colorado.

Ulrich, J.C., 1910b, *Specifications for Tunnel Construction*: San Luis Valley Irrigation District Archives, Center, Colorado.

Ulrich, J.C., 1910c, *Specifications for Construction of Dam for the Rio Grande Reservoir*: San Luis Valley Irrigation District Archives, Center, Colorado.

Ulrich, J.C., 1905, *Report Upon The Farmers Union Irrigation Company's Reservoir Dam*: San Luis Valley Irrigation District Archives, Center, Colorado.

U.S. Bureau of Reclamation (USBR), 1987, *Design of Small Dams*: Third Edition, U.S. Government Printing Office, Washington D.C.

Weaver, K.D., and Bruce, D.A., 2007, "*Dam Foundation Grouting*," ASCE Press.

City of Dallas Floodway System (DFS) Case Study: 100-Year Levee Remediation

Brad Barth, M. ASCE, P.E.[1], Stephen W. Ringen, A.M. ASCE, E.I.T.[2], and Jeffrey H. Sallas, Aff.M.ASCE[3]

[1]Sr. Geotechnical Engineer, HNTB Corporation 10000 Perkins Rowe Suite 640 Baton Rouge, LA 70810; brbarth@hntb.com
[2]Project Engineer, Magnus Pacific Corporation, 100 W. Oak Street Suite 301 Denton, TX 76201; sringen@magnuspacific.com
[3]Project Director, Magnus Pacific Corporation, 100 W. Oak Street Suite 301 Denton, TX 76201; jsallas@magnuspacific.com

ABSTRACT: The Dallas Floodway System (DFS) consists of 37 km of earthen levees, pump stations, gravity sluice gates, and pressure storm sewers along the Trinity River in Dallas, Texas. Construction of the original system was completed in the 1930s after the region experienced catastrophic flooding from the Trinity River in 1908. The DFS was strengthened in the 1950s by U.S. Army Corps of Engineers (USACE). In 2009, USACE through the Levee Safety Program rated the DFS as "Unacceptable" during Periodic Inspection No. 9. As a result of this inspection USACE rescinded their letter of support for accreditation from Federal Emergency Management Agency (FEMA). The City of Dallas worked with HNTB Corporation (HNTB) and USACE to assess the levees, design improvements to the levees, including over 5,700 m of seepage cutoff walls. In March of 2012, the City of Dallas awarded Magnus Pacific Corporation (Magnus Pacific) the 100-year Levee Remediation – Cutoff Wall Improvement project, a critical step toward regaining FEMA 100-year accreditation. Magnus Pacific was the prime contractor for the project, supported by specialty subcontractors Layne Geo and SMB Enterprises, Incorporated. This paper presents a case study of the levee assessment, design, and construction of over 5,700 m of seepage cutoff wall.

INTRODUCTION

The DFS is located within Dallas, Texas and consists of 37 km of earthen levees, pump stations, gravity sluice gates, and pressure storm sewers, see Fig. 1. The East Levee protects the reclaimed industrial corridor east of the Trinity River, while the West Levee protects West Dallas which is primarily residential.

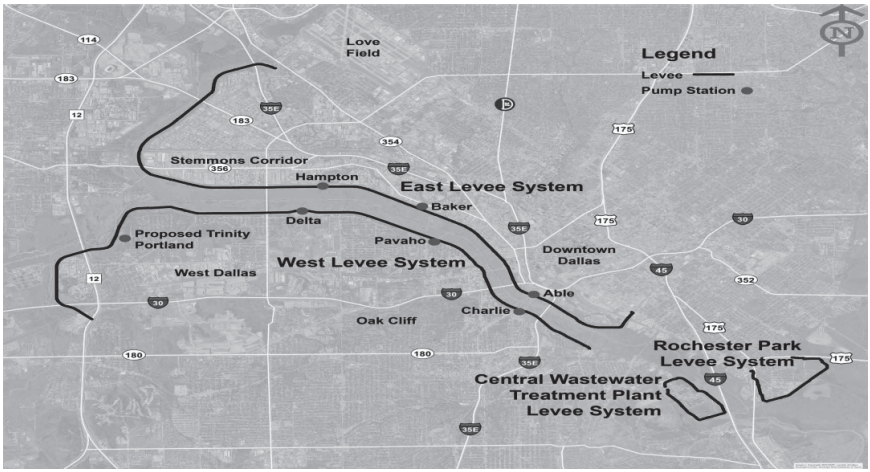

FIG. 1. Dallas Floodway System.

Construction of the original system began in July 1928 after the region experienced catastrophic flooding in 1908 from the Trinity River. The river's course was shifted approximately 0.8 km to the southwest and 37 km of flood protection levees were built. The natural channel of the Trinity River was maintained for storm water storage and drainage within the protected area of Dallas. The construction was completed in 1932 and has since controlled the Trinity River's alignment. Currently, the West and Elm Forks converge west of Dallas to form the Trinity River (re-aligned) flowing through the floodway, with the East Fork converging with the river to the east. In the 1950s USACE strengthened the DFS by flattening the levee slopes to reduce excessive levee slides and maintenance issues.

The original DFS levees were reportedly constructed with 2.5:1 (H:V) side slopes, which were later deemed too steep because of instability issues, and were flattened in the 1950s re-strengthening to 3:1 to 4:1 side slopes. The system has experienced shallow slough slides since the completion of the 1950s re-strengthening. In the roughly fifty years since the re-strengthening, 305 slough-type slides of the levee embankments have occurred. These shallow slides have been addressed through operation and maintenance of the levee system.

The highest recorded flood since the 1950s re-strengthening of the East and West Levees by USACE was in 1990, which was approximately 0.6 m below the current 100-year water surface elevation and approximately 4.3 m below the Standard Project Flood (SPF). Approximately 4.5 m of freeboard exists above the 100-year water surface elevation.

In 2009, U.S. Army Corps of Engineers (USACE) through the Levee Safety Program rated the DFS as "Unacceptable" during Periodic Inspection No. 9. As a result of this inspection USACE rescinded their letter of support for accreditation from Federal Emergency Management Agency (FEMA). In addition to maintenance related deficiencies, USACE also noted concern for slope stability, underseepage, and

excessive vegetation. FEMA began the de-accreditation process for the DFS. The City of Dallas worked with HNTB Corporation (HNTB) and USACE to assess the levees, design improvements to the levees including over 5,700 m of seepage cutoff walls. In March of 2012, the City of Dallas awarded Magnus Pacific Corporation (Magnus Pacific) the 100-Year Levee Remediation – Cutoff Wall Improvement project, a critical step toward regaining FEMA 100-year accreditation. Magnus Pacific was the prime contractor for the project, supported by specialty subcontractors Layne Geo and SMB Enterprises, Incorporated. The scope of work included the construction of 4,800 m of cutoff walls along the East Levee, 800 m of cutoff wall along the West Levee, rehabilitation of three outfall structures, and construction of a 1,600 m long maintenance path.

LEVEE ASSESSMENT

Geotechnical data available for the system included more than 2,200 borings, 500 Cone Penetrometer Tests (CPTs), and over 30 piezometers, which were obtained from historic and nearby on-going projects, and a subsurface exploration program implemented by the City of Dallas for consideration in evaluation of the system. The subsurface exploration program implemented by the City of Dallas specifically to address the FEMA accreditation included over 400 CPTs, 500 soil borings, geoprobes®, test trenches, associated laboratory testing, and 50 piezometers. Borings were drilled and sampled along the levee crown, toes and mid-slopes, as well as within the floodway. Boring and laboratory test data was used to support evaluation of geomorphology, subsurface stratigraphy, piezometric levels, and other geotechnical engineering analyses.

The levee embankments are generally comprised of lean clay and fat clay and founded on recent alluvial soils. The alluvial floodplain soils generally consisted of alluvial clay deposits. These clay deposits, which are predominately comprised of fat clays, serve as the river side and protected side clay blankets and as the levee foundation material. These alluvial clays vary in thickness from 1.5 m to 3.0 m thick to greater than 7.6 m to 10.7 m thick. The alluvial clay blanket thickness is directly related to the geomorphology specifically related to the downward cutting which formed the bedrock terracing of the historical Trinity River valley. The upper clay blankets are underlain by sandier deposits (becoming coarser with depth), followed by a typically thin layer of basal sand and gravel. The basal sands and gravels mark the bedrock contact with the Eagle Ford Shale or the Austin Chalk formations. From the subsurface exploration a series of isolines, bedrock contact contours, and stratigraphy roll plots with geomorphological interpretation were developed to support the levee assessment.

These contours and isolines were used in the geomorphological interpretation to show the cutting of the more recent bedrock terraces within the current alluvial valley. Fig. 2 shows a portion of the bedrock contact contours in the area of the project and associated subsurface exploration sites. Fig. 3 shows an example of the stratigraphy roll plots with geomorphological interpretation which were developed along the entire system for the floodside levee toe, levee centerline, and land side levee toe. The figure presents the stratigraphy in the form of fence diagrams.

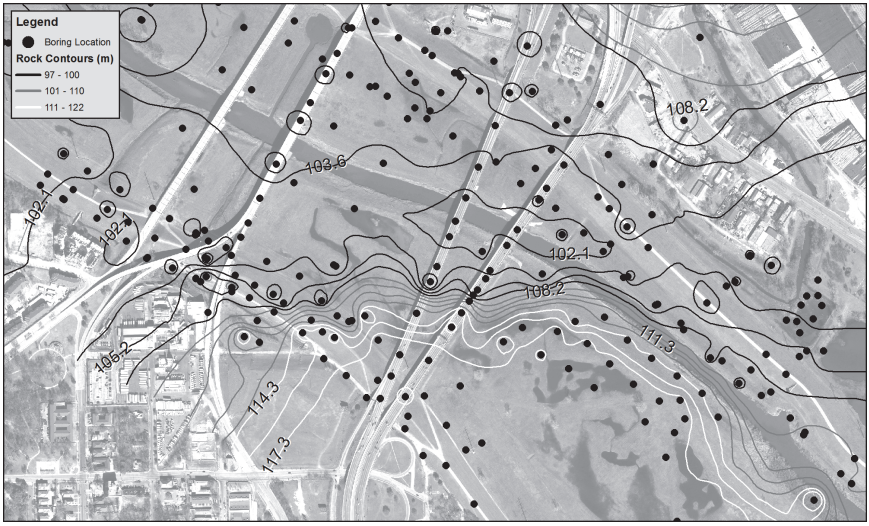

FIG. 2. Bedrock contact contours.

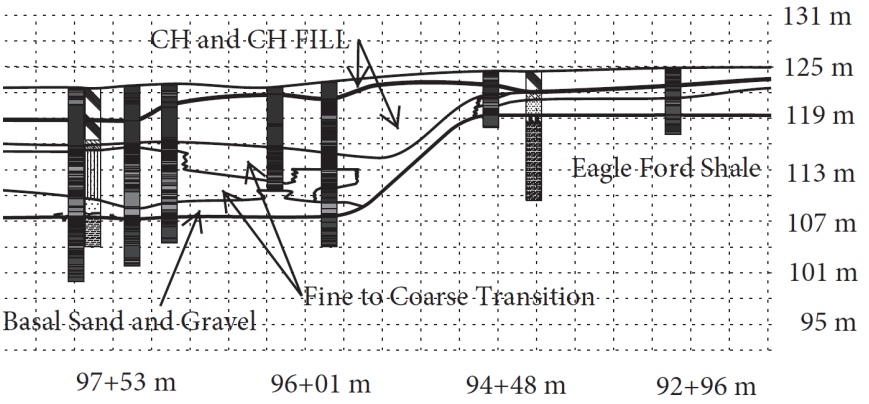

FIG. 3. Stratigraphy roll plots with geomorphic interpretation.

Building on the geologic interpretation work of the 1960s, and Brillinger (1985), generally in the area of Dallas' Central Business District, the bedrock contact elevation of 120.4 m was considered the break between the current surface terrace (floodplain) and the next oldest terrace. Review of the contours suggests a continuance of this older bedrock terrace, as evident of the terraces between elevations 117.3 m to 122.0 m. Further review shows two additional or newer terraces at 106.7 m to 109.7 m and the newest or deepest bedrock elevation of 100.6 m to

106.7 m (paleo channels) which may represent the deepest cutting action of the historic system prior to the re-deposition to the current floodplain surface elevations.

The paleo channels representing the 106.7 to 106.7 m elevation are seen in the upper East Levee Reaches at the Park Cities Treatment Facility and at the Texas Highway 183. Below the confluence of the Elm and West Forks, similar paleo channels are noted at the West Fork crossing just east of Hampton/Delta pump stations, the Hampton meander just downstream of Hampton pump station, the Reunion in area of Commerce to Interstate 35, and Combs Creek area. These locations represent areas with deep alluvial deposits on the order of 15.2 m to 21.3 m or greater above bedrock contact.

The highest bedrock terrace representing the 117.3 m to 122.0 m elevations are seen along portions of the East and West Levees. Accordingly, these locations represent the areas with the thinnest alluvial deposits of approximately 4.6 m to 7.6 m thick.

The intermediate bedrock terrace at elevations 106.7 m to 109.7 m within the current alluvial floodplain represents areas were the alluvial depositions lie between the above two terrace/paleo channels thus representing deposits on the order of approximately 7.6 m to 15.2 m.

The levee assessment included evaluation of levee height, closure structures, erosion, embankment and foundation stability, seepage, and settlement. The historical shallow slough slides which are currently repaired through operation and maintenance of the levee system were determined to be non-catastrophic in nature, therefore risk reduction measures were not pursued for embankment stability. Erosion issues were addressed through maintenance repairs, while levee height was not a consideration for this project as the levee project grade is on the order of 4.5 m higher than the 100-year water surface elevation. Only the potential for underseepage was determined to warrant risk reduction measures.

LEVEE DESIGN

Seepage analyses revealed the potential for landside heave of the resisting clay blanket based on USACE design criteria. As evaluated from the levee assessment, the position of the levee system relative to the geology and geomorphology greatly forecast potential engineering concerns. Areas of high bedrock terraces with landside sumps (old Trinity River channel) with connecting basal sands and gravels were determined to be of concern. Therefore, levee reaches and sub-reaches were established based on engineering judgment which accounted for historical performance, topographic features, river location, sump location, geology or bedrock terraces, and geomorphology. The East Levee was subdivided into 24 sub-reaches, the West Levee into 21 sub-reaches. Coupling detailed geologic mapping with engineering seepage analyses allowed for narrowing the areas of concern.

The geology and geomorphology directly affected the solution to minimize seepage concerns as the head pressure in the basal sands would need to be reduced or the resisting clay blanket weight would need to be increased. Considering the geomorphology and current land use it was not feasible to consider filling in the landside sumps to minimize the potential seepage issue through thickening of the resisting clay blanket. Therefore, to minimize the potential seepage, a cutoff wall

which reduces the total head within the basal sands and gravels was the least impactful solution for the system.

As result of seepage analyses across the DFS, two areas did not meet USACE seepage design criteria for the 100-year event. These areas included a section of the East Levee, 4,800 m long from approximately East Irving Boulevard to approximately Hampton Road and a section of the West Levee, 800 m long just upstream of Corinth Street. The seepage cutoff wall was positioned along the riverside levee toe. The seepage cutoff wall was extended through the underlying basal sands and gravels and keyed into either the Eagle Ford Shale or the Austin Chalk bedrock formations. The cutoff wall limits were selected based on seepage models and knowing the geology and geomorphology especially considering the bedrock terrace elevation along the wall alignment, the thickness of the resisting clay blanket, as well as the protected side sump locations. The seepage cutoff wall was designed to consist of soil-bentonite (SB), cement-bentonite (CB), and Jet-Grout elements. The CB cutoff wall was utilized were a more robust or resilient component was desired such as at the pump station outfalls. The Jet-Grout elements were used around utilities and in areas of low vertical clearance.

CUTOFF WALL CONSTRUCTION

On the East Levee, SB, CB, and Jet-Grout cutoff walls were installed to achieve a maximum specified permeability of 2.1 x 10^{-6} cm/sec. All three wall types were seamlessly tied together to achieve a continuous wall 4,800 m long at depths of up to 18.9 m below grade keyed into the Eagle Ford Shale, see Photograph 1.

Photograph 1. East Levee SB cutoff wall construction, heading 1 PC 1250.

Magnus Pacific self-performed the installation of the SB and CB cutoff walls and subcontracted Layne Geo to install the Jet-Grout cutoff wall. The SB wall was excavated with a bentonite slurry allowing for stable excavations. The bentonite construction slurry was hydrated and mixed within a slurry pond. The bentonite construction slurry was then used to stabilize the vertical excavations. The construction slurry was pumped to the location of the traversing excavation. Stable excavations required the slurry level to be maintained above the water table, as such it was maintained near the flood plain ground surface elevation. As the upper clay blanket materials were relatively thick within the geologic profile, the excavated material was processed directly adjacent to the trench to uniformly blend the sand and gravel layer to make a relatively uniform backfill material. The excavated material was processed with a bull-dozer and an excavator. Due to the high clay content of the mixed materials no additional dry bentonite was incorporated into the backfill other than the natural mixing of the excavation bentonite slurry to achieve the desired backfill slump. The CB wall was constructed in approximately 8 m to 12 m panels. The CB wall was excavated with the CB Slurry which was batched by panel.

Quality control sampling and testing occurred several times per shift and per square foot of wall. Testing and sampling included the bentonite construction slurry, the SB backfill, and the CB slurry. The SB backfill was tested for permeability, index properties, slump, and unit weight. While the CB slurry was tested for permeability, shear strength, and unit weight.

Both the SB and CB cutoff walls were constructed with conventional long reach excavation equipment with rock buckets for excavation into the underlying bedrock formations. The walls were terminated a minimum of 1.5 m into the Eagle Ford Shale or the Austin Chalk. As the wall alignment traversed several different bedrock terraces, on site Geotechnical Engineers verified the top of the key material and the minimum key depths. One area of difficulty was near Hampton Pump Station at ancestral confluence of the East and West Forks of the Trinity River. As such the downstream terrace was situated on a cut bank around elevation 117.3 m whereas the upstream terrace was situated at 106.7 m terrace elevation. Due to the position of this an ancestral cut bank more frequent inspections were required by the Geotechnical Engineer to ensure a proper key into the Eagle Ford Shale.

The wall alignment transected two pump station outfall structures. By installing a CB cutoff wall through these outfalls Magnus Pacific was able to avoid shutting down both pump stations at the same time. One pump station was shut down first and a work platform was constructed across the outfall and the CB wall was installed. After sufficient curing and strength gain, the section through the outfall was excavated allowing the pump station to be placed back online before second pump station was shutdown, see Photograph 2.

The CB cutoff wall was 200 m long and totaled 2,400 m^2. After the CB wall was constructed through each outfall structure a clay cap was placed over the wall and on the slope of the outfall. After the clay cap was placed a three layer filter was placed followed by rip rap to protect the slope and outfall from erosion. A completed photo of the Old Hampton Pump Station Outfall prior to being returned to service is shown in Photograph 3.

Photograph 2. East Levee over-excavation of CB cutoff wall at pump station outfall.

Photograph 3. East Levee Old Hampton Outfall.

The Jet-Grout cutoff wall was comprised of three sections. Each section presented unique challenges. The first challenge encountered was low vertical clearance underneath bridges in two of the three sections. Layne Geo utilized three different drill rigs to accommodate the various clearance limits. The next challenge was protecting existing utilities in the cutoff wall alignment. These utilities ranged from a 1.2 m water main that was nearly 6 m below ground to a 15 cm jet fuel line which supplied jet fuel to Dallas Love Field. In order to prevent impacts to these utilities, Magnus Pacific excavated and surveyed the exact locations of the lines. After the locations were known, Layne Geo was able to install the Jet-Grout columns underneath the utilities while maintaining a clearance or window around each utility. The SB cutoff wall was tied into both the CB and Jet-Grout cutoff wall sections to complete a continuous cutoff wall. Through all phases of construction, Magnus Pacific adhered to a comprehensive quality control program that ensured the wall met or exceeded the design requirements.

On the West Levee, 800 m of SB and Jet-Grout cutoff walls were installed to depths of 5.8 m below grade. The SB wall was constructed on both sides of a low clearance bridge and keyed into an underlying Austin Chalk, see Photograph 4.

Photograph 4. West Levee SB cutoff wall construction.

The Jet-Grout cutoff wall was installed under a low clearance bridge and around a 0.6 m water main. The water main was below the top elevation of the cutoff wall or window and therefore still needed to maintain clearance around the utility without compromising the design permeability. To accomplish this, Layne Geo installed Jet-Grout columns as close as possible to the water main prior to Magnus Pacific excavating and exposing the gap between the water main and the jet-grout columns which was subsequently sealed with low permeability flowable fill.

SUMMARY

The DFS 100-Year Levee Remediation – Cutoff Wall Improvement project demonstrated that geologic and geomorphic modeling can be effectively used to support geotechnical analyses in the evaluation, selection, design and construction of levee risk reduction systems. Intimate knowledge of the geology and geomorphology directly relate to levee embankment materials, flood plain foundation soils, critical failure modes such as underseepage, project limits, and which mitigation measures would be feasible. For this project, the site specific geology, geomorphology, and urban land-use made cutoff walls as the most practical approach to reducing risk for levee underseepage affecting levee stability. The project reached substantial completion in March of 2013 with the completion of the cutoff walls and the rehabilitation of the pump station outfall channels. These documented improvements will accompany the FEMA 65.10 documentation to recommend levee certification such that FEMA may accredit the system to remain within the National Flood Insurance Program.

ACKNOWLEDGMENTS

The authors appreciate the support of the City of Dallas, Ms. Liz Fernandez, Mr. Kelly High, and Mr. Than Nguyen, Magnus Pacific Corporation, Rodney Louviere, USACE, Mr. Rob Newman, and HNTB Corporation, Mr. Scott Breen, Mr. David Jaromin, Mr. Darin Maciolek, Mrs. Lesley Schwalje, and Mr. Brad Wilder.

REFERENCES

Brillinger, A. B. (1985). “Investigation of Trinity River Paleochannels in the Central Business District, Dallas, Texas.” *Master’s Thesis*, Department of Geology, Texas A&M University, College Station.

Design and Construction of an Earthen Impoundment for Water Management

Thomas Chapel[1], F. ASCE, P.G., P.E., Jon Jaffe[2], and Caleb Stock[3], M. ASCE, P.E.

[1]Principal Engineer, Tetra Tech, Inc., 3801 Automation Way, Suite 100, Fort Collins, CO 80525; tom.chapel@tetratech.com
[2]Production Engineering Manager, Anadarko Petroleum Corporation, 4000 Burlington Ave., Evans, CO 80620; jon.jaffe@anadarko.com
[3]Project Engineer, Tetra Tech, Inc., 3801 Automation Way, Suite 100, Fort Collins, CO 80525; caleb.stock@tetratech.com

ABSTRACT

Tetra Tech, Inc. (Tetra Tech) provided engineering support to Anadarko Petroleum Company (Anadarko) for water storage alternatives proposed for use in hydraulic fracturing operations. Tetra Tech conducted a geotechnical investigation to determine the suitability of an Anadarko site located south of Greeley, Colorado. The property, which is located near the geologic floodplain of the South Platte River, is underlain by clayey sand and low plasticity clay, gravelly sand, and claystone bedrock.

An earthen impoundment was designed to maximize storage capacity and balance earthwork quantities. The footprint of the facility was 6.3 hectares (15.5 acres) with impoundment dimensions of 107 m by 235 m (350 ft by 770 ft). The embankment crest ranged from 1.5 m to 2.9 m (5 ft to 9.5 ft) above existing grade, and the capacity was approximately 79,500 m^3 (500,000 barrels or 21,000,000 gal).

During construction coarse gravel that would not be a suitable liner subgrade was encountered. The material was removed and stockpiled; clay material from other Anadarko sites was trucked in and used as liner subgrade. The gravel was screened on site and used by Anadarko as road base at various other sites.

Construction of the impoundment was completed in summer 2013, and has performed well; it was not damaged during the flooding of September 2013.

INTRODUCTION

The Greater Wattenberg Area (GWA) has been producing oil and gas since the early 1970s. The field covers more than approximately 400,000 hectares (1,000,000 acres) within the greater Denver Basin, generally located between Denver and Greeley, Colorado. As development of shale resources continues, the lateral extent of the producing area continues to increase. The location of the Wattenberg Field is shown in FIG. 1.

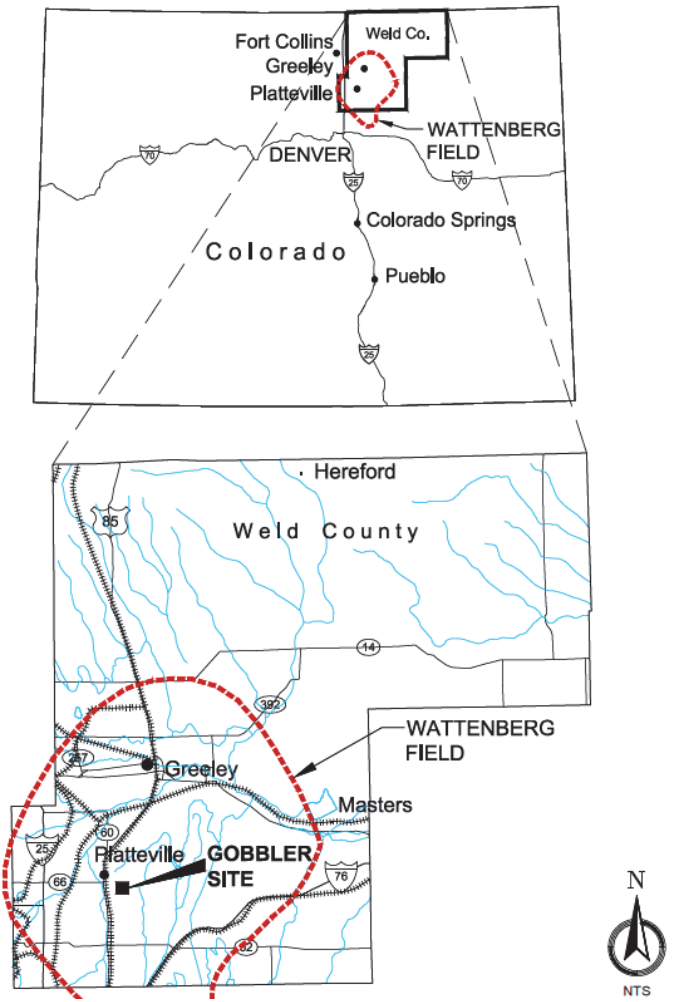

FIG. 1. GWA Location Map

Anadarko has an extensive development planned in the GWA. In 2011, Anadarko realized that the water supply necessary for development activities would be a key component for successfully developing the field. In an effort to significantly reduce trucking, Anadarko implemented their "Water On Demand" (WOD) system. The WOD system delivers water throughout Anadarko's planned development areas using buried large diameter, 51 cm and 61 cm (20 in and 24 in), high density polyethylene (HDPE) pipe and smaller diameter surface pipe for transfers from the buried HDPE pipe to each location. The WOD system as currently installed has over 128 km (80 miles) of buried HDPE pipe. To provide surge and storage capacity, Anadarko

required water storage alternatives, and retained Tetra Tech to assist in evaluation of an appropriate site for the facilities needed for the WOD system.

SITE AND PROJECT DESCRIPTION

Anadarko owned a parcel of land situated on a geographical high spot within their area of interest. Aided by gravity flow, this site would allow smaller pump sizes for providing water to the WOD system than other sites considered. Historically, the property had been the site of a turkey farming/ranching operation; thus the site was eventually named "the Gobbler Site".

The Gobbler Site is located approximately 12 km (7.6 miles) southeast of Platteville and approximately 6 km (4 miles) east of U.S. Highway 85. The site is generally flat, with a maximum elevation of 1,571 m (5,155 ft) near the center of the proposed facility and a minimum elevation of 1,568 m (5,145 ft) near the northwest, northeast, and southeast corners of the proposed impoundment, based on land surveying conducted by Petroleum Field Services, LLC. The portion of the Gobbler Site planned for construction of water storage facilities was the northern portion, which consisted of undeveloped land vegetated with prairie grasses generally less than 15 cm (0.5 ft) in height. Fig. 1 shows the property location.

ENGINEERING EVALUATION AND COST ANALYSIS

An engineering evaluation and cost analysis (EE/CA) was prepared to compare water storage alternatives, including an earthen impoundment, above-grade steel tanks, above-grade concrete tanks (both pre-cast and cast-in-place), and Portadams®. Portadams are above ground impoundments constructed of a steel frame and geosynthetic liner. They are considered temporary storage options and can constructed and deconstructed relatively quickly. Criteria identified by Anadarko that were used to compare the water storage options included: initial cost, time to construct, availability of material, and maintenance requirements.

Tetra Tech and Anadarko developed a weighting system to facilitate quantitative comparison of the alternatives. Cost was considered a key criterion for comparison of the water storage facilities; it was therefore given a weighting factor of 5. The time needed for construction was assigned a weighting factor of 2. Material availability and maintenance requirements were assigned weighting factors of 1. Each storage option was presumed to be environmentally acceptable.

Direct quantitative comparisons were made where possible; for example, estimated construction cost and the construction timeframe. Qualitative analyses were used for the material availability and maintenance requirements. Based on scores using the criteria above, each option was assigned a rating of very good, good, average, below average, or poor, relative to the other alternatives. An integer one through five was assigned to each rating to provide a numerical value.

The results of the EE/CA indicated that an earthen impoundment was the most desirable water storage option based on the system described above. The earthen impoundment was rated "very good" in the *time to construct* category and "good" in the *construction cost* and *material availability* categories with an "average" score for

maintenance requirements. Portadams® were the second most desirable water storage option, followed by cast-in-place concrete tanks, then steel tanks. Pre-cast concrete tanks ranked the lowest of the alternatives considered.

Table 1. EE/CA Results

Item	Criterion	Value	Weighted Score
Earthen Pit	Cost	Good	37
	Construction Time	Very Good	
	Material Availability	Good	
	Maintenance Requirements	Average	
Portadams	Cost	Average	32
	Construction Time	Very Good	
	Material Availability	Good	
	Maintenance Requirements	Average	
Cast-In-Place Concrete Tanks	Cost	Average	28
	Construction Time	Below Average	
	Material Availability	Good	
	Maintenance Requirements	Very Good	
Steel Tanks	Cost	Below Average	19
	Construction Time	Poor	
	Material Availability	Good	
	Maintenance Requirements	Average	
Pre-Cast Concrete Tanks	Cost	Poor	16
	Construction Time	Poor	
	Material Availability	Good	
	Maintenance Requirements	Very Good	

SITE GEOLOGY

The Gobbler Site occupies a broad hill that slopes gently to the north. The USGS geologic map of the Hudson Quadrangle (Soister, 1965) shows that the near-surface geology generally consists of Holocene- to Pleistocene-age windblown sand (Q_{es}). A broad northwest- to southeast-trending ridge includes deposits of Holocene colluvium (Q_c), and the tops of hills are capped by Pleistocene-age Rocky Flats Alluvium (Q_{rf}), Quaternary Loess (Q_l), and Cretaceous Demetrie Volcanics (Q_{dw}). The underlying bedrock is mapped as claystone/shale of the Tertiary/Cretaceous-age Denver Formation.

GEOTECHNICAL INVESTIGATION AND SUBSURFACE CONDITIONS

To compare the actual subsurface conditions with published geologic mapping, and to evaluate the Anadarko property for the design and construction of an earthen impoundment, Tetra Tech drilled four borings to a depth of 12 m (40 ft) below the existing ground surface as shown on Fig. 2. Drive samples were collected at 1.5 m (5

ft) intervals using a thick-walled California type sampler, and blow counts were recorded for each sample interval. Blow counts indicate the consistency of the fine-grained soil was medium stiff to hard. The coarse-grained material had a consistency ranging from very loose to dense.

To evaluate materials for use in construction of the embankments, bulk samples were collected from auger cuttings from depths up to 4 m (14 ft) below the existing ground surface, and on materials visually classified as low-plasticity clay and gravelly sand.

Samples were examined and classified according to the Unified Soil Classification System (USCS). A laboratory testing program was developed to identify key engineering properties of the soils to evaluate seepage potential and stability of the embankments for engineering design. Selected samples were tested in the laboratory for in-situ density and water content, gradation, Atterberg limits, swell and consolidation, compaction, permeability, and shear strength. Soil classifications were determined in accordance with ASTM D2487.

SUBSURFACE CONDITIONS

Fifteen cm (6 in) or less of topsoil-like material were encountered at the ground surface in all four borings. Below the topsoil, the soils encountered consisted of alternating layers of clayey sand and low-plasticity clay to depths between 3 m and 4 m (10 ft and 14 ft) below existing grade. These layers were underlain by gravelly sand or sand to a depth of up to 8 m (25 ft).

The upper subsurface zone, including primarily clays and sands, was anticipated to be the primary borrow source of fill used in embankment construction. The lower zone, where bedrock predominates, would form the embankment foundation.

The *in-situ* water content of samples tested ranged from 2.2 percent to 18.7 percent and the *in-situ* dry density ranged from 1,420 kg/m^3 to 2,080 kg/m^3 (89 lb/ft^3 to 130 lb/ft^3). Atterberg limits testing indicated the liquid limit (LL) of the clayey soils ranged from 21 to 62 and the plasticity index (PI) ranged from 6 to 37. Grain size distribution testing was performed on twelve samples, and indicated that the upper 2 m to 4 m (6 ft to 14 ft) ranged from clayey sand to lean clay. Bedrock was classified as high-plasticity clay containing up to 93 percent clay and silt sized particles (passing the No. 200 sieve).

Standard compaction (Proctor) testing was performed in accordance with ASTM D698 on two bucket samples collected from 0 to 2 m (7 ft) and from 4 m to 6 m (14 ft to 21 ft) below existing grade. Samples of similar materials from each borehole were combined to provide representative samples of similar materials from the site. Standard Proctor compaction testing determined the maximum dry density and optimum water content to be 1,910 kg/m^3 (119.4 lb/ft^3) at 10.3 percent and 2,060 kg/m^3 (128.7 lb/ft^3) at 9.0 percent for shallow and deep samples, respectively. The degree of compaction of the embankments was determined relative to the Proctors. Construction specifications required a minimum of 95 percent of standard Proctor maximum dry density and a moisture content within two or three percent of the optimum moisture content for granular or fine grained soils, respectively.

Two remolded direct shear tests were conducted on potential embankment material from the two bulk samples collected. Test results indicated a total cohesion of 19 kPa

(400 lb/ft^2) with an angle of internal friction of 35 degrees for the shallow sample. A total cohesion of 47 kPa (980 lb/ft^2) with an angle of internal friction of 28 degrees was determined for the deep sample.

Three permeability tests were conducted: two remolded samples on potential embankment material from the two bulk samples collected (as described previously) and one on *in-situ* soils from a depth of 2.7 m (9 ft). The two remolded samples were compacted to 95 percent of the maximum standard Proctor dry density. The remolded test using material from the shallow sample indicated a saturated hydraulic conductivity of 2.06 x 10^{-4} cm/s. The remolded test using material from the deep sample indicated a saturated hydraulic conductivity of 1.67 x 10^{-5} cm/s. The *in-situ* sample tested had a saturated hydraulic conductivity of 4.47 x 10^{-4} cm/s.

Two swell-consolidation tests were performed on remolded embankment materials. The remolded samples were compacted to 95 percent of the standard Proctor maximum dry density and optimum water content. Under an inundation pressure of 24 kPa (500 lb/ft^2), the remolded bulk samples from 0 to 2 m (7 ft) and 4 m to 6 m (14 ft to 21 ft) exhibited no volume change. The compression index (C_c) ranged from 0.04 to 0.05 and the recompression index (C_s) was 0.02 for both remolded samples.

Groundwater

At the time of drilling, water was not encountered in any of the four exploratory borings to the maximum drilled depth of 12 m (40 ft). After 24 hours, water was measured at 9.4 m (31 ft) below ground surface in one of the borings. We concluded that the water, which had seeped into the borehole, was from a porous, discontinuous sandstone lens within the claystone bedrock and would have little to no effect on facility construction, operations, or sustainability.

CIVIL ENGINEERING DESIGN

Anadarko required a minimum capacity of 40,000 m^3 (250,000 barrels or 10,500,000 gal) for the impoundment, but a preference was specified to maximize the design capacity to the extent possible given site conditions. The final design capacity is approximately 80,000 m^3 (500,000 barrels or 21,000,000 gal) assuming that 0.61 m (2 ft) of freeboard is maintained. The impoundment was designed such that it would not be classified as a jurisdictional dam by the State of Colorado. That is, the embankment does not have a statutory height greater than 3 m (10 ft) to the spillway crest, the reservoir volume is less than 123,400 m^3 (100 acre-ft), and the surface area is 8 hectares (20 acres) or less at the high waterline (Colorado Division of Water Resources, 2013).

As designed, the Gobbler Site impoundment is a rectangular structure with interior dimensions of approximately 107 m by 235 m (350 ft by 770 ft). The interior slopes are 3H:1V. To balance the excavation and fill quantities as closely as possible, the 3m (10 ft) wide crest was set at approximately 1.5 m to 2.9 m (5 ft to 9.5 ft) above existing grade and exterior slopes are between 5H:1V and 50H:1V. The exterior slopes of the embankment were flattened on one side to dispose of excess material on site, which was determined to be more cost-effective than hauling the material off site. The impoundment floor slopes at one percent towards the northeast, and a 6.7 m

(22 ft) by 6.7 m (22 ft) by 0.9 m (3 ft) deep sump is located at the northeast-side midpoint to collect seepage through the primary liner.

The impoundment has an average depth from the embankment crest to the floor of approximately 4.5 m (15 ft). The crest elevation does not exceed 3.0 m (10 ft) above existing grade in any location. The designed facility is shown below as Fig. 2.

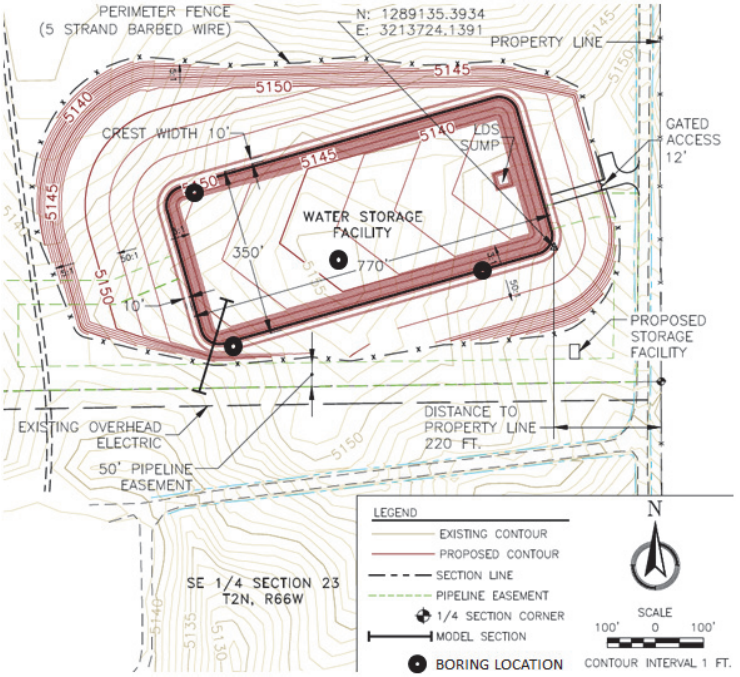

FIG. 2. Site Design

A barbed wire fence and gate system was installed around the perimeter. Weather and UV-resistant safety lines with floats were included in the design as a safety feature in the event of accidental entrance into the impounded water by workers.

The impoundment would initially be used to store fresh water; however, Anadarko wanted the option to be able to store process water in the impoundment should operations change. Therefore a double-liner system incorporating a smooth 1.5 mm (60 mil) HDPE secondary (lower) geomembrane liner, overlain by HDPE geonet, overlain by a smooth 1.5 mm primary (upper) geomembrane liner was designed. The geomembrane liner system covers the floor of the impoundment and interior slopes, and was anchored at the crest using an anchor trench 0.5 m (18 in) deep and constructed in accordance with Colorado Oil and Gas Conservation Commission (COGCC) rule 904.c.(1) which specifies a minimum liner thickness of 0.6 mm (24 mil) and an anchor trench at least 0.3 m (12 in) deep. Methodology from Giroud et al (1997) was used to design the leak detection system between the two liners. The

sump was designed to allow capacity to store two days of leak detection system flow with a factor of safety of 1.5.

To evaluate the potential for overtopping the embankment, potentially causing excessive surface erosion and possible failure, analysis was conducted to determine the freeboard needed for this facility and to verify that the 0.6 m (2 ft) specified by COGCC rule 902.b. is adequate to protect the impoundment from overtopping due to wind and wave action. Since the impoundment would have a maximum water-surface length less than 1.6 km (1 mile), "standard" calculations for determining the wave height were not considered appropriate. Therefore, the wave height was calculated based on methods described by Julien (2006). A maximum wave height of 0.33 m (1.1) ft for standard operation was calculated. Wave run-up and wave set-up heights were calculated based on figures and equations provided in "Hydraulics of Dams and Reservoirs" (Sentürk, 1994) and were determined to be insignificant (less than 3.05 cm or 0.1 foot). A design wind speed of 145 km/h (90 mi/h) was used in accordance with the Bureau of Reclamation method presented in Sentürk for determining the operational design freeboard. A wind speed of 80.5 km/h (50 mi/h) was used for determining the minimum freeboard.

Potential settlement of the embankment was incorporated in the freeboard analysis. Results of the analysis indicated that the operational freeboard should be at least 0.6 m (2 ft) at any given time. Therefore the COGCC minimum requirement of 0.6 m (2 ft) was determined to be appropriate.

GEOTECHNICAL ENGINEERING ANALYSIS

To evaluate the potential for instability of the embankments, the finite element computer modeling program GeoStudio 2007 by Geo-Slope International, Ltd (2007) was used. The most critical cross-section was identified based on the proposed design and the site survey of existing ground, and that section was analyzed for seepage and slope stability.

For modeling purposes, the elevation of the fluid in the impoundment was assumed to be at the maximum design capacity (freeboard elevation, 0.6 m (2 ft) below the crest) and full (at the crest of the embankment). Although the impoundment would be lined, modeling scenarios omitted the liner system to simulate a worst case seepage scenario in which a liner breach occurred, resulting in a steady state seepage scenario, reducing the stability of the embankments by increasing pore water pressures and decreasing the effective strength of the embankment soils.

Analysis of the embankment was conducted according to Natural Resources Conservation Service (2005) criteria governing the design and construction of earth dams and reservoirs.

The horizontal acceleration used for the pseudo-static analysis was 0.05g, which for this site corresponds to the Peak Ground Acceleration (PGA) with a 2 percent probability of exceedance in 50 years, according to the U.S. Geologic Survey's (USGS) Earthquake Hazards Program Seismic Hazard Maps (2010).

Laboratory testing was performed on samples collected during drilling operations as described above. Due to the uncertainty and variability of the site soils and the inherent differences normally observed between laboratory results and actual field

conditions, engineering judgment and a measure of conservatism were applied to the laboratory results for their use in the computer models. Design parameters used in the model are shown in Table 2.

Table 2. Model Input Material Properties

Soil Type	Depth Below Crest (m) (ft)	Unit Weight (kN/m^3) (lb/ft^3)	Hydraulic Conductivity (cm/s)	Effective Cohesion (kPa) (lb/ft^2)	Effective Friction Angle (deg)
Embankment Clayey Sand	0 – 2.90 (0 - 9.5)	19.79 (126)	1.00×10^{-4}	3.59 (75)	20
Natural Clayey Sand	2.90 – 5.03 (9.5 – 16.5)	18.07 (115)	5.00×10^{-4}	2.39 (50)	25
Lean Clay	5.03 – 7.77 (16.5 – 25.5)	16.49 (105)	5.00×10^{-6}	4.79 (100)	20
Gravel	7.77 – 9.60 (25.5 – 31.5)	19.64 (125)	1.00×10^{-3}	0	28

Seepage and slope stability analyses were conducted on the most critical two-dimensional cross-section of the proposed embankment as defined by the highest elevation differential, the steepest and longest slopes, and/or the weakest materials. All interior embankment slopes were designed at 3H:1V and the exterior embankment slopes ranged from 5H:1V to 50H:1V.

The analyses were performed using the Seep/W and Slope/W components of GeoStudio 2007 by Geo-Slope International, Ltd (2007). Seep/W was used to conduct steady-state finite element seepage analyses. Constant boundary conditions included a potential seepage face, fluid total head elevation, and groundwater levels as measured in the exploratory borings after drilling.

A steady-state seepage analysis implies that the seepage occurred over a period of time sufficient enough to fully define the phreatic surface and provide continuous seepage magnitudes at all locations through and under the embankments. The static condition describes the normal, long-term operating levels of the impoundment. Rapid drawdown occurs when the impoundment has achieved steady-state seepage and a constant phreatic surface, and then the water surface elevation is rapidly lowered such that the saturated embankment is no longer supported by hydrostatic pressures.

The pseudo-static stability analysis condition adds an additional horizontal loading that occurs due to seismic loading.

Seepage

Seepage analyses were performed to evaluate the performance of the embankment, to estimate seepage flux (volume of seepage per unit time) on the downstream side of the embankment, and to estimate porewater pressure conditions within the

embankment for use in effective-stress slope stability analyses. The HDPE double liner with geonet was neglected in the analysis for conservatism, as discussed above.

The fluid level was modeled at the freeboard elevation and at the maximum embankment height, which are approximately 4.6 m and 5.2 m (15 ft and 17 ft) above the base of the earthen impoundment at the deepest location, respectively. These water surface elevations were selected for modeling the impoundment because they represent the critical design water elevations for this facility. For this impoundment, the fluid was assumed to be fresh water with a specific gravity of 1.0. Should site operations change, an alteration in the fluid specific gravity of up to 1.25 was also modeled and provides factors of safety above the required limits.

Boundary conditions equal to the respective water heights were applied on the upstream face of the embankment while the boundary condition of a potential seepage face was applied to the downstream face of the embankment.

The seepage flux was determined at the downstream toe of the modeled embankment, at the location most susceptible to piping. The maximum flux at the downstream toe of the impoundment embankment was calculated to be 1.9×10^{-7} m^3/sec (6.8×10^{-6} ft^3/sec).

These results indicate that the seepage is negligible and will not yield problematic piping. Seepage analyses were conducted for the embankments assuming a no liner condition, simulating a total liner failure which is an unexpected and conservative assumption for seepage analysis. The seepage flux was approximately equal for both water surface elevations modeled.

The hydraulic gradient of the downstream slope at the toe of the embankment (the location most susceptible to piping) was calculated to be 0.354. According to methodology recommended by the USACE (1993), the factor of safety against piping caused by an excessive hydraulic gradient can be calculated as the critical hydraulic gradient divided by the measured hydraulic gradient. The critical hydraulic gradient is the ratio of the buoyant unit weight of soil to the unit weight of water. For our calculations, a conservative moist unit weight of 19.79 kN/m^3 (126 lb/ft^3) was applied at the toe of the embankment resulting in a critical hydraulic gradient of 1.7. Thus, the factor of safety against piping was calculated as 4.8. These calculations indicate a low risk of embankment distress or failure due to seepage.

Slope Stability

Slope stability was analyzed using limit equilibrium principles. Potential failure surfaces were analyzed using the Spencer method, which satisfies both force and moment equilibrium in and between slices. The Slope/W program incorporates a search routine to locate the failure surface with the lowest factor of safety within user-defined search limits. Trial failure surfaces were defined with “entry and exit” parameters, resulting in a range of possible locations to search for the critical potential failure surface (lowest factor of safety). Effective stress stability analyses were performed using Mohr-Coulomb failure criteria for the soil materials.

For the porewater pressure conditions, the steady-state seepage files from SEEP/W were used as the parent analysis for the slope stability analyses’ input data, except for the rapid drawdown case where the phreatic surface was drawn manually to indicate

the dividing line between saturated and unsaturated conditions, as discussed above. Slope stability analyses were performed for both upstream and downstream side slopes, assuming static and pseudo-static seismic loading conditions, for fluid at freeboard elevation and at the maximum embankment elevation, and for the upstream, static, rapid drawdown scenario as described above.

Upstream and downstream slopes of impoundment embankments were analyzed under static, rapid drawdown, and pseudo-static loading conditions and with the impounded water at both freeboard and full-crest elevations. The lowest calculated factors of safety for the downstream slope of the embankment were 1.6 for the static, steady-state seepage condition and 1.3 for the pseudo-static (seismic) condition. The rapid drawdown scenario resulted in a calculated factor of safety of 1.9. For the three most critical modeled scenarios, the water was at the embankment crest.

Settlement

Consolidation-swell tests were conducted on representative samples of embankment material to provide differential strain estimates upon inundation and with differing applied vertical stresses. Testing indicated that the embankment materials were non-expansive. The test data were used to estimate the amount of settlement that can be expected in the embankment materials post compaction. Remolded consolidation-swell samples were compacted to 95 percent of the maximum dry density and at the optimum moisture content based on standard Proctor compaction testing, which will provide a valid representation of the swell-compression behavior given the boundaries specified for embankment compaction (greater than 95 percent of the maximum Proctor dry density and within 3 percent of the optimum moisture content).

The behavior of the soils at the site was analyzed in accordance with volume change theory and general settlement calculations (Budhu, 2011). The embankment and foundation soils were subdivided into layers according to similar consolidation characteristics and material classifications. The differential vertical height change of each layer was calculated based on laboratory test results, experience with similar materials, and overburden soil and water pressures. The net vertical height change was analyzed for the embankment height relative to the existing grade to determine potential discrepancies in impoundment storage due to differential settlements.

The maximum settlement for the facility was calculated to be 9.6 cm (3.8 in) using a profile to a depth of 15.2 m (50 ft) below the final crest elevation. The differential settlement of the embankment portion was calculated as less than 0.25 cm (0.1 in) and will not have significant effects on the overall facility.

CONSTRUCTION

Construction of the Gobbler Site impoundment occurred between April 1, 2013, and June 13, 2013. During excavation operations, the gravelly sand encountered in three of the four soil borings at depths ranging from 4 m to 6 m (13 ft to 19 ft) was more prevalent and shallower in much of the impoundment area than had been anticipated based on the widely-spaced borings. Further, the material graded over

short distances to coarse, sandy gravel with clast diameters greater than 2.5 cm (1 in) in many parts of the excavation. Five test pits were excavated to determine the extent of the coarse sandy gravel layer. It was determined that approximately 15,900 m^3 (20,800 yd^3) of this gravelly material would need to be excavated to remove the unsuitable material from beneath the liner. This resulted in over-excavation of a layer approximately 0.3 m (1 ft) thick from the base of the impoundment.

Because of the gravelly nature of the material, Anadarko decided to stockpile it for use as road and pad surfacing at this and other sites. Lean clay material that had been excavated from another Anadarko project site was determined to be a suitable subgrade soil for the Gobbler site, and was hauled to the Site to provide the liner subgrade fill following over-excavation of the coarse sandy gravel. Quality assurance and control testing was performed on the imported material to verify that the engineering properties were suitable.

CONCLUSIONS

The design and construction of the Gobbler Water Storage Facility illustrate a successful integration of geologic science and geotechnical engineering practice to solve practical design and construction problems. Engineering concepts were used to determine a cost-effective solution to Anadarko's water storage needs. Through collaboration between the engineering team and Anadarko's construction team, geologic conditions were considered and the design was revised to solve an unsuitable gravelly soil issue for this site. Clay soils that were unsuitable for use at other Anadarko sites and would have been wasted were identified as an excellent material for the geomembrane liner subgrade at this site, and the gravel, which was problematic for this site, solved a road and pad surfacing need that would have otherwise required Anadarko to purchase and import produced aggregate.

The design and construction were successfully completed. The Gobbler Water Storage Facility was placed in service as part of Anadarko's WOD program in June 2013. The design was tested during the historic flooding that occurred in September 2013, and the facility performed as intended. Key elements of the design, such as freeboard, seepage, and slope and erosional stability of the embankments functioned as predicted.

REFERENCES

ASTM Standard D 698, 2012, "Standard Test Methods for Laboratory Compaction Characteristics of Soil Using Standard Effort (12 400 ft-lbf/ft^3 (600 kN-m/m^3))," ASTM International, West Conshohocken, PA, 2011, DOI: 10.1520/D0698

ASTM Standard D 2487, 2011, "Standard Practice for Classification of Soils for Engineering Purposes (Unified Soil Classificaiton System)," ASTM International, West Conshohocken, PA, 2011, DOI: 10.1520/D2487-11

Budhu, M. (2011). *Soil Mechanics and Foundations*. John Wiley & Sons Inc., Hoboken, NJ.

Colorado Division of Water Resources. 2013. Design Review and Construction Inspection, http://water.state.co.us/SurfaceWater/DamSafety/DesignConstruction/Pages/default.aspx. Viewed March 29, 2013.

Geo-Slope International, Ltd. (GEO-SLOPE). 2007. "Geostudio 2007" Version 7.13. Calgary, Alberta, Canada.

Giroud, J.P., Gross, B.A., Bonaparte, R., and McKelvery, J.A. (1997). "Leachate flow in leakage collection layers due to defects in geomembrane liners." *Geosynthetics International,* 4(3-4): 215-292.

Julien, P.Y. (2006). *River Mechanics*. Cambridge University Press, New York. 395pp.

National Resources Conservation Service (NRCS). (2005). Earth Dams and Reservoirs TR-60.

Sentürk, F. (1994). *Hydraulics of Dams and Reservoirs*. Water Resources Publications, Highlands Ranch. January.

Soister, P.E. (1965). Geologic map of the Hudson quadrangle, Weld and Adams Counties, Colorado. U.S. Geological Survey.

United States Army Corps of Engineers (USACE). (1993). Seepage Analysis and Control for Dams. Engineering Manual 1110-2-1901. April 30.

U.S. Geologic Survey (USGS). (2010). Earthquake Hazards Program. Seismic Hazard Map, http://earthquake.usgs.gov/earthquakes/states/texas/hazards.php. Viewed April 20, 2013.

Dealing with Tricky Soils at the SDS Water Treatment Plant

Steven Kuehr[1], M. ASCE, P.E., Rebecca Brock[2], M. ASCE, P.E., and Alexander Vega[3], M. ASCE, E.I.T.

[1]Principal and C.O.O., Brierley Associates, 990 S. Broadway, Suite 222, Denver, CO 80209; skuehr@brierleyassociates.com
[2]Senior Engineer, Brierley Associates, 990 S. Broadway, Suite 222, Denver, CO 80209; rbrock@brierleyassociates.com
[3]Staff Engineer, Brierley Associates, 990 S. Broadway, Suite 222, Denver, CO 80209; avega@brierleyassociates.com

ABSTRACT: The Southern Delivery System's (SDS) 189,300 m^3/d (50-mgd) water treatment plant and finished water pump station in southeast Colorado Springs is the largest and most complex component of the regional project. The project is also being built on some of Colorado's most complex geology. Foundation components of the project are constructed and construction continues on the various facilities. The geology of the water treatment plant site consists of eolian deposits over alluvium. Two large site structures were founded within the eolian deposits at depths ranging from 9.1 m (30 ft) below to 3 m (10 ft) above existing grade. The eolian soils are windblown soils that were deposited in a loose condition and later the individual grains were fused with weak water-soluble "cement." When these soils become wetted, particularly under conditions of increased loading, they collapse. Design, construction, and operation measures were necessary to mitigate the potential for water to collect below grade or to pond above grade, as well as minimizing the potential for pipe or tank leakage. The design-build project team mitigated the collapse potential of the site soils. Ground improvement included deep dynamic compaction (DDC) for areas of the site. A test pilot program was successful in demonstrating that DDC could be used as a cost effective method to mitigate the soils across large areas of the site. Using DDC saved 1,704,957.3 m^3 (2,230,000 yd^3) of over-excavation that would have otherwise been required.

INTRODUCTION

The Southern Delivery System (SDS) project is a large regional water supply project designed to transmit water from Pueblo Reservoir to Colorado Springs Utilities and other project participants. The project includes a connection to the outlet works at Pueblo Dam, 80.4 km (50 miles) of raw water pipeline, three booster pump stations, and a 189,300 m^3/d (50-mgd) water treatment plant (WTP). The project location is shown on Figs. 1 and 2.

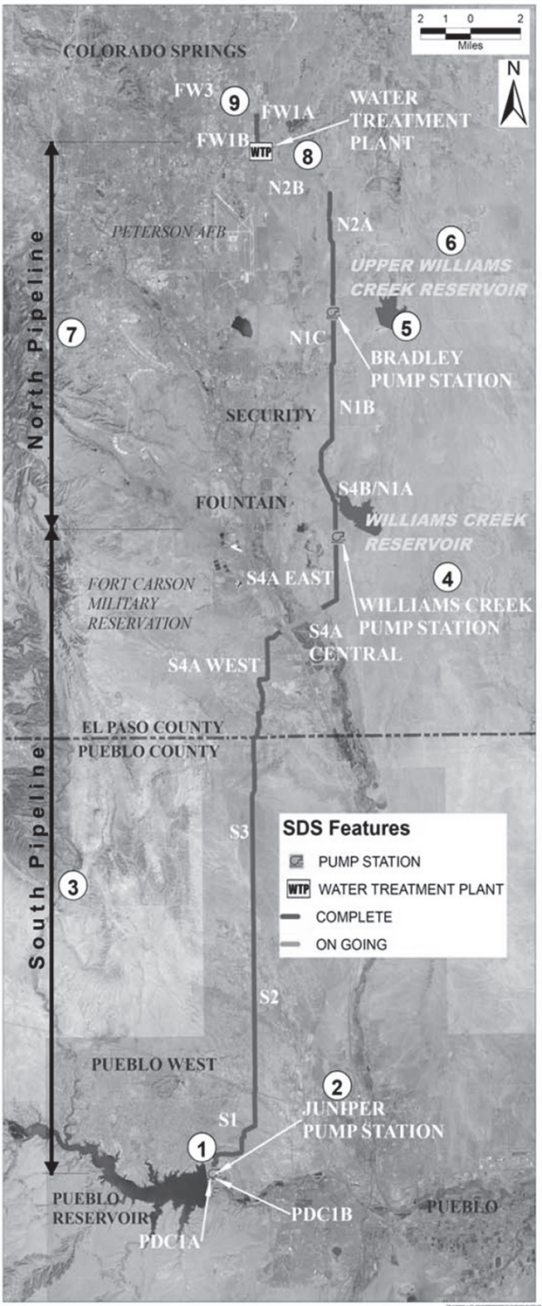

FIG. 1. SDS Pipeline Alignment Progress Map (Image Source: Colorado Springs Utilities, February 2014)

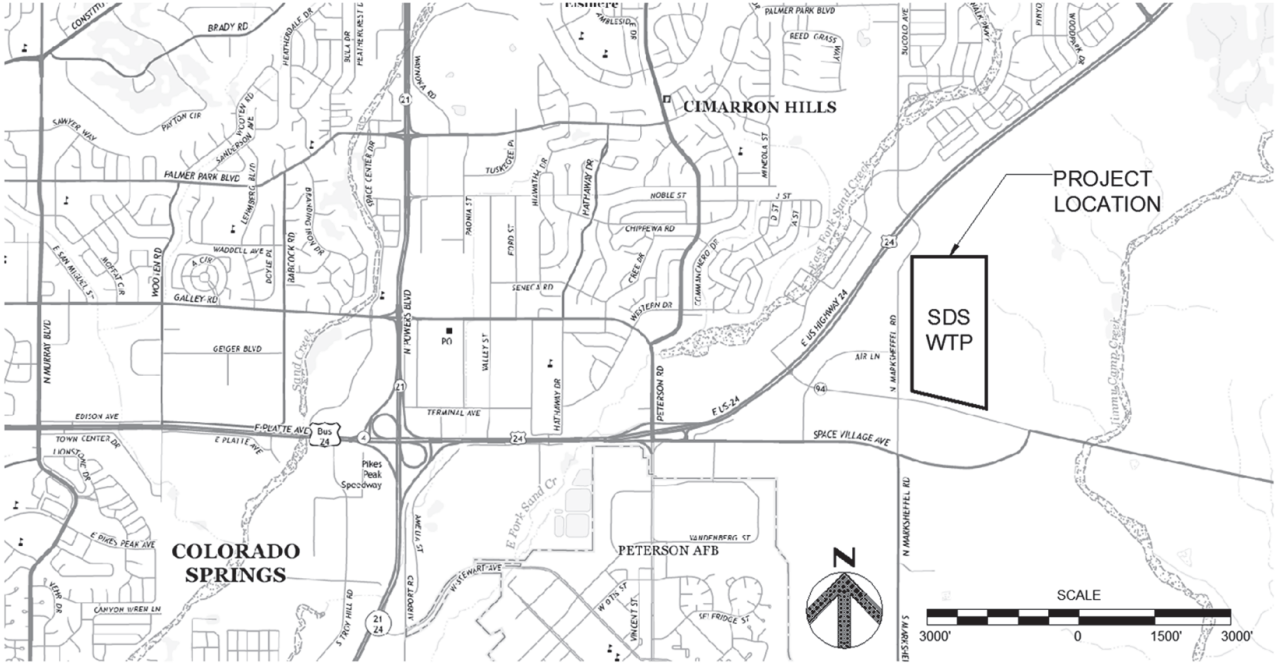

FIG. 2. Project Location (Image Source: USGS Elsmere, Colorado Quadrangle, Revised 2013)

The treatment plant consists of an above-grade raw water tank, a main process building, a below-grade finished water tank, sediment drying beds, and backwash recovery lagoons at the site as shown on Fig. 3.

Brierley Associates (Brierley) was the geotechnical team member for the design-build team of Carollo Engineers (designer) and McCarthy (contractor). R. E. Monks was the earthwork and grading contractor and Densification, Inc. was the specialty deep dynamic compaction subcontractor.

BACKGROUND

A preliminary geotechnical investigation for the site had been performed by RJH Consultants (RJH 2009). As summarized in the RJH report (RJH 2009), the WTP site is within the Great Plains physiographic province of the Colorado Plateau region. The Great Plains Province is characterized by smooth uplands and gently sloping grasslands dissected by wide, shallow valleys. Surficial soils in the site vicinity generally consist of Quaternary-age eolian, alluvial, colluvial, and terrace deposits. The bedrock within the Great Plains Province consists of relatively flat-lying Mesozoic and Cenozoic formations (less than 254 million years old) (USGS 2013). The bedrock at the site is typically about 21.3 m (70 ft) to 30.5 m (100 ft) below ground surface (bgs) and dips gently to the northeast.

The geology of the WTP site consists of unconsolidated surface deposits consisting of eolian, alluvium, and clay in localized areas. These soils are typically silty sands and poorly- to well-graded sands. The thickness of these soils over the bedrock formations in this area can vary from 21.3 m (70 ft) to 30.5 m (100 ft) Claystone and sandstone exist beneath the alluvium as part of the Dawson Formation.

The RJH investigation revealed significant thicknesses of eolian deposits (dune sand) at the site. Eolian soils are collapsible. These are windblown soils that were deposited in a loose condition and later the individual grains were connected with weak water-soluble “cement.” As identified by the Colorado Geological Survey (White and Greenman 2008), collapsible soils are dry with low density and a high void ratio. When these soils become wetted, particularly under conditions of increased loading, they can collapse several percent. This phenomenon is also known as hydro-collapse. At this site, the eolian soils are much thicker than other similar deposits in Colorado (White and Greenman 2008). The increased thickness further complicates the design and construction measures necessary to build within and upon these soils.

Photograph 1 shows a microscopic photograph of typical collapsible soil. Collapsible soils have caused structural damage to buildings and infrastructure, including damaging differential settlements and pipeline ruptures as shown in Photograph 2.

The design-build request for proposals (RFP) called for the complete removal and recompaction of the collapsible soils. By removing, reworking, replacing, and recompacting the collapsible soils, the fragile soil matrix would be destroyed and a suitable structural fill would result. Brierley was asked to evaluate whether or not a less “brute-strength” approach could be utilized and result in savings to the project.

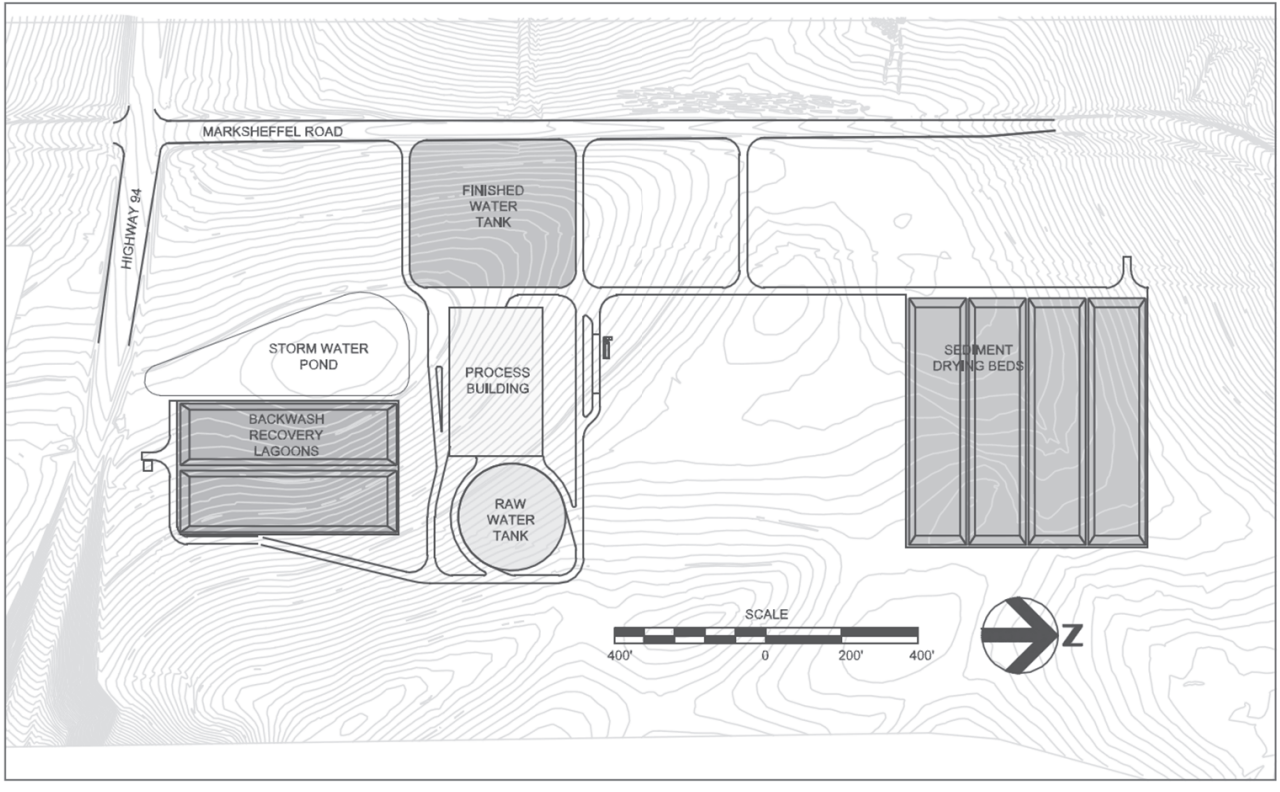

FIG. 3. Site Plan showing the proposed major structures (Image Source: Carollo Engineers)

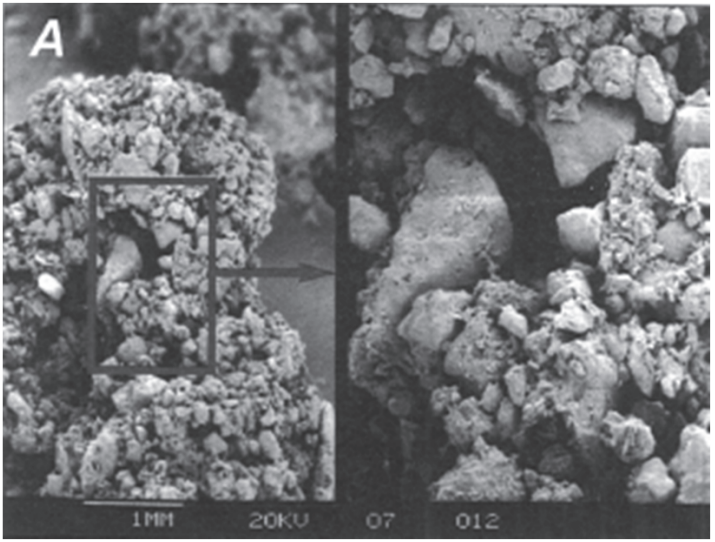

Photograph 1. Microscopic image of collapsible soil (Image Source: White 2008)

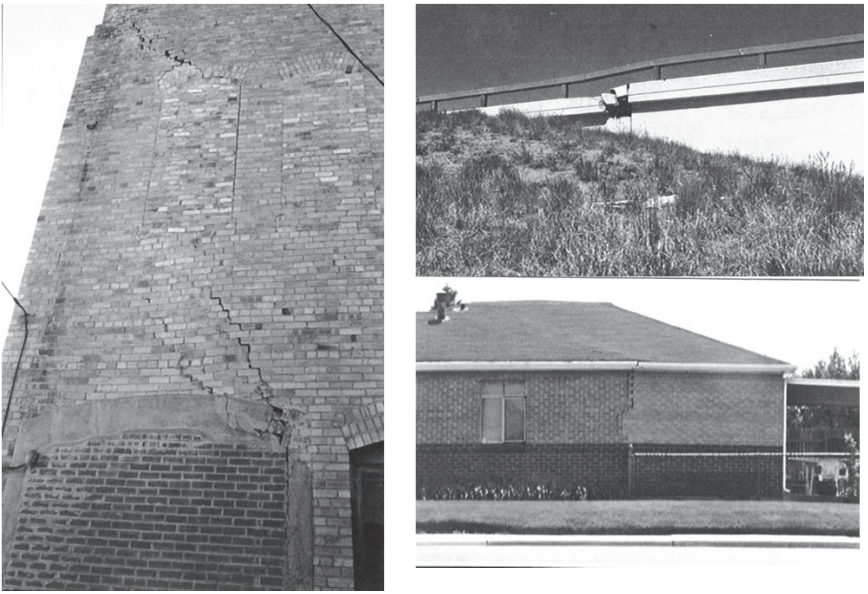

Photograph 2. Photographs of damaged structures resulting from collapsible soils (Image Source: White 2008)

PROJECT CHARACTERISTICS

The SDS project is being developed by Colorado Springs Utilities (CSU) to meet its service area demands for approximately the next 50 years. The SDS project consists of multiple components to convey, store, and treat raw water for the cities of Colorado Springs, Fountain, and Security. One of the key components of SDS project is the WTP.

The WTP site is approximately 489,670 m^2 (121 acres) and is located at the northeast corner of the intersection of Highway 94 and Marksheffel Road in Sections 4, 9, and 16, T14S, R65W. The site location is identified on Figs. 1 and 2. The WTP site was formerly used for ranching. Topographical relief at the site is about 40 ft with the highest elevation (El.), about 1935.2 m (6349 ft), near the eastern edge, approximately 335.3 m (1,100 ft) north of Highway 94 and the lowest area, near El. 1923 m (6309 ft), in the southern "low area." Based on topographic contours, the site generally drains from north to south, along the west side of the site and eventually discharges from the site through a culvert under Highway 94.

The current long-term plan for the WTP includes an ultimate plant configuration of three parallel, separately designed and constructed treatment trains. The first train will have a treatment capacity of about 189,300 m^3/d (50-mgd). The ultimate WTP capacity will be about 681,374 m^3/d (180 mgd). The current construction project includes a Process Building, a Raw Water Tank, a Finished Water Tank and Pump Station, a Backwash Recovery Lagoon, Sediment Drying Beds, a Stormwater Pond, and a Decant Pump Station.

GEOTECHNICAL INVESTIGATION

The RJH investigation included 13 geotechnical borings, which were drilled with hollow-stem augers and Standard Penetration Test (SPT, ASTM D1586) sampling. RJH also performed nine Cone Penetrometer Tests with a 266.9 kN (30-ton) truck-mounted cone rig in general accordance with ASTM D 5778. Tip resistance, sleeve resistance, and pore pressure were measured electronically as the 35.7 mm (1.4 in) diameter cone was advanced. Brierley performed 32 additional SPT borings to further define the nature and variable thickness of the collapsible soils. Additionally, thin-walled 76.2 mm (3 in) diameter relatively-undisturbed Shelby tube samples were successfully obtained within the eolian soils to reduce the potential for disturbance to the soil matrix, thus enabling higher-quality laboratory tests.

The borings indicate that subsurface materials generally consist of 8.5 m (28 ft) to 18.3 m (60 ft) of eolian soils. The eolian soils are underlain by dense, coarse alluvium, which was measured to be at least 6.7 m (22 ft) thick in areas. The alluvium is underlain by claystone, siltstone, and sandstone of the Dawson Formation. A generalized soil profile is shown on Fig. 4 and a geologic profile through the treatment train area (not including bedrock) is shown on Fig. 5.

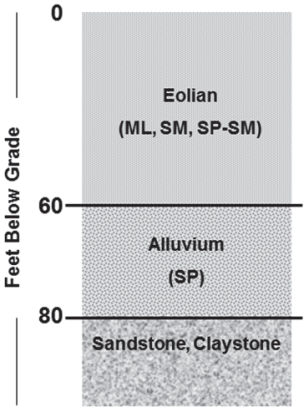

Structure	Eolian Thickness (ft)
Raw Water Tank	60
Process Building	40
Finished Water Tank	40
Sediment Drying Beds	40
Backwash Recovery Lagoons	50

FIG 4. Generalized soil profile created from geotechnical borings and the anticipated eolian thickness beneath proposed structures

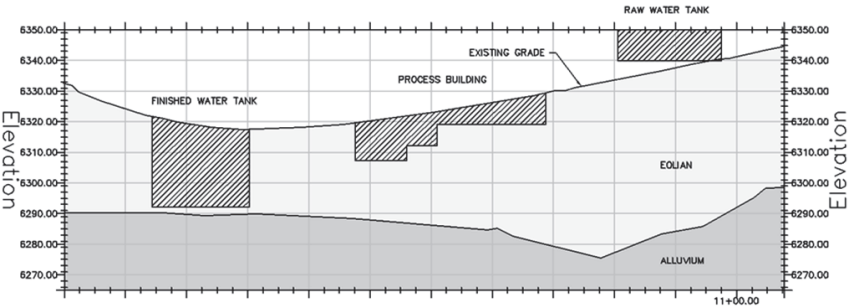

FIG. 5. Geological profile through the treatment train

Laboratory classifications (ASTM D2487) of the eolian soils deposit ranged from silt (ML) to poorly-graded sand with silt (SP-SM) with the majority of the samples classifying as silty sand (SM). Fines (minus No. 200 sieve) contents ranged from 7 percent to 51 percent and liquid limits ranged from 23 to 25. Samples showed a collapse potential (ASTM D4546) of 0.5 percent to 6.8 percent when inundated under a seating load of 47.9 kN/m^2 (1,000 lb/ft^2).

ALTERNATIVES ANALYSIS

Brierley determined that if the WTP structures were built directly on the eolian soils, settlements of up to 279.4 mm (11 in) could occur due to the collapse potential. Potential settlements of this magnitude were clearly unacceptable. Mitigation techniques, including full-depth over-excavation and replacement with compaction, pre-wetting and surcharging the site, stone columns, and deep dynamic compaction

(DDC), were considered by Brierley and the design-build team. These methods are shown in Fig. 6.

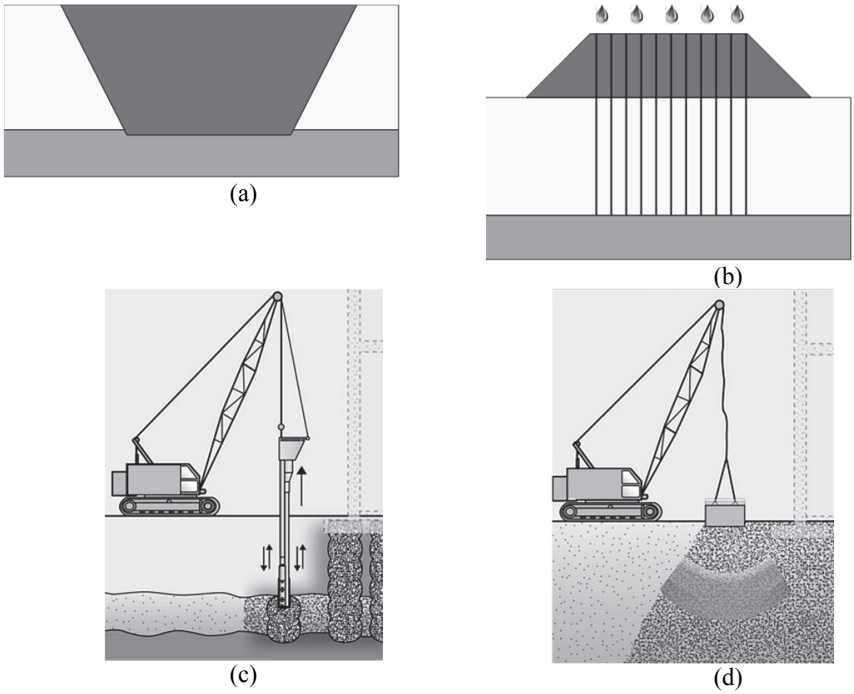

FIG. 6. Illustration of techniques used to mitigate collapse potential of eolian soils: (a) Over-excavation, replacement, and recompaction; (b) Pre-wet with wells and surcharge; (c) Stone columns (Image Source: Hayward Baker); and (d) Deep dynamic compaction (Image Source: Hayward Baker).

Pre-wetting with drains and surcharging was considered from the fundamental point of view that, if the soils were subjected to wetting via closely-spaced gravity standpipe wells and a surcharge similar to the anticipated structure loads was applied, that the collapse would be induced prior to construction, thus rendering a suitable subgrade. This method was not pursued because the amount of water needed would be tremendous and the project team did not consider this to be a tried and proven technique. The authors later realized that a method similar to this had been employed by the Bureau of Reclamation at Pueblo Dam where a 9.1 m (30 ft) thickness of similar soils was treated along a portion of the dam embankment foundation.

Stone columns are installed with large vibratory probes that penetrate into a soil deposit and introduce compacted aggregate material, which form a column of densely compacted soil as the vibratory probe is progressively raised to the ground surface.

The stone columns are installed in a grid pattern at regularly spaced intervals that reinforce and densify a zone of soil. Stone columns have the advantage of transferring structure loads to lower strata. Due to the large number of stone columns that would be required and the significant depth to deeper stable strata, stone columns were considered to be too expensive for the project.

DDC consists of repetitious free-drops of a 88.9 kN (10-ton) to 266.9 kN (30-ton) weight from a height of 15.2 m (50 ft) to 21.3 m (70 ft) (Photograph 3). This puts enormous energy into the ground and in the right soil conditions it can improve soil density for tens of feet in depth. DDC is commonly used for loose, granular soils, for old construction debris fills, and other urban "junk" fills. The application of DDC to collapsible soils is not well documented in the literature; however, a few case histories were identified. Because the eolian soils deposit is essentially loose sand cemented at the grain to grain contacts, it was reasoned that if the compactive energy from the falling weight was enough to break these bonds, then the DDC concept would be effective.

(a)

(b)

Photograph 3. Photographs of DDC equipment: (a) Crane with a 21-m height boom; and (b) 14.5-metric ton weight.

DDC was considered a viable option for subgrade improvement beneath the concrete-lined lagoon structures (sediment drying beds and backwash recovery lagoons). These structures are not as critical or as sensitive to differential settlement as the main treatment train structures. Therefore, DDC was pursued further for the lagoons and over-excavation, replacement, and recompaction was used for the main treatment train structures (Photograph 4).

Photograph 4. Aerial photograph of the main treatment train area (Source: Colorado Springs Utilities, August 2013)

DEEP DYNAMIC COMPACTION

Because the lagoons are lightly loaded structures, Brierley determined that the depth of over-excavation at the lagoons could be limited to 6.1 m (20 ft). It was further considered that if DDC was effective to a depth of about 6.1 m (20 ft), it could be applied in lieu of over-excavation. However, because DDC has not been used on Colorado's collapsible wind-blown sands, Brierley recommended that the owner and the contractor conduct a pilot test to demonstrate its effectiveness. Because of the potential for significant cost saving, a pilot test was performed.

The design-build team assembled a RFP package, which outlined locations of test plots and desired outcomes in the two areas of lagoon structures. The RFP required SPT borings and laboratory testing to be performed both before and after the DDC trials. Before and after ground surveys were also required. The grid pattern spacing was varied so that an optimized foundation treatment approach could be developed. The design-build team interviewed two specialty DDC contractors and chose Densification, Inc. to perform the pilot test, which included the anticipated DDC equipment.

The pilot test was completed in May 2013 and resulted in an average increase in SPT N-value of more than 5 blows per 30.5 cm (1 ft) (N) over roughly the upper 6.1 m (20 ft) of the eolian soils deposit and average surface settlements greater than 6 in, as determined by comparing the before and after ground surface elevations. The pilot test was deemed a success and full production DDC work began in July 2013.

The pilot test and the production DDC work utilized a 142.3 kN (16-ton) weight dropped from a height of 21.3 m (70 ft). The weight was dropped seven times per point on a 4.6 m (15 ft) by 4.6 m (15 ft) offset grid pattern as shown in Fig. 7. A total of 1,989 drops was performed for the Backwash Recovery Lagoons and 3,916 drops for the Sediment Drying Beds. The DDC work created craters, which were typically 2.7 m (9 ft) in diameter and 0.3 m (3 ft) to 1.2 m (4 ft) deep (Photograph 5). On average, soil density as inferred from the SPT tests improved by an average N-value of 6 bpf over an improvement depth of 5.5 m (18 ft) to 7.3 m (24 ft) (Fig. 8). Soil samples collected during SPT tests indicated an average increase in dry unit weight of 80.1 kg/m^3 (5 lb/ft^3) over an improvement depth of 4.6 m (15 ft) to 7.3 m (24 ft) (Fig. 9). Ground surface settlements, as measured by before and after ground surveys, ranged from 177.8 mm (7 in) to 215.9 mm (8.5 in).

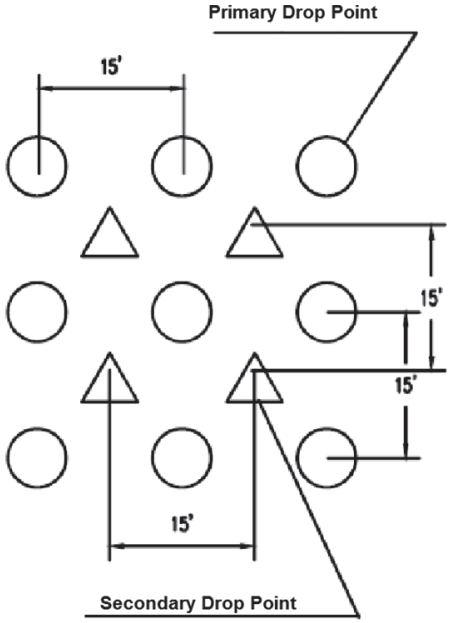

FIG. 7. DDC drop point grid pattern

(a)

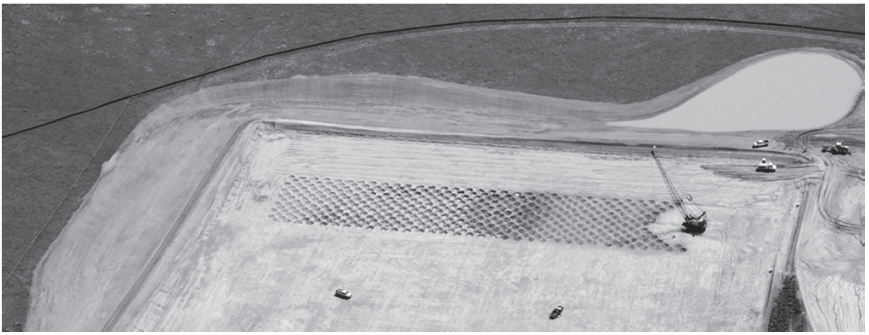

(b)

Photograph 5. Photographs of DDC at the Sediment Drying Beds: (a) Craters formed during the DDC pilot test; and (b) Aerial view of DDC craters formed during production (Source: Colorado Springs Utilities).

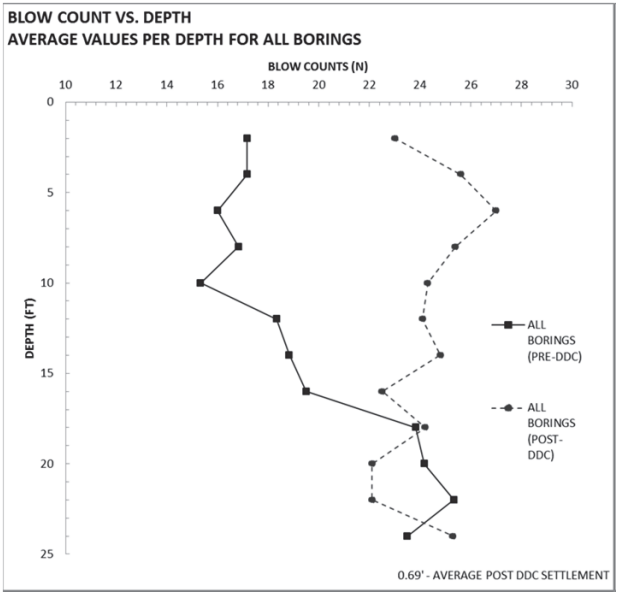

(a)

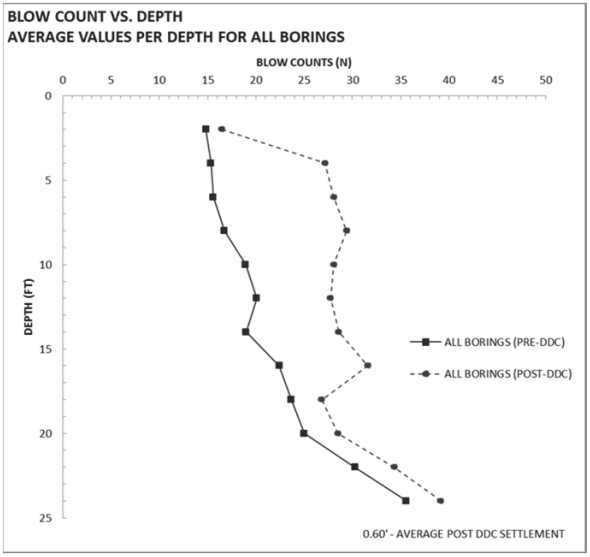

(b)

FIG. 8. Blow count versus depth: (a) Backwash Recovery Lagoon (b) Sediment Drying Beds

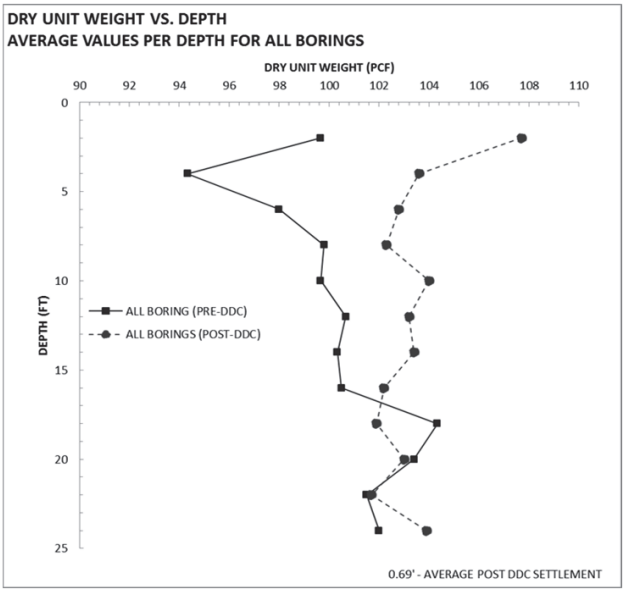

(a)

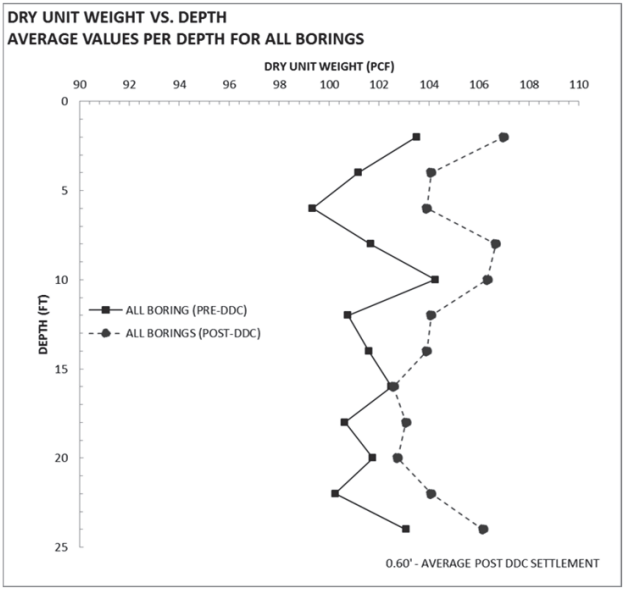

(b)

FIG. 9. Dry unit weight versus depth: (a) Backwash Recovery Lagoon (b) Sediment Drying Beds

CONCLUSION

Ground improvement using Deep Dynamic Compaction was tested and implemented in lieu of massive over-excavation for certain structures at the Southern Delivery System Water Treatment Plant. The WTP is currently under construction in Colorado Springs, Colorado. DDC was successful in increasing soil density and significant pre-construction ground surface settlement was induced by the method. Compared to the alternative of 6.1 m (20 ft) of over-excavation, the use of DDC eliminated approximately 1,682,020.7 m^3 (2,200,000 yd^3) of excavation, replacement, and recompaction. Although not specific to this project, DDC typically costs about $5 per 0.8 m^3 (1 yd^3) of improved soil. Over-excavation, replacement, and recompaction is estimated to cost approximately twice that amount. It is clear that DDC resulted in significant cost savings to this project.

REFERENCES

Lovelace, A.D., Bennet, W.D., & Lueck, R.D., (1982), "Test Section for the Stabilization of Collapsible Soils on Interstate 25, Project 1-025-4 (58) 243, Algodones, New Mexico, Santa Fe". *New Mexico State Highway Department* Report MB-RR-83-1.

RJH (2009). "Southern Delivery System Geotechnical Engineering Report for the Water Plant."

Rollins, K.M. and Kim, J. (1994) "U.S. Experience with Dynamic Compaction of Collapsible Soils." ASCE, *Geotechnical Special Publication* No. 45, In-Situ Deep Soil Improvement, p. 26-43.

United States Geologic Survey (2013). "Elsmere Quadrangle".

White, J. and Greenman, C. (2008). "Collapsible Soils in Colorado." *Colorado Geological Survey Engineering Geology 14*.

Needle's Eye Tunnel Repair Feasibility Study

Christoph Goss[1], P.E., Ph.D. M. ASCE and Don W. Deere[2], P.E. M. ASCE

[1]Principal, Deere & Ault Consultants, Inc., 600 South Airport Road, Suite A-205, Longmont, CO 80503; christoph.goss@deereault.com
[2]Chairman, Deere & Ault Consultants, Inc., 600 South Airport Road, Suite A-205, Longmont, CO 80503; don.deere@deereault.com

ABSTRACT: The Needle's Eye Tunnel is located at elevation 3536 m (11,600 ft) near the top of Rollins Pass on Boulder County Road 117/US Forest Service Road 149 approximately 32 km (20 miles) west of Rollinsville, Colorado. The location of the Needle's Eye Tunnel is shown on Fig. 1. The curved tunnel is approximately 46 m (150 ft) long, 6.7 m (22 ft) wide, and 7.3 m (24 ft) tall. A sketch of the plan and profile is found in Fig. 2. The tunnel was blasted through a mixture of granite and gneiss, typical in the Front Range of the Rocky Mountains. Current ground support consists of rock bolts and wire mesh. During the 20th Century, the tunnel was part of a railroad and vehicle road alignment. Since 1990, the tunnel has been closed to traffic. In 2012, Deere and Ault Consultants, Inc. (D&A) was hired by the Rollins Pass Restoration Association (RPRA) to evaluate the feasibility of repairing the tunnel so that it could be re-opened for low volume vehicle and pedestrian traffic between Rollinsville and Winter Park. The evaluation by D&A showed that the tunnel is currently unsafe for traffic but could be rehabilitated with a mixture of shotcrete, rock bolts, and drains.

HISTORY

The tunnel was originally the temporary "Hill Route" section of the standard gage Moffat Railroad (Denver Northwestern and Pacific Railway) constructed between 1903 and 1905 between Denver and Hot Sulphur Springs. It remained in use until the Moffat Tunnel was completed in 1928. During that time, it was used to both transport goods and tourists between Denver and the mountain communities. There was even a hotel and restaurant at the summit. In 1937, the railroad alignment was converted to a primitive road and in 1955 it was upgraded to a 4.8 m (16 ft)-wide auto road. In 1979, the road was closed to traffic. Engineering studies were conducted in 1981 (Amuedo & Ivey), 1985 (MSHA), and 1986 (Centennial Engineering plans and specifications, Rocky Mountain Consultants review letter). Repairs were completed in 1987 and the road was re-opened in 1988. In 1990, a rock fall near the northeast portal resulted in a

tunnel closure that is still in effect today. In 1992, a repair alternatives study was conducted, but no construction work was performed.

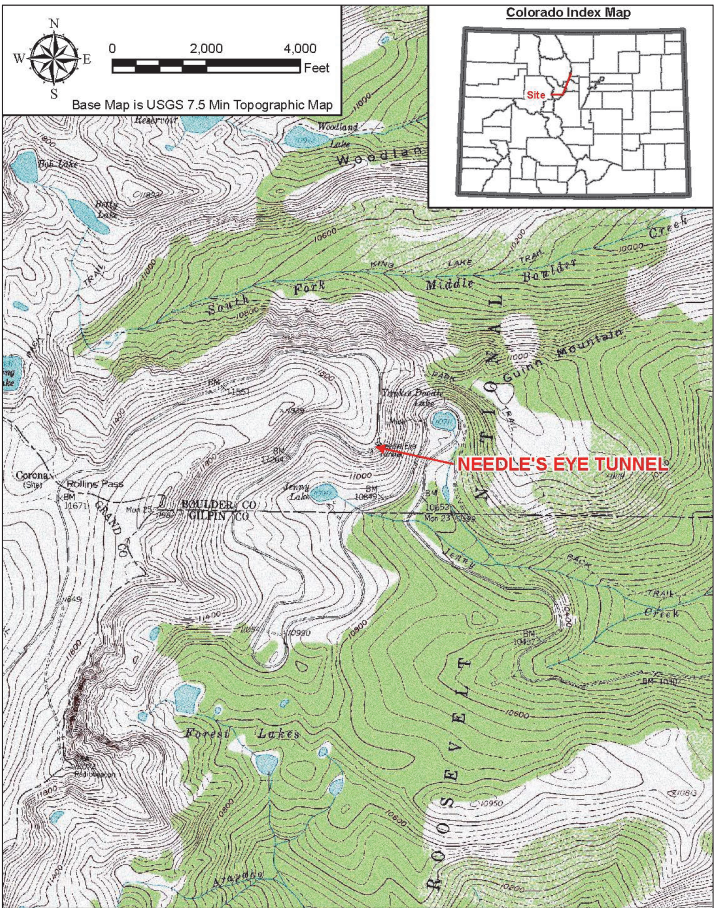

FIG. 1. Vicinity Map

LITERATURE REVIEW

As part of the feasibility study, D&A reviewed two existing reports. The first report was by Dr. Ron Heuer to Boulder County, dated October 3, 1990. This report was written in response to the July 15, 1990 rock fall. D&A generally agreed with the report, in particular Dr. Heuer's rock mass descriptions:

- Granitic or gneissic rock
- Closely to moderately jointed

- Slightly to moderately weathered
- Discolored joint surfaces
- Small amounts of weaker material present in joints
- Blocky to very blocky
- Locally moderately blocky and seamy
- Overall fair quality

D&A shared Dr. Heuer's concerns that the circumferential spacing of the bolts as installed was too wide (particularly at the portals) and that this was the primary cause of the rock fall. D&A also pointed out his concerns about ice wedging and its ability to loosen the rock blocks.

The second report that D&A reviewed was "*Repair Alternatives, Risk Analysis, and Remedial Measures for the Needle's Eye Tunnel*" prepared by Parsons Brinkerhoff Quade & Douglas, Inc. (PB) for Boulder County, dated March 1992. It evaluated various repair alternatives including costs and potential risks. D&A used their tunnel stationing and dimensions in the evaluation. D&A generally agreed with PB's geologic descriptions, freeze-thaw concerns, and repair alternatives but did not agree with the specifics of their risk analysis, particularly the annual probability of failures with various repair alternatives.

Both reports refer to the joint sets originally mapped by Amuedo & Ivey in 1981.

Table 1: Joint Sets Mapped by Amuedo & Ivy 1981

Joint Number	Strike	Dip
1	N45°W +/-12°	90°+/-29°
2	N52°E +/-22°	80° SE+/-22°
3	N17°W +/-19°	26°SW +/-16°
4	N37°E +/-26°	42°NW +/- 42°

Based on PB's plan sheets, the alignment of the tunnel varies from N65°E at the southwest portal to N40°E at the northeast portal (see Fig. 2).

SITE VISIT

On September 12, 2012, D&A and RPRA staff visited the tunnel to observe and photograph the conditions of the rock and the rock support. Aside from its high elevation, two of the striking features of the tunnel are its short length and shallow cover (height of rock above the tunnel). Photograph 1 shows the southwest portal (Rollinsville side). Of note are the steeply dipping joints on the left with accompanying loose rock on the ground. Photograph 2 shows a rock fall from the north crown in the middle of the tunnel. The bolts and mesh are generally in good shape with little corrosion, this is typical for dry, high altitude environments. Photograph 3 shows the shear that forms the north wall and the 1990 rock fall at the northeast portal. Photograph 4 shows the northeast portal looking southwest.

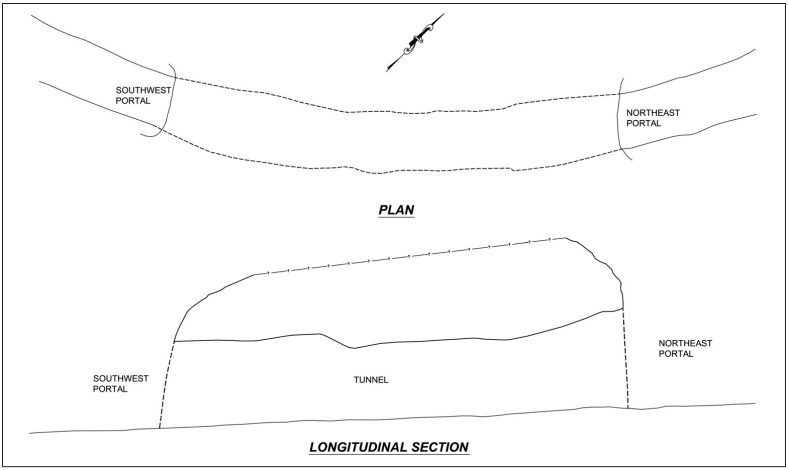

FIG. 2. Tunnel plan and profile (adapted from Parsons Brinckerhoff Quade & Douglas Inc, 1992)

Photograph 1. Southwest portal overview; note loose rock on left side and low cover over tunnel

During the site visit, D&A staff examined the geology. The rock types are partially igneous and metamorphosed migmatite/granite gneiss. This agreed with Dr. Heuer's description of granitic or gneissic rock, PB's description of quartz monzonite gneiss, and geologic mapping by Gable in 2000 that shows quartz monzonite with sillimanite-biotite gneiss. The rock condition ranged from fresh to moderately weathered.

Photograph 2. Failed mesh and loose rock in mesh near tunnel middle; partial source of rock fall

Photograph 3. Looking southwest with both rock falls visible; note angled tunnel walls

D&A observed the same joint sets noted previously, but took particular notice of Amuedo & Ivey's joint set number two. It strikes northeast and dips sharply to the southeast. This key joint set locally contains hydrothermally altered shears (zones of displacement containing ground up rocks and clay) and controls the tunnel behavior. It forms the smooth-faced north wall and controls the shape of the south wall. Shears in this joint set are most visible on the north wall where zones of alteration and moderate weathering appear as weak or "punky" rocks.

Photograph 4. Northeast portal overview looking southwest; note the low cover over the tunnel

Two significant rock falls were visible in the tunnel. The first was the 1990 rock fall at the northeast portal. There has been some additional raveling of the rock in that area. The second was a previously undocumented rock fall along the north wall near the middle of the tunnel. There appeared to be two sources of this rock fall, both associated with the north wall shear zone. Some of the rock appeared to have come from the north wall below the bolts and mesh. The rest of the rock came from the upper left crown where dangling wire mesh is visible. This confirmed the previous evaluations that the tunnel was not stable with the existing support.

Overall, the ground conditions in the tunnel can be described as per Heuer: blocky to very blocky, locally moderately blocky and seamy, and overall fair (to locally poor) quality. D&A noted that due to the shallow cover of approximately 5m (16 feet), the rock blocks are de-stressed or looser than in a deeper tunnel. This makes them more prone to sliding. The shallow, de-stressed, blocky ground at high altitude on the southeast face of a mountain also makes the tunnel particularly susceptible to freeze-thaw damage. As snow melts during the day, water seeps into the rock joints and freezes during the night. The "swelling" pressure from the ice loosens and jacks out individual rock blocks.

ANALYSES

D&A performed several analyses to evaluate the ground conditions and potential support options. The first analysis was a Tunneling Quality Index (Q system) rock mass classification. The Q system was developed by Dr. Nick Barton in 1974 and has been periodically revised. It is a classification system developed from many tunnel case histories that takes into account various components of the rock mass through which the tunnel is advanced. A detailed discussion of this and other rock mass classification systems can be found in Hoek (2007) and at www.nickbarton.com. For the Needle's Eye Tunnel analysis, D&A used the parameter ranges in Table 2.

Table 2. Q System Parameters Used in Analysis

Parameter	Value	Description
Rock Quality Designation (RQD)	75-90	Fair-Good
Joint Set Number J_n	9-12	3 joint sets to 3 joint sets + random
Joint Roughness Number J_r	1-1.5	Smooth planar-rough planar
Joint Alteration Number J_a	1-2	Unaltered joints-slightly altered joints
Joint Water Reduction J_w	1	Dry or minor inflow
Stress Reduction Factor (SRF)	5	Single shear zone in shallow rock or loose open joints
$Q = \frac{RQD}{Jn} \times \frac{Jr}{Ja} \times \frac{Jw}{SRF}$	**Q=**	**0.6-3**

Fig. 3 shows a support chart developed by Grimstad and Barton (1993) that recommends rock reinforcement categories for various combinations of tunnel size, type, and rock mass classification. For this tunnel with an ESR of 1, it recommends 5 cm to 8 cm (2 in to 3 in) thick fiber reinforced shotcrete (sprayed concrete) and rock bolts at 1.5 m to 2 m (5 ft to 6 ft) spacing.

Another commonly used rock mass classification is the Geomechanics Classification or Rock Mass Rating (RMR) system (Bieniawski, 1989). Like the Q system, it combines various geologic parameters that affect ground behavior. For the Needle's Eye Tunnel analysis, D&A used the parameter range in Table 3.

The recommended support for this category is systematic bolts 1.5 m (5 ft) on center in the crown and walls with wire mesh and 5 cm to 10 cm (2 in to 4 in) of shotcrete. This is very similar to the Q system result.

To validate the rock mass classification system recommendations, D&A utilized a computer model to evaluate the specific conditions at the Needle's Eye Tunnel. Given that the rock in this tunnel is hard but jointed, the most likely type of ground failure will be a block failure, where a block or group of blocks falls out along joints or cracks in the rock mass. D&A used the computer software Unwedge 3.0 by Rocscience to model a 6.7 m (22 ft) by 7.3 m (24 ft) rough horseshoe tunnel on an axis 40 to 65 degrees. D&A input the joint orientations per Amuedo & Ivey and assigned joint properties to both the typical and sheared joints. No groundwater pressure was modeled at this design level. Finally, D&A added the existing support of 25 mm (1 in) diameter, 2.4 m (8 ft)-long rock bolts 1.5 m (5 ft) on center along the tunnel and 2 m (7 ft) on center across the tunnel walls and crown. The model then computed the largest rock blocks that could form given the combination of joints, tunnel size, tunnel orientation, and support. Fig. 4 shows the graphical result of this analysis at the north wall.

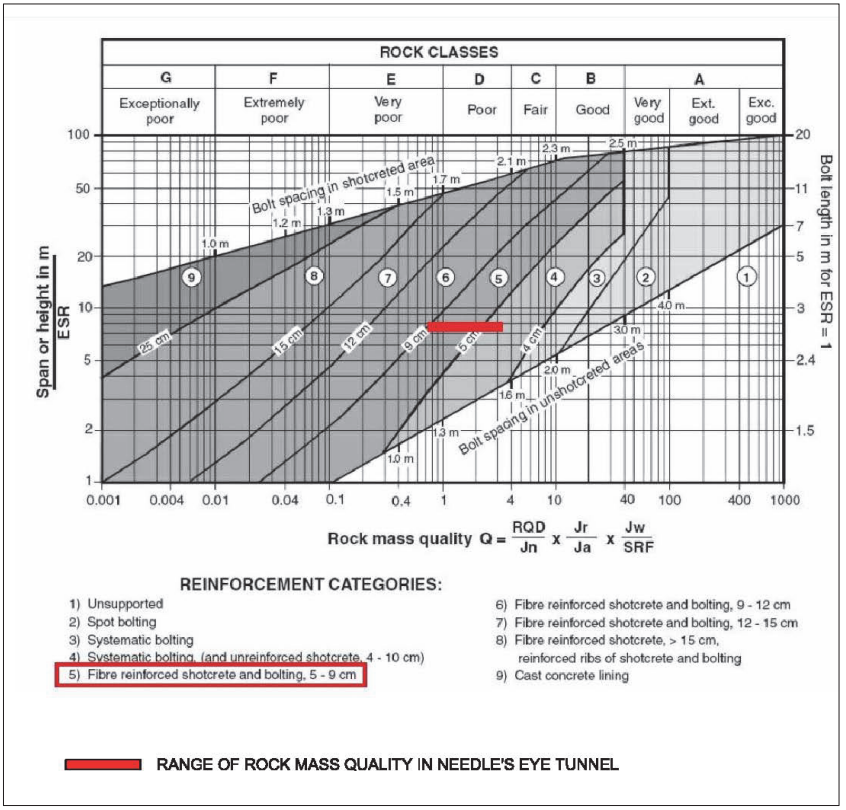

FIG. 3. Q System Support Chart (Grimstad and Barton 1993)

Table 3: RMR Parameters Used in Analysis

Parameter	Value	Description
Intact Rock Strength	7	50-100 MPA (7250-14,500 psi); medium strength
Rock Quality Designation (RQD)	17	75-90%; Fair-Good
Discontinuity Spacing	10	20-60cm (0.7-2 ft)
Discontinuity Condition	20	Slightly rough surface, highly weathered walls
Groundwater Inflow	10	Damp
Strike & dip orientation	-12	Very unfavorable; steep shear parallel to tunnel
RMR	**52**	**Class III Fair Rock**

For the existing conditions, the model showed two failures, one in the north wall (shown on Fig. 4) and one at the northeast portal (not shown). Computed factors of safety were 0.7 and 0.1, respectively. Any factor of safety at or below 1.0 is considered to be unsafe. In the authors' opinion, for a tunnel with occasional public foot and vehicle traffic, a factor of safety around 1.5 should be considered the minimum. The model results confirmed what had been observed in the field. Rock falls occurred at the north wall and the northeast portal. In fact, the lowest factor of safety was at a tunnel orientation of 52 degrees (parallel to the main shear), which is essentially the tunnel alignment near the middle where the new rock fall had occurred.

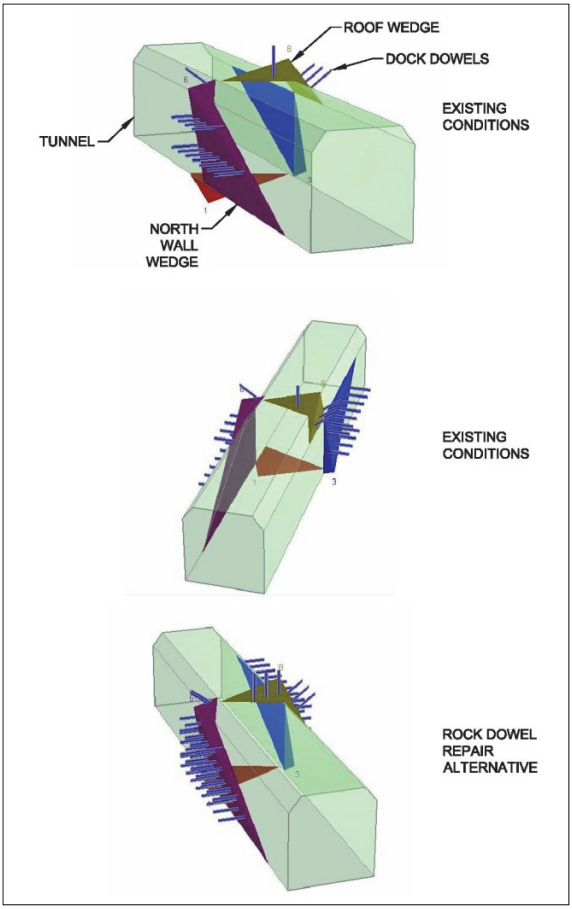

FIG. 4. Unwedge Rock Block Analysis

Comfortable that the model results were reasonable, D&A tested several rock bolt layout scenarios to evaluate their impact on the factor of safety. All bolts were 25 mm (1 in) diameter and 2.4 m (8 ft)-long. Changing the rock bolt spacing to1 m (3.5 ft) on center (i.e., placing a new bolt between each existing one) increased the factor of safety to 1.2. Adding a 1.5 m (5 ft) by 1.5 m (5 ft) pattern between existing bolts in the north crown and wall increased the factor of safety to 1.3. Doing both scenarios increased the factor of safety to 1.9. This shows that by doubling the existing number of bolts in each row and adding a new row of bolts between the existing rows, along with some spot bolting in the north wall and crown, should adequately stabilize the ground.

Next D&A modeled a mixture of rock bolts and shotcrete. New rock bolts were placed between the existing ones in the north wall and crown. A 34 MPa (5,000 lb/in^2) compressive strength (1.2 MPa (174 lb/in^2) shear strength) layer of shotcrete was then added to the inside of the tunnel from 1m (3 feet) above the floor up both walls and across the entire crown. The resulting minimum factors of safety were 2.6 for a 75 mm (3 in)-thick layer and 3.0 for a 100 mm (4 in)-thick layer of shotcrete. In all scenarios, the controlling wedges were located at the north wall and the portals.

REPAIR OPTIONS

Based on the empirical analyses and modeling, D&A concluded that there are two technically feasible repair options that rely on a combination of rock bolts, wire mesh, and shotcrete. The first option is a significant amount of rock bolting throughout the tunnel and installation of additional wire mesh with a minor amount of shotcrete placement at the portal brows and the north wall shear. The second option is a smaller bolting effort focused on the north wall with a shotcrete lining of the entire tunnel. Figs. 5 and 6 show sketches of the two repair options.

While repairs can be completed with small equipment that can be hauled up in pickup trucks, there would likely be some required road improvements for easier equipment and materials access. Once at the site, the contractor would have to carefully remove sections of the wire mesh to let the accumulated loose rock out. The contractor would then have to scale the ground to remove any other loose rocks and replace the mesh. The existing and new rubble (muck) would then have to be hauled out of the tunnel. Depending on permit requirements, it may be possible to dispose of the waste rock near the tunnel, but for planning purposes a longer haul should be assumed. Next the contractor would have to replace the chain link at portals with wire mesh (or just add wire mesh to the top).

For the rock bolts and wire mesh option (1), the contractor would install new rock bolts in each row half way between the existing bolts (9 bolts per 30 rows or 270 bolts) and bring the bolting further down to 3 feet above the floor. Next bolts would be installed on a 1.5 m by 1.5 m (5 ft by 5 ft) pattern in the crown and north wall (6 bolts per 30 rows or 180 bolts). Then additional bolts would be installed in the portal areas both inside and outside (60 bolts per portal for a total of 120). Finally, there would be some local spot bolting for specific blocks, particularly in the shear area (assume 30 bolts). The total number of bolts would be around 600. Note that this spacing is much closer than typical for mining and underground construction. New

wire mesh would be placed throughout the tunnel and around the portals. To help drain the ground and thereby make the tunnel more resistant to freeze/thaw damage, around 75 weep holes 3 m to 4 m (10 ft to 15 ft) long and inclined upward would be drilled from inside the tunnel on a regular spacing. Local shotcrete is recommended on the north wall shear and around the portals. Given the small estimated quantity of shotcrete, around 15 m^3 (20 cy), the most likely placement method would be the dry-mix process using a small, portable pot and premixed sacks. Since both new and existing wire mesh will act as reinforcement, fiber reinforcement is not required.

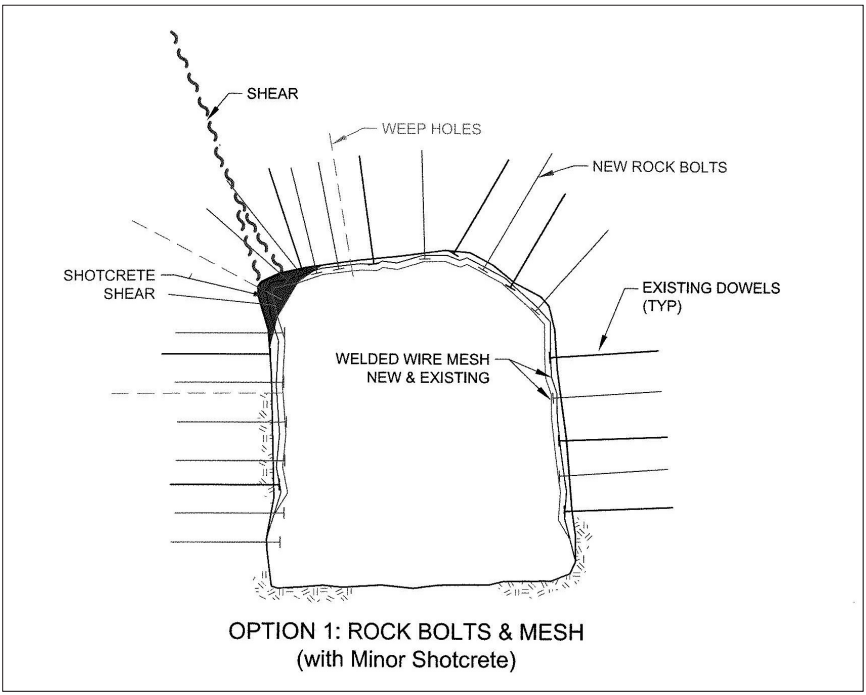

FIG. 5. Rock Bolts and Mesh

For the shotcrete option (2), the contractor would first install new rock bolts between the existing ones in the north wall and crown (5 bolts per 30 rows or 150 bolts). Then additional bolts would be installed in the portal areas both inside and outside (30 bolts per portal for a total of 60 bolts). Finally, there would be some local spot bolting for specific blocks, particularly in the shear area (assume 30 bolts). The total number of bolts would be around 240. Then 8 cm (3 in) of shotcrete would be sprayed inside the tunnel from 1 m (3 ft) above the floor up both walls, and across the crown. The shotcrete would be thickened around the north wall shear. Shotcrete would also be placed around both portals. Given the large shotcrete quantity, approximately 95 m^3 (125 cy), a modular batch plant would likely be set up on site

and the shotcrete sprayed using the wet-mix method. Since the existing wire mesh will act as reinforcement, fiber reinforcement is not required. To help drain the ground and thereby make the tunnel more resistant to freeze/thaw damage, around 75 weep holes 3 m (10 ft) to 4.5 m (15 ft) long and inclined upward would be drilled from inside the tunnel on a regular spacing after the shotcrete was placed.

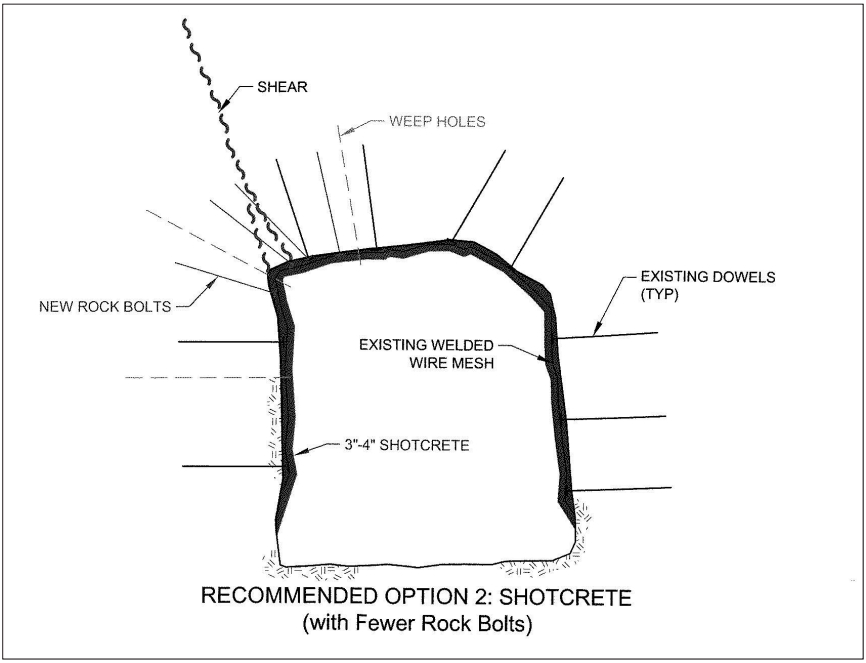

FIG. 6. Shotcrete and Rock Bolts

RECOMMENDATIONS

As shown both in the field and in the model, the Needle's Eye Tunnel is currently not safe for public access. Continued weathering and spalling will likely result in more rock falls in the future. Repairing the Needle's Eye Tunnel will require both additional bolting and shotcrete. Two options have been presented in this paper. The proportions of bolting and shotcreting can be adjusted for cost effectiveness and other considerations during the final design. While the bolt and wire mesh option (1) is estimated to be somewhat cheaper than the shotcrete option (2), it would require regular long-term inspection and maintenance. The shotcrete lining presents a low maintenance option that would be easier to construct, be more typical for public structures, and likely be more acceptable. The disadvantage of the shotcrete option is that it would cover historic soot marks and change the look and feel of the tunnel. Given the relatively small price difference, constructability, and lower maintenance, D&A recommended the shotcrete lining (2) as the preferred option.

ACKNOWLEDGEMENTS

The authors would like to thank the Rollins Pass Restoration Association for the opportunity to work on this project with them and to allow the publication of this paper.

REFERENCES

Amuedo & Ivey, 1981, Geotechnical Investigations report dated March 3, 1981

Barton, N.R., Lien, R. and Lunde, J. 1974. Engineering classification of rock masses for the design of tunnel support. *Rock Mech.* **6**(4), 189-239.

Bieniawski, Z.T. 1989. *Engineering rock mass classifications.* New York: Wiley.

Gable, Dolores, 2000, *Geologic Map of the Proterozoic Rocks of the Central Front Range, Colorado*, Geologic Investigations Series I-2605, USGS

Grimstad, E. and Barton, N. 1993. Updating the Q-System for NMT. *Proc. int. symp. on sprayed concrete - modern use of wet mix sprayed concrete for underground support*, Fagernes. 46-66. Oslo: Norwegian Concrete Assn.

Hoek, Evert, 2007, *Practical Rock Engineering,* Rocscience, Toronto, Ont, Canada

Heuer, Ron, 1990, Letter Report to Boulder County titled *File 9015 Needles Eye Tunnel*, dated October 3, 1990

Parsons Brinckerhoff Quade & Douglas Inc, 1992, Report to Boulder County titled: *Repair Alternatives, Risk Analysis, and Remedial Measures for the Needle's Eye Tunnel*, dated March 1992

Ground Classification for Trench, Shaft, and Slope Excavations

Sarah Myers[1], E.I.T., M.ASCE, Bill Zietlow[2], P.E., Robin Dornfest[3], P.G., M.ASCE, and Rebecca Brock[4], P.E., P.G., M.ASCE.

[1]Staff Engineer, Brierley Associates, 990 S. Broadway, Suite 222, Denver, CO 80209; smyers@brierleyassociates.com
[2]Senior Associate Engineer, Brierley Associates, 990 S. Broadway, Suite 222, Denver, CO 80209; bzietlow@brierleyassociates.com
[3]Central Region Manager, Brierley Associates, 2629 W. Redwing Road, Suite 150, Fort Collins, CO 80526; rdornfest@brierleyassociates.com
[4]Associate Engineer, Brierley Associates, 990 S. Broadway, Suite 222, Denver, CO 80209; rbrock@brierleyassociates.com

ABSTRACT: Soft ground tunnel/trenchless designers and contractors have used the Tunnelman's Ground Classification system (Heuer, 1974 after Terzaghi, 1950) for over 60 years to describe potential ground behavior for tunneling. Geotechnical baseline reports (GBRs) utilize the Tunnelman's Ground Classification system to baseline ground behavior for trenchless construction. More recently, GBRs are being used to describe soil behavior for shafts and open-cut excavations utilizing the same method. Use of this system for shafts and open-cut construction is outside the original intent of the classification scheme and subsequent modifications. While many ground types behave similarly in tunnels, shafts, and open-cut excavations, there are considerations that are unique to shaft and open-cut excavations. This paper introduces a modified ground behavior classification system for use specifically in describing ground behavior for trench, shaft, and sloped excavations in soils based on the Tunnelman's Ground Classification system. This system provides classification of different ground behaviors, descriptions of the ground behavior, typical soil types associated with those behaviors, and impacts of groundwater on the behaviors. The proposed classification system could be used in not only GBRs but incorporated into traditional geotechnical evaluation and recommendation reports, which commonly refer to OSHA guidelines for minimum slopes, but do not address ground behavior.

INTRODUCTION

Data from infrastructure projects, geotechnical evaluations, and recommendation reports typically provide the designer with the information needed to design both open-cut sections and trenchless crossings. The designer prepares construction documents which typically include a clause that the contractor cannot rely on

anything aside from the factual data contained in the geotechnical report. Contractors therefore are not able to rely on the discussions and other pertinent information contained within the reports when preparing bids and defending differing site condition claims.

For trenchless projects, geotechnical engineers commonly produce geotechnical data reports (GDRs) and geotechnical baseline reports (GBRs). These documents are typically included as contract documents and have become an effective tool to manage risks and control cost. The GBR becomes a contractual document upon which the contractor is to rely on during the bidding phase and when determining if a differing site condition has been encountered. The GBR explicitly states how the contractor should expect the ground to behave. For trenchless projects, GBR writers often rely on a classification of ground behaviors that was originally developed by Terzaghi (1950) and modified by Heuer (1987) as a baseline of the ground behavior anticipated throughout a project. This modified version of the Tunnelman's Ground Classification system is an empirical classification scheme whereby the ground is categorized in different groups based on typical behavior at the face of a small diameter tunnel open to the atmosphere.

Although not intended for open-cut construction, the Tunnelman's Ground Classification system is frequently used in GBRs to describe potential ground behavior in open-cut portions of the alignment, as well as the trenchless reaches of a project where a GBR is provided.

Our proposed *Trench, Shaft, and Slope Ground Classification for Soils* system is intended to utilize the Tunnelman's Ground Classification system but provide appropriate terminology and explanations for ground behaviors specific to trench, shaft, and/or slope excavations, independent of construction means and methods. This proposed classification system provides the appropriate equivalent to the Tunnelman's Ground Classification system which was developed specifically for tunneling. Our intent is to introduce a modified system that removes confusion or ambiguity experienced in past instances where the Tunnelman's Ground Classification system was applied to non-tunnel projects. Descriptions of ground behavior that are relevant to the type of project would be beneficial for general communication as well as for GBRs, as they become more common for projects outside of tunneling.

GROUND BEHAVIOR CLASSIFIATION FOR TUNNELS

In 1946, Dr./Prof. Karl Terzaghi introduced what has come to be known as the Tunnelman's Ground Classification system for rock that was published in "Rock Tunneling with Steel Supports" by Proctor, White, and Terzaghi who labeled "terms describing rock condition.". In 1950, Terzaghi presented the equivalent classifications for soil in a chapter of "Applied Sedimentation" by Task and Parker entitled "Geologic Aspects of Soft-Ground Tunneling" that Terzaghi called "TunnelMan's Ground Classification". In both cases, Terzaghi's apparent intent was to provide descriptions of ground behavior during tunnel construction that were distinct from geologic descriptions of the type of ground. The idea was that formations that were geologically distinct and perhaps very different may behave similarly under similar conditions induced by construction, and vice versa. The grouping by behavior rather

than by geologic classification was a breakthrough concept and important for engineering purposes. These descriptions gave the tunnel engineering community both a standard way of discussing ground conditions relevant to their work and a design tool useful in different methods of ground support design.

The Tunnelman's Ground Classification system has since been used extensively in tunnel engineering and has become part of the standard of practice for geotechnical engineers in designing underground structures. It has been referenced by many and has been slightly modified over the years by Peck, Deere, Brandt, Heuer, and Rose. Several empirical tunnel support design methods have been developed based on the Tunnelman's Ground Classification system. Most recently, the Tunnelman's Ground Classification system has become part of most tunneling project's contract documents through the use of the GBR.

CURRENT PRACTICE FOR GEOTECHNICAL REPORTS

The U.S. Department of Transportation - Federal Highway Administration states "the importance of preparing an adequate geotechnical report cannot be overstressed." Geotechnical reports summarize the results of the subsurface investigation, provide design recommendations and criteria and construction considerations. Geotechnical design and recommendation reports are commonly utilized during the project design and construction phases, and, if needed, when resolving disputes that arise during construction.

A geotechnical design and recommendation report typically includes geotechnical/geologic data, design recommendations, design criteria, and construction considerations. The report is typically written primarily for the designer and is not usually included in the contract documents. Geotechnical design and recommendation reports may sometimes be referred to as the basis of design report, the geotechnical investigation report, or a topic-specific technical memorandum.

In the tunneling industry, there are two common types of geotechnical reports, GDRs and GBRs. For these tunneling projects, the GDR and GBR are often included as a part of the contract documents. In the contract hierarchy of documents, the GBR usually takes precedence over the GDR.

The GDR typically includes the factual findings of the field exploration program (borings and geologic mapping), in-situ testing, and laboratory testing. A summary of the background and literature review(s) conducted prior to the development of the exploration plan is often included. The GDR does not contain interpretations, design criteria, or construction recommendations. The purpose of separating the relevant data in the GDR from interpretation is to create a single location for unbiased factual data for use by the design team and the contractor.

As previously mentioned, geotechnical design and recommendation reports may be created for use in conveying information within the design team, and it is within these documents that design parameters related to recommended slopes, which may refer to OSHA Health and Safety Standards for Excavations (29 CFR Part 1926) for specific slope height, slope inclination, excavation depths, and subsurface classification. Additionally, other recommendations, such as lateral earth pressures, compaction requirements, and other necessary design information, would be presented.

The GBR is an interpretation of the factual data presented in the GDR. The GBR describes the anticipated subsurface conditions and ground behavior. The baseline statements are contractual assumptions and are not necessarily geotechnical facts. The GBR is intended to establish contractual geotechnical baseline conditions on which the contractor can base his bid; this approach results in fair and comparable bids, not based on assumptions of risk. GBRs are also used during administration of the construction contract where measurable and impartial baselines set the mark for fair compensation if differing site conditions are encountered during construction. While the GBR may address construction considerations for the contractor, specific design recommendations are generally not included. Typically, GBRs are prepared in general accordance with the Geotechnical Baseline Reports for Underground Construction, Guidelines and Practices published by ASCE (2007).

The use of geotechnical reports as contract documents was fairly unique to the tunneling industry. However, incorporating GDRs and GBRs into the contract documents is becoming more prevalent for not only the tunnel and trenchless portions of projects, but for the shafts and open-cut excavation (or cut-and-cover) components of the same or standalone projects.

PROPOSED GROUND CLASSIFICATION SYSTEM

Currently, when baselines of ground behavior for shafts and open-cut excavation portions of projects are included in the GBR, the Tunnelman's Ground Classification system is often utilized to describe and baseline ground behavior during the unsupported phase of excavation. Our proposed *Trench, Shaft, and Slope Ground Classification for Soils* system allows the GBR writer a more appropriate reference to describe how the ground will behave. It should be noted that the purpose of the proposed classification system is to describe ground behavior caused by unsupported excavations. The time period after excavation during which these behaviors occur varies from short-term (minutes to hours) to medium-term (days to weeks) to long-term (months to years). Changing the groundwater table by dewatering may or may not change ground behavior, partially in silts and lean clays, and should be explicitly discussed in the GBR.

Our proposed classification system solely describes anticipated ground behavior during unsupported excavation of slopes and vertical cuts. The intent of this proposed system is to describe ground behavior independent of construction means and methods. There are a number of other behaviors related to the ground that may be appropriate to include as baselines for a particular project, such as base and global stability, ability to dewater, reuse of spoils for fill, and others discussed in the ASCE suggested guidelines (2007). If used, these other behavior descriptions should be included as part of the construction considerations. Ground support and safety regulations should refer to OSHA guidelines. Our proposed classification system should be used in conjunction with OSHA guidelines and is not intended to replace OSHA guidelines.

The proposed *Trench, Shaft, and Slope Ground Classification for Soils* system is as follows:

Firm

Firm ground is likely to be encountered in stiff to hard clays, cemented granular soils, and dense, silty, or clayey granular soils. Soils exhibiting firm ground behavior are generally above the groundwater table. Vertical excavations will display stable behavior. Long-term sloped excavations at 1:1 (horizontal:vertical) will exhibit stable behavior. Firm ground may be difficult to excavate but generally requires little excavation support.

Slow Raveling

Slow raveling ground is common in silty to clayey granular soils above the groundwater table. In slow raveling ground the stand-up time for trench and shaft excavations is considered short-term. Gravel-to cobble-sized clasts within the soil begin to fall out of the excavation face within a few minutes to a few hours. This behavior can cause difficulties in removing trench boxes. In sloped excavations of 1.5:1, slow raveling ground has long-term stability but may be subject to rilling (formation of small, shallow erosion channels parallel to the slope fall line).

Fast Raveling

Fast raveling ground is likely to develop in silty to clayey granular soils below the groundwater table and in cleaner granular soils above the groundwater table. There is essentially no stand-up time when encountering fast raveling ground for trench and shaft excavations. Gravel- to cobble-sized clasts within the soil fall out of the excavation face continuously to every few minutes. This behavior typically results in the necessity for pre-excavation shoring systems. Slopes up to 1.5:1 have medium-term stability but may be subject to rilling.

Running

Running ground is typically observed in clean dry sand and gravel. There is no stand-up time when encountering running ground in trench and shaft excavations. In running ground, the soil moves like sugar or beach sand until reaching the angle of repose immediately following excavation. Pre-excavation supports, such as sheet piles, are often necessary for stable vertical excavation in running ground. Sloped excavations will not stand steeper than the angle of repose.

Flowing

Flowing ground is typically encountered in clean granular soils or silts below the groundwater table. There is no stand-up time in trench and shaft excavations for flowing ground. The flowing ground moves like a viscous fluid. Flowing ground will not stand at any slope for any length of time.

Cohesive Running

Cohesive running ground is characterized by changing behavior due to changing moisture content, typically due to either drying after excavation exposure or wetting due to weather. Dry to moist clays may change from firm ground to cohesive running ground with an increase in moisture content. Silty to clayey sand may change from firm ground to cohesive running ground with loss of apparent cohesion due to drying. In shaft and trench excavation, the stand-up time is considered short-term in cohesive running ground. Cohesive running ground is similar to slow raveling ground for short periods of time. Cohesive running ground for sloped excavations has a short stand-up time before the change in moisture content, and then will not stand any greater than the angle of repose. Many soils may change from one behavior type to another after changes in moisture content, and this should be noted as applicable in the baseline description.

Squeezing

Squeezing ground may occur in very soft to medium stiff clay, silt and peat, at high moisture contents or below the groundwater table. In shaft and trench excavation, the stand-up time is short-term. In squeezing ground, there is slow extrusion of soil into the excavation due to over-stress conditions. Depending on excavation depth, lateral forces on excavation support may greatly exceed typical lateral earth pressures and must be considered in the support-of-excavation design. Slopes up to 2:1 have medium-term stability.

Slabbing

Slabbing ground is typically observed in moist to saturated clay or clayey or silty sand and gravel. Slabbing ground behavior is exhibited particularly in the presence of fissures or slickensides and firm ground may change to slabbing ground with a change in moisture content. In trench and shaft excavations, slabbing ground is considered to have a short- to medium-term stand-up time. Slabbing ground is similar to raveling ground except that tension cracks form parallel to the excavation face when the soil tensile strength is exceeded and larger soil blocks break off into the excavation. Similar to slow raveling ground, slabbing ground may make trench box removal difficult. For excavations sloped up to 1:1, slopes have medium-term stability depending on the moisture content.

CONCLUSIONS

The proposed *Trench, Shaft, and Slope Ground Classification for Soils* system is a tool for geotechnical engineers and geologists to communicate using a uniform system for describing and/or providing baselines for unsupported ground behavior. This proposed classification system could be used in both GBRs and conventional geotechnical reports. The use of GBRs in construction is quickly expanding to

incorporate non-tunnel projects. Therefore, this proposed classification system is suggested to complement the existing Tunnelman's Ground Classification system

Table 1. Trench, Shaft, and Slope Ground Classification for Soils

Ground Classification	Trench and Shaft Excavation Behavior	Slope Excavation Behavior	Typical Soil Types
Firm	Stable, short vertical excavations	Long-term, slopes stable at 1:1	Stiff to hard clay, loess, weakly cemented sand, dense sandy silty or clayey gravel, all above the groundwater table
Slow Raveling	Short-term stand-up, gravel to cobble sized pieces of soil fall out of the excavation face every few minutes to few hours	Long-term, slopes stable at 1.5:1 but may be subject to rilling	Generally silty to clayey granular soils above the groundwater table, or slits and clays below the groundwater table
Fast Raveling	Essentially no stand-up time, gravel to cobble sized pieces of soil fall out of the excavation face continuously to every few minutes	Medium-term, slopes stable at 1.5:1 but may be subject to rilling	Generally silty to clayey granular soils below the groundwater table, cleaner granular soils above the groundwater table,
Running	No stand-up time, moves like sugar or beach sand to angle of repose immediately following excavation	Will not stand steeper than angle of repose	Clean dry sand and gravel
Flowing	No stand-up time, flows like a viscous fluid	Will not stand at any slope	Granular soils or silt below the groundwater table
Cohesive Running	Short-term stand-up time, similar to slow raveling for short periods of time, as material dries it changes to running	Short-term stand-up before loss of moisture content, then will not stand steeper than angle of repose	Dry to moist clays may change from firm to cohesive running with change in moisture content. Silty to clayey sand may change from firm to cohesive running with loss of apparent cohesion due to drying

Ground Classification	Trench and Shaft Excavation Behavior	Slope Excavation Behavior	Typical Soil Types
Squeezing	Short-term stand-up, slow extruding of soil into excavation due to overburden conditions	Medium-term slopes stable at 2:1	Very soft to medium stiff clay and silt, peat, at high moisture contents or below the groundwater table
Slabbing	Short to medium-term stand-up time, similar to raveling except that larger blocks break off to tension cracks parallel to excavation face when soil tensile strength is exceeded	Depending on moisture content, medium-term slopes stable up to 1:1	Moist to saturated clay or clayey or silty granular soils, particularly in the presence of fissures or slickensides, may change from firm to slabbing ground with change in moisture content

while providing necessary distinctions regarding ground behavior more specific to non-tunnel excavations.

REFERENCES

American Society of Civil Engineers. (2007). "Geotechnical Baseline Reports for Underground Construction, Guidelines and Practices." *Technical Committee on Geotechnical Reports of the Underground Technology Research Council.*

Deere, D.U., Peck, R.B., Monsees, J.F., and Schmidt, B. (1969). "Design of Tunnel Liners and Support Systems." *U.S. Department of Transportation.*, OHSGT Contract 3-0152. NTIS.

Deere, D.U., Peck, R.B., Parker, H.W., Monsees, J.F., and Schmidt, B. (1970). "Design of Tunnel Support Systems." *Highway Research Record,* No. 339, pp. 26-33.

Heuer, R.E. and D.L. Virgens, (1987). "Anticipated behavior of silty sands in tunneling." *In Proceedings of the Rapid Excavation and Tunneling Conference.* Littleton, CO: Society of Mining Engineers, Inc.

Heuer, R.E. (1974). "Important ground parameters in soft ground tunneling." *Proceedings of Specialty Conference on Subsurface Exploration for Underground Excavation and Heavy Construction*, New York: ASCE, pp. 41-55.

Occupational Safety & Health Administration. "Regulations (Standards – 29 CFR)." U.S. Department of Labor.

Peck, R.B. (1969). "Deep Excavation and Tunneling in Soft Ground." *Proceedings of the 7th International Conference of Soil Mechanics,* Mexico, State-of-art Vol. 1969, pp. 225-290.

Terzaghi, K. (1977). "Earth tunneling with steel supports." *Commercial Shearing and Stamping Co.*, Youngstown, OH.

Terzaghi, K. (1950). "Geologic aspects of soft ground tunneling." *Chapter 11 in Applied Sedimentation,* R. Task and D. Parker, eds. New York: John Wiley & Sons, pp. 193-209.

A Landslide Hazard Rating System for Colorado Highways

Dan Pratt[1] and Paul Santi[2], P.G.

[1]Project Engineer, Sanborn Head and Associates, 3770 Embassy Parkway, Suite 110, Fairlawn, OH 44333, dpratt@sanbornhead.com
[2]Professor, Department of Geology and Geological Engineering, Colorado School of Mines, 1500 Illinois St., Golden, CO 80401, psanti@mines.edu

ABSTRACT: Landslides pose hazards along many stretches of Colorado highways. To assist in quantifying hazards and risks from known, existing landslides and to help prioritize their importance, the Colorado Landslide Hazard Rating System (CLHRS) was developed as a companion to the existing rockfall rating system used by CDOT. A preliminary version of the CLHRS was generated based on a review of the current body of technical literature regarding the factors that contribute to landslide hazard, consequence, and risk. It consisted of eleven Hazard Factors and eight Consequence Factors to calculate an overall risk score. The preliminary CLHRS was used to evaluate 69 landslides distributed throughout western Colorado. The resulting scoring distributions were then subjected to a suite of statistical analyses in order to identify the factors that possessed the greatest statistical merit. The statistical screening led to a final functional version of the CLHRS consisting of six Hazard Factors (geology, vegetative cover, slope aspect, surface water influence, failure frequency, and slope angle) and six Consequence Factors (depth to slide plane, length of highway affected, average daily traffic, detour options, worst-case scenario detour time, and annual maintenance cost). The CLHRS total risk scores clearly identify a subset of the landslides with both highest hazard characteristics and potential consequences.

INTRODUCTION

Many vital transportation routes in Colorado pass through mountainous terrain that is susceptible to geological hazards such as rockfall and landslides. The Colorado Department of Transportation (CDOT) currently uses a rockfall hazard rating system (RHRS) to evaluate rockfall hazard potential and risk for such areas (Pierson, 1991; Santi et al., 2009). In addition to the RHRS, CDOT has created a risk rating system for landslides based in part on Washington State DOT's Unstable Slope Management System (USMS) (Lowell and Morin, 2000). The aim of this research is to develop a more comprehensive landslide hazard rating system (LHRS) with the cooperation of CDOT for use as a companion to the RHRS. This new system will address deficiencies found in current landslide rating systems by including factors relating to

climatic, seismic, geologic, and hydrologic influences on landslide stability. Additionally, the Colorado LHRS (CLHRS) will serve as a time-efficient and cost-effective means of assessing landslide risk by evaluating the potential for failure (i.e., hazard) and the resulting impacts of failure (i.e., consequences) separately to produce a final risk score. Failure is defined as discernable movement of the landslide (assumed to be on the order of millimeters per day). The advantage of this system is that it allows for the identification, ranking, and comparison of slopes that pose the most immediate threat to public safety as well as the justification of resources for mitigation. Also, through routine application of the CLHRS to known landslides, a working inventory of slope characteristics can be maintained, thus highlighting changes in slope conditions over time.

CURRENT LANDSLIDE RATING SYSTEMS

Several scoring systems have been developed to assess the relative hazard and/or risk from landslides and are currently in use by several domestic DOTs and other agencies (Dalqamouni, 2011; Liang et al., 2006; Lowell and Morin, 2000; Oregon DOT, 2001; Saldivar-Sali and Einstein, 2007). These systems take into consideration a wide variety of factors that cover both slope and road characteristics, evaluating conditions that contribute to or trigger a landslide failure, or conditions related to the potential negative impacts or consequences of a landslide failure. Each characteristic is broken into three or four severity categories, each with a corresponding numerical score that increases exponentially with severity. Final scores are reported based on the system-specific scoring procedure to yield a value that reflects the overall hazard potential or risk. Most existing systems sum the numerical scores assigned to each factor to produce a risk value. The systems for Oregon (Oregon DOT, 2001) and the Philippines (Saldivar-Sali et al., 2007) differ in that multipliers are applied to the summed scores to arrive at a final value. Both approaches allow ranking of scores, although multiplying scores stretches the ranges for easier visual assessment. Multiplying scores also follows the general format of quantifying risk as the product of hazard factors and consequence factors.

CDOT currently maintains a working database of risk characteristics for 124 landslides threatening Colorado transportation routes. These characteristics are summarized in “Landslide Database Reports” and are stored electronically. A “Risk Value” is generated for each landslide based on the evaluation of seven “landslide properties” (Failure Frequency, Extent of Slide Beyond ROW, Size, Detour Options, Average Daily Traffic, Annual Maintenance Costs, and Road Width Affected). For each landslide property there are five possible degrees of severity. The risk values assigned to each category increase exponentially with severity using a base of three (i.e., 0, 3, 9, 27, 81). An exponential scale allows for greater distinction between severity values. All values are assigned using the base three system for consistency. Five of the seven landslide properties, as well as the scoring procedure were directly adopted from WSDOT’s Unstable Slope Management System (USMS) (Lowell and Morin, 2000). Final Risk Values can range from 0 to 567 and are divided into 4 categories: Low (0-21), Moderate (22-63), High (64-189), and Extreme (190-567).

PROJECT GOALS

The purpose of this research project, which is a summary of Pratt (2014), was to develop a risk rating system specifically for landslide hazards that threaten transportation routes throughout the state of Colorado. The new system is a revision of the existing CDOT risk rating system with substantial additions, incorporating new factors that specifically evaluate the hazard, including:

- Local geologic conditions (e.g., soil slope vs. rock slope, etc.);
- Climatic factors (e.g., annual precipitation, vegetation, slope aspect);
- Hydrologic factors (e.g., seepage conditions, surface water influences);
- Seismic susceptibility; and
- Slope morphology (e.g., slope angle).

The new system is validated by statistical testing of each included parameter. The CLHRS is intended to serve as an inventory tool applied to existing landslides to assess overall risk, and not in a predictive capacity for areas that have not experienced landslides. While potential loss of life is clearly one of the most important drivers of landslide hazard analysis, it is difficult to predict and quantify and was not included in this system.

CDOT's current Landslide Database Reports record information for 124 sites. However, many of these files document landslide features that are decades old and have not been updated either due to lack of additional movement or because they have been mitigated. Of the original dataset, 78 landslides experience movement regularly and/or continue to be of concern to CDOT. Nine of these 78 slides were eliminated from the dataset because they represented failures of mechanically-stabilized earth (MSE) walls and it was judged that the geometry of these features and the set of factors that contribute to their failure are sufficiently unique to exclude them from further evaluation. Therefore, all subsequent analyses were developed based on a dataset consisting of 69 landslides. The spatial distribution of the 69 landslide sites throughout western Colorado is presented in Fig. 1. Each site was visited during the summer of 2011 to record data needed for the hazard rating system.

HAZARD FACTOR SELECTION AND EVALUATION METHODOLOGY

Eleven Hazard Factors were initially selected for use in the CLHRS, based on a review of recent technical literature. These factors and the scoring options are shown in Table 1. Several factors used in other rating systems were deliberately omitted from the CLHRS due to their lack of suitability for rapid evaluation.

Geologic Problem Type

The occurrence and behavior of landslides is influenced by local geologic conditions. The CLHRS allows the investigator to choose one of four geologic problem types: colluvial soils, interbedded rock units, weak rock, and rock discontinuity-controlled slides.

A mantle of colluvial soil covers the natural slopes in many areas throughout Colorado and the overall stability of these soils can be related to the Unified Soil

Classification System (USCS) designation. Silts and clays of high plasticity and organics (i.e., MH, CH, PT, etc.) typically correlate with lower shear strengths and therefore represent the most hazardous condition, whereas predominately clean sands and gravels represent the least hazardous condition (i.e., GW, SW, etc.) due to their typically higher shear strengths.

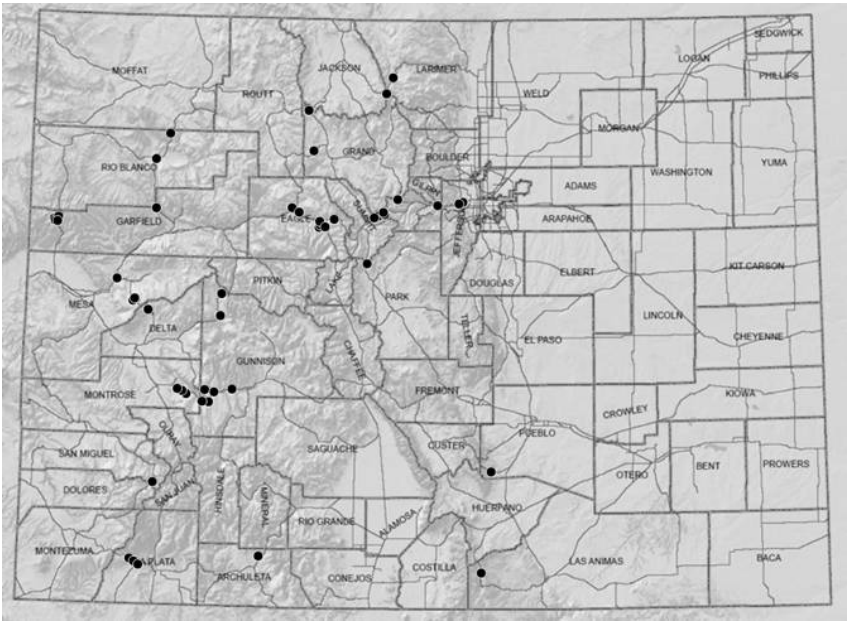

FIG. 1. Landslide location map. Dots indicate locations of 69 landslide centroids.

In areas where landslides are present in predominately interbedded sedimentary rock strata, the differences in permeability or strength between the units can play an important role in slope stability (Eberhardt et al., 2005). The CLHRS score is based on the magnitude to the difference in values between interbedded units of either the unconfined compressive strength or the permeability. These engineering properties are difficult to evaluate without performing geotechnical analyses. However, they can be estimated by using published tables of typical ranges of values (e.g., EPFL LMR, 2013).

For landslides developed on slopes consisting predominately of weak rock material (e.g., shale slopes), the results of a modified jar slake test (Santi, 2006) may be used to evaluate landslide hazard potential. Materials that slake can experience rapid physical degradation and a decrease in strength. The six possible outcomes of the modified jar slake test were divided into four hazard categories in the same manner used by Santi et al. (2009) for rockfall hazard assessment. A modified jar slake result of “no reaction” represents the least hazardous condition while degradation to flakes or mud represents the most hazardous condition. For this test, a small hand sample of

Table 1. Preliminary CLHRS evaluation sheet

Hazard Factor			Hazard Category			
			3 points	9 points	27 points	81 points
Geology (Choose One)	Cohesive Soil	USCS Classification	GW, SW, GP, GC, SP	GM, SM, SC	CL, ML	CH, MH, OL, OH, PT
	Interbedded Rock (Choose One)	Strength Difference (D_S)	1:1	1:1 < D_S ≤ 2:1	2:1 < D_S ≤ 3:1	D_S > 3:1
		Permeability Difference (D_P)	$D_P < 10^2$	$10^2 < D_P \leq 10^3$	$10^3 < D_P \leq 10^4$	$10^4 < D_P$
	Weak Rock	Jar Slake Test	No reaction	Slabs	Fractures or Chips	Flakes or Mud
	Rock	Discontinuity vs. Slope Orient.	0 < AD ≤ 0.25θ	0.25θ < AD ≤ 0.5θ	0.5θ < AD ≤ 0.75θ	0.75θ < AD < θ
Climatic Conditions		Benefical Vegetative Cover (BVC)	BVC > 75%	50% < BVC ≤ 75%	25% < BVC ≤ 50%	BVC < 25%
		Annual Precipitation (AP)	AP < 15"	15" < AP ≤ 30"	30" < AP ≤ 45"	AP > 45"
		Slope Aspect	N	NW, NE	E, SE, SW, W	S
Hydrology		Groundwater Seepage	Dry	Damp/Wet	Dripping	Running Water
		Influence of Surface Water Bodies	None or Distant	Seasonal Drainages	Small Stream Erosion/Ponded Water	Contact w/ River/Reservoir
		USDA Soil Capacity	Low/Very Low	Moderate	High	Very High
Seismic Susceptibility		Peak Ground Acceleration (%g)	%g ≤ 12	12 < %g ≤ 14	14 < %g ≤ 16	%g > 16
Existing Movement		Pavement Damage	Warping only	No Cracking, 1-2" offset	Some Cracking, 2-6" offset	Extensive Cracking, >6" offset
		Failure Frequency	No failures in previous 5 yrs	1-2 periods of movement in previous 5 yrs	Movement observed annually	Multiple movement episodes throughout year
Slope Morphology		Slope Angle (β)	β < 20°	20°< β ≤ 30°	30° < β ≤ 40°	β > 40°
HAZARD TOTAL:						

Consequence Factor		Consequence Category			
		3 points	9 points	27 points	81 points
Slide Size	Depth to Slide Plane (D_{sp})	D_{sp} < 5ft	5ft ≤ D_{sp} < 10ft	10ft ≤ D_{sp} < 15ft	D_{sp} ≥ 15ft
	Map Area Affected (A_m)	$A_m \leq 1{,}000\ m^2$	$1{,}000\ m^2 < A_m \leq 10{,}000\ m^2$	$10{,}000\ m^2 < A_m \leq 100{,}000\ m^2$	$A_m > 100{,}000\ m^2$
	Length of Highway Affected (L_h)	$L_h \leq 100$ ft	100 ft < $L_h \leq 500$ ft	500 ft < $L_h \leq 1{,}000$ ft	$L_h > 1{,}000$ ft
Proximity of Slide to Road (P_r)		$P_r \geq 40$ ft	40ft > $P_r \geq 15$ft	$P_r \leq 15$ft	Intersecting
Socioeconomic Impacts	Average Daily Traffic	<5,000	5,000-10,000	10,000-20,000	> 20,000
	Detour Options	None required	Onsite, lane shift, red. Speed	Offsite, <5 mi	>5 mi or none
	Worst Case Detour Time	<10 min	10-30min	30-60min	>60min
	Annual Maintenance Costs	<$7K	$7-14K	$14-34K	> $34K
CONSEQUENCE TOTAL:					

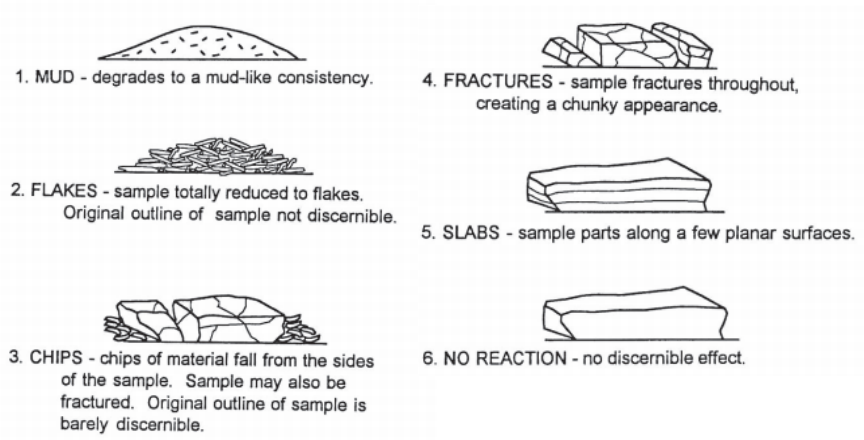

FIG. 2. Illustrated representation of modified jar slake test categories (Santi, 2006).

rock is collected and placed in a transparent container filled with water. Visual observations are made after a period of 30 minutes regarding the physical state of the sample. The criteria used to judge the relative degradation of the weak rock sample at the conclusion of the test follows the methodology presented by Santi (2006) and shown in Fig. 2.

In areas of Colorado where exposed rock masses have discontinuities such as bedding planes or metamorphic foliations daylighting in a slope, potential sliding hazards exist (Norrish and Wyllie, 1996). For the CLHRS, the orientation of such discontinuities relative to the measured slope angle can be used as a form of rapid kinematic analysis of hazard potential. It is important to note that landslides within this geologic problem type are assumed to be experiencing translational movement along a single dominant set of discontinuities. Hazard assessment for rock slopes involving other types of movement (e.g., topple, wedge failure, etc.) is not the intended function of the CLHRS.

The hazard categories for this Hazard Factor are based on the principles of kinematic analysis and the structural conditions for planar failures summarized by Norrish and Wyllie (1996). Because the CLHRS specifically evaluates known, active landslides, several of the conditions required for planar failures to occur are assumed to be present. Specifically, the dip direction of the planar discontinuity is assumed to be within 20 degrees of the dip direction of the slope face, the dip of the planar discontinuity is assumed to be less than the dip of the slope face and greater than the angle of friction for the surface, and the lateral extent of the failure mass is assumed to be defined by lateral release surfaces that do not contribute to the stability of the mass (Norrish and Wyllie, 1996). Horizontal, vertical, and opposite dip directions of discontinuities relative to the slope angle, as well as discontinuities that dip more steeply then the slope angle are judged to represent zero sliding hazard conditions, either because planar geometry does not allow for failures to threaten the roadway or because discontinuities do not daylight in the slope. Therefore, hazard score increases

with increasing steepness of the dip of the planar discontinuity, , up to the slope angle, due to increasing driving forces due to gravity.

Beneficial Vegetative Cover

The influence of vegetation on slope stability is complex and difficult to quantify and has historically been omitted from slope stability analyses (Greenway, 1987). However, more recent research by Huat et al. (2006), Nott (2006), Sidle and Ochiai (2006), Goudelis et al. (2007), Morgan (2007), Stokes et al. (2009), and Ghestem et al. (2011) shows that vegetation can impart both mechanical and hydrological benefits to slope stability. Woody roots have the potential to anchor unstable soil slopes to stable substrate for shallow landslides, although the potential benefits could be negligible if the failure plane is located deeper than the maximum depth of the tree roots. Canadell et al. (1996) and Crow (2005) give lists of maximum root depths for many plant species, which are useful guides for field evaluation. Specifically, the upper limit of root depths varies with soil type and plant species and reaches a maximum upper limit at approximately 10 to 15 feet (3.0 to 4.6 meters) below ground surface (Crow, 2005). Therefore, if the estimated depth to the slide plane is within this general region, the likelihood of trees providing anchoring support is small and the most severe hazard score should be assigned in order to reflect the absence of an important beneficial characteristic. Because grasses and shrubs do not intuitively possess the same anchoring potential as trees, the relative benefit of grasses versus trees should be weighted in favor of the trees for shallow landslides.

In order to meet the goal of developing a rapid and comprehensive risk rating system, this study has simplified the assessment of vegetation's effect on the hazard by requiring an investigator to evaluate beneficial vegetative cover as a percentage of the landslide map area.

Average Annual Precipitation

Rainfall commonly functions as a triggering mechanism for shallow landslides. Specifically, the intensity and duration of rainfall leads to rapid water infiltration and a temporary rise in pore-water pressures that may ultimately trigger failure (Wieczorek, 1996). Rainfall intensity and duration data can be obtained through instrumenting landslide sites with rain gauges or through regional summaries of average annual precipitation.

Slope Aspect

Slope aspect is defined as the compass direction in which a slope dips. According to Dai and Lee (2002), slope aspect affects moisture retention and the development of vegetation, which in turn may affect soil strength and landslide susceptibility. Furthermore, Wieczorek, et al. (1997) have shown slope aspect can influence the amount of rainfall that a slope receives in the case of rainfall direction controlled by a prevailing wind. Dai and Lee (2002) have shown that landslide frequency decreases with increasing northern orientation and increases to a maximum on south-facing

slopes. Additionally, Maharaj (1993) has observed a similar trend of increased landslide frequency on slopes with more southerly aspects. Conversely, Gokceoglu and Aksoy (1996) have noted a greater occurrence of landslides on north-facing slopes.

The utility of using slope aspect in the context of landslide stability lacks general agreement among the scientific community (Ercanoglu and Gokceoglu, 2002). The differences in observed landslide frequencies relative to slope aspect may be attributable to the specific environmental conditions in a given region of the world. In Colorado, and in the context of rockfall hazard assessment, north-facing slopes generally experience less variation in solar radiation throughout the day and consequently more readily establish stabilizing vegetation. Conversely, south-facing slopes experience higher evaporation rates and temperature fluctuations due to extended exposure to sunlight, creating drier soils that lack stabilizing vegetation and experience more erosion (Santi et al., 2009). For the dataset used in this study, landslide occurrence appears to be greatest for slopes with south-facing aspects. Thus, north-facing slopes were judged to represent the least hazardous condition and south-facing slopes the most hazardous condition.

Groundwater Seepage

The presence of water within a landslide mass contributes to the hazard by increasing driving forces and decreasing resistance. High groundwater levels present on steep mountain slopes saturate existing landslide masses and decrease the effective strength of the soil material and/or create pore pressures within rock discontinuities (Regmi et al., 2013). On-site observations regarding the presence and intensity of groundwater seepage are indicative of the subsurface hydrogeologic conditions. Hazard scores increase with increasing magnitudes of soil saturation. Hazard categories are distinguished using identical criteria used in Santi et al. (2009) for the RHRS.

In cases where multiple seepage states are identified, scores are assigned based on the most severe result in order to maintain conservatism. The time of year for evaluating this factor is also a key consideration, and multiple visits in different seasons are recommended. For this study, groundwater seepage was evaluated during the dry summer months of 2011, resulting in over 90 percent of the scores falling into the “none observed” category. For this reason, the importance of this factor has likely been obscured. Future improvements to the model should include seasonal groundwater information. However, it is expected that groundwater is a contributing factor in the majority of the landslides, so this information may not serve to separate the rating scores among the landslides.

Influence of Surface Water

In addition to instabilities created by groundwater seepage, the external influence of surface water bodies contributes to landslide hazard. For example, seasonal drainages and active streams can deliver water to a landslide and saturate the slope, thus increasing the driving forces. Rivers can actively cut the toe of a landslide, potentially

removing support for the landslide mass and reducing resisting forces. Additionally, landslides developed on the margins of active reservoirs can experience regular movements due to rapid drawdown as the buttressing support of the water is removed faster than the water can drain from the slope thus increasing driving forces and decreasing resistance due to heavy saturation (e.g., Walker and Santi, 2004).

USDA Available Water Capacity

The USDA defines available water capacity as "the amount of water that a soil can store that is available for use by plants" (USDA, 1998). This soil property was judged to serve as an acceptable indicator of the drainage behavior for a soil. Soils listed in USDA soil survey data as possessing very low to low available water capacity were considered to represent the least hazardous condition while soils listed as having "very high" available water capacity were considered to represent the most hazardous condition. Water capacity of residual soils in the vicinity of rockslides was considered to provide a reasonable indication of the drainage parameters of these areas as well.

Peak Ground Acceleration

Landslides may be triggered by ground accelerations resulting from seismic activity (Jibson and Harp, 2011, and a specific example for Colorado is found in Walker and Santi, 2004). Though Colorado is not typically associated with active seismicity, the diverse tectonic history of the Rocky Mountains has left a multitude of faults throughout the state. Fig. 3, which shows peak ground accelerations as a percentage of gravitational acceleration with a two percent probability of exceedance in 50 years, is used to evaluate seismic hazard for the CLHRS. No landslide site is located within an isopleth with a peak ground acceleration of less than 12 percent g, nor is any landslide site located within an isopleth that delineates a peak ground acceleration of greater than 16 percent g. Therefore, areas with accelerations less than 12 percent g are judged to represent the least hazardous condition and accelerations greater than 16 percent g are judged to represent the most hazardous condition. Intermediate numerical values are divided evenly between the upper and lower boundaries.

Pavement Damage

Field observations of existing road damage serve as indicators of relative hazard with large cracks, bulges, and pavement displacements indicating recent or un-mitigated ground movements.

Failure Frequency

Landslide failure frequency is based on a review of maintenance records from both recent slope movements and historical failures.

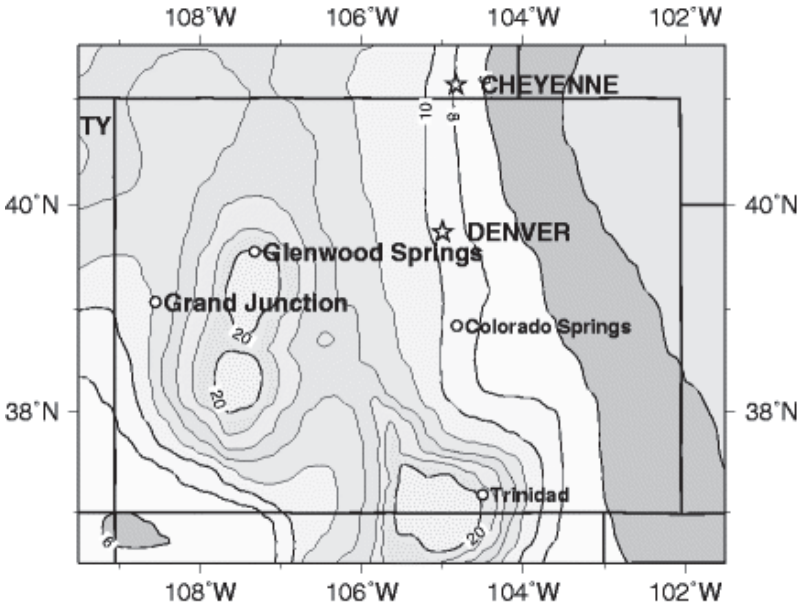

FIG. 3. Peak acceleration (percent g) with 2 percent probability of exceedance in 50 years (USGS, 2012).

Slope Angle

Slope angle is considered in most soil slope stability analysis methods and is typically used to calculate stability factors from empirical charts or for use in factor of safety (FS) calculations. Research conducted on landslides developed in mudstone terrain by Iwahashi et al. (2003) in the northern highlands of Japan show that mean slope angle frequency distributions for nearly 7,800 landslide masses are most closely approximated by Weibull distributions. The breaks in severity for this hazard category are based on their findings.

CONSEQUENCE FACTOR SELECTION AND EVALUATION METHODOLOGY

Eight Consequence Factors were selected for use in the preliminary CLHRS, based on a review of recent technical literature. Descriptions of the significance of each factor, evaluation method, and category break justifications are presented below. Five of the six consequence-related factors in the current CDOT system were retained for use in the new CLHRS: extent of the slide beyond right-of-way, size, detour options, average annual daily traffic (AADT), and annual maintenance costs. The length of roadway affected by the landslide is currently recorded in CDOT's landslide database reports but was not previously included in the risk score calculation. This value has

been added in the new CLHRS. In addition to the CDOT-derived Consequence Factors, two new factors were developed for this study: depth to slide plane and worst-case scenario detour time.

Depth to Slide Plane

The consequences of failure of a landslide are related to the total volume of the slide mass, which can be judged to some degree by measurement of the depth to the slide plane. More massive slides can deposit greater volumes of material on a roadway and adjacent structures, thus necessitating mobilization of labor to remove larger quantities of material. The depth of movement below the ground surface is not typically greater than the width of the zone of surface motion, and the maximum depth to the slide plane is typically equal to the distance from the break in the original ground surface slope to the most uphill crack or scarp (McGuffey, 1991).

Map Area Affected (Landslide Size)

The map area affected by the landslide has been used as a substitute for landslide "size" by CDOT. The boundaries for a given slide feature can be observed directly in the field and corroborated by aerial photography (or vice versa), and approximate boundaries can be traced in ArcGIS to create closed polygons for each landslide.

Length of Roadway Affected

The length of the roadway affected by a landslide refers to the total length of road segment that intersects the landslide mass or the total length of roadway that is immediately adjacent to the slide mass. Larger exposed segments of road will suffer more severe consequences from failure due to the increased size of the section of road that must be repaired or replaced. The range of road lengths used for this factor fully encompass the measured affected road lengths encountered in this study.

Proximity of Slide to Road

Intuitively, the closer a slide is to the roadway, irrespective of its vertical distance from that roadway, the greater the consequences of failure. In the worst case, the roadway passes through the landslide with the toe and headscarp located on opposite sides of the ROW.

Average Daily Traffic (ADT)

Landslide-affected routes that receive large volumes of traffic daily are likely to experience high economic losses due to the delay and/or rerouting of commercial traffic. This factor is retained from the original CDOT system and the breaks in consequence categories are unchanged.

Detour Options

Sites that lack expedient detour options will require more effort to design, implement, and maintain a detour for the duration of repairs following blockage or damage from a landslide. Through observations in the field of the landslide geometry, size, historical movement behavior, and current damage area, a reasonable detour solution can be assumed based on the area affected and likely mitigation/repair efforts. Situations in which onsite detour options are very limited or impossible are assigned higher consequence scores.

Worst-Case Scenario Detour Time

In the event of the total failure of a landslide such that a segment of a road is completely destroyed or damaged severely enough that mitigation efforts require temporary closure of the road (i.e., no on-site detour), a worst-case scenario detour time Consequence Factor has been included in the system. The detour time from the shortest alternative path is found through trial and error via any conventional internet-based mapping site (e.g., Google Maps).

Annual Maintenance Costs

Landslides that experience movements regularly and cause significant damage to the roadway require frequent monitoring, maintenance, and mitigation. These efforts have their associated costs in terms of labor and materials. The current CDOT system is largely based on Lowell and Morin's (2000) USMS. These dollar amounts have been adjusted for inflation to reflect costs in 2013 dollars.

VALIDATION OF FACTORS

Statistical analyses were conducted on the dataset in order to validate each factor included in the CLHRS, as presented in detail in Pratt (2014). First, initial data screening was intended to identify factors that lack sufficient variability to distinguish subdivisions of landslides. Factors were retained if two of their scoring categories contained at least 15 percent of the data points. Parameters that showed a narrow distribution of scores were deleted because the lack of variation would not be useful for describing how that parameter contributes to landslide hazard or consequence (Santi et al., 2009). Using this criterion, two Hazard Factors, groundwater seepage and pavement damage, were eliminated because 90 percent or greater of the observations fell into one hazard category. We recognize that a groundwater contribution factor that adequately distinguishes activity level amongst the landslides is an important gap in the current system that should be addressed in future revisions.

Correlation analysis was used to identify the existence and magnitude of relationships between each individual factor and the final total scores. The results of these analyses were intended to serve as justification for the removal of factors that lacked predictive power and tracked poorly with the total score. Three factors (annual precipitation, drainage (soil capacity), and proximity of slide to roadway) do not have

a statistically significant relationship to the total hazard score and were removed from the CLHRS.

Next, ordinal logistic regression was used to identify factors that tracked poorly with the overall total score. Two factors, the seismic Hazard Factor and the landslide size Consequence Factor, both lack statistically significant relationships to the scores they are respectively trying to predict. Therefore, they were not included in the final hazard rating system. One would expect that the landslide size and the length of roadway would show similar trends, since both relate to the overall volume of the slide. As it turns out, only the length of roadway factor closely mimics the overall score, and the landslide size does not necessarily indicate the expected damage or likelihood of movement.

FINAL CLHRS

Based on the results of the statistical analyses, a final modified draft of the CLHRS was produced with the remaining twelve of the initial nineteen factors, presented as Table 2. Individual factor scores were summed to produce final aggregate scores, and the aggregate hazard and consequence scores were multiplied together to create a final risk score (risk = hazard x consequence). A ranking of all landslides by total hazard, consequence, and risk scores is included as Figs. 4, 5, and 6, respectively.

Landslides were categorized into severity classes using breaks based on median, quartiles, and outliers as shown in Fig. 7 and Table 3. In this case, the median is a score of 20,880 (division between classes II and III), the lower quartile break is 8,712, the upper quartile break is 37,278, and the cutoff for outliers is 76,032.

In creating a rating system that evaluates geologic environments, it becomes necessary to simplify complex and interrelated environmental and geological relationships in order to meet the project goals of creating a simple and rapidly applicable system. There is no substitute for a thorough investigation of any phenomenon that poses a potential threat to human health and safety, property, or critical infrastructure. The CLHRS provides a current “snapshot” of risk-related conditions and is not intended to function in either a predictive capacity or as a foundation for designing a mitigation program.

Table 2. Final CLHRS Evaluation Reference Sheet

Hazard Factor			Hazard Category			
			3 points	9 points	27 points	81 points
Geology (Choose One)	Cohesive Soil	USCS Classification	GW, SW, GP, GC, SP	GM, SM, SC	CL, ML	CH, MH, OL, OH, PT
	Interbedded Rock (Choose One)	Strength Difference (D_S)	1:1	$1:1 < D_S \leq 2:1$	$2:1 < D_S \leq 3:1$	$D_S > 3:1$
		Permeability Difference (D_P)	$D_P < 10^2$	$10^2 < D_P \leq 10^3$	$10^3 < D_P \leq 10^4$	$10^4 < D_P$
	Weak Rock	Jar Slake Test	No reaction	Slabs	Fractures or Chips	Flakes or Mud
	Rock	Discontinuity vs. Slope Orient.	$0 < AD \leq 0.25\theta$	$0.25\theta < AD \leq 0.5\theta$	$0.5\theta < AD \leq 0.75\theta$	$0.75\theta < AD < \theta$
Climatic Conditions		Benefical Vegetative Cover (BVC)	BVC > 75%	50% < BVC ≤ 75%	25% < BVC ≤ 50%	BVC < 25%
		Annual Precipitation (AP)	AP < 15"	15" < AP ≤ 30"	30" < AP ≤ 45"	AP > 45"
		Slope Aspect	N	NW, NE	E, SE, SW, W	S
Hydrology		Groundwater Seepage	Dry	Damp/Wet	Dripping	Running Water
		Influence of Surface Water Bodies	None or Distant	Seasonal Drainages	Small Stream Erosion/Ponded Water	Contact w/ River/Reservoir
		USDA Soil Capacity	Low/Very Low	Moderate	High	Very High
Seismic Susceptibility		Peak Ground Acceleration (%g)	%g ≤ 12	12 < %g ≤ 14	14 < %g ≤ 16	%g > 16
Existing Movement		Pavement Damage	Warping only	No Cracking, 1-2" offset	Some Cracking, 2-6" offset	Extensive Cracking, >6" offset
		Failure Frequency	No failures in previous 5 yrs	1-2 periods of movement in previous 5 yrs	Movement observed annually	Multiple movement episodes throughout year
Slope Morphology		Slope Angle (β)	β < 20°	20°< β ≤ 30°	30° < β ≤ 40°	β > 40°
HAZARD TOTAL:						

Consequence Factor		Consequence Category			
		3 points	9 points	27 points	81 points
Slide Size	Depth to Slide Plane (D_{sp})	$D_{sp} < 5ft$	$5ft \leq D_{sp} < 10ft$	$10ft \leq D_{sp} < 15ft$	$D_{sp} \geq 15ft$
	Map Area Affected (A_m)	$A_m \leq 1{,}000\ m^2$	$1{,}000\ m^2 < A_m \leq 10{,}000\ m^2$	$10{,}000\ m^2 < A_m \leq 100{,}000\ m^2$	$A_m > 100{,}000\ m^2$
	Length of Highway Affected (L_h)	$L_h \leq 100$ ft	$100\ ft < L_h \leq 500$ ft	$500\ ft < L_h \leq 1{,}000$ ft	$L_h > 1{,}000$ ft
Proximity of Slide to Road (P_r)		$P_r \geq 40$ ft	$40ft > P_r \geq 15ft$	$P_r \leq 15ft$	Intersecting
Socioeconomic Impacts	Average Daily Traffic	<5,000	5,000-10,000	10,000-20,000	> 20,000
	Detour Options	None required	Onsite, lane shift, red. Speed	Offsite, <5 mi	>5 mi or none
	Worst Case Detour Time	<10 min	10-30min	30-60min	>60min
	Annual Maintenance Costs	<$7K	$7-14K	$14-34K	> $34K
CONSEQUENCE TOTAL:					

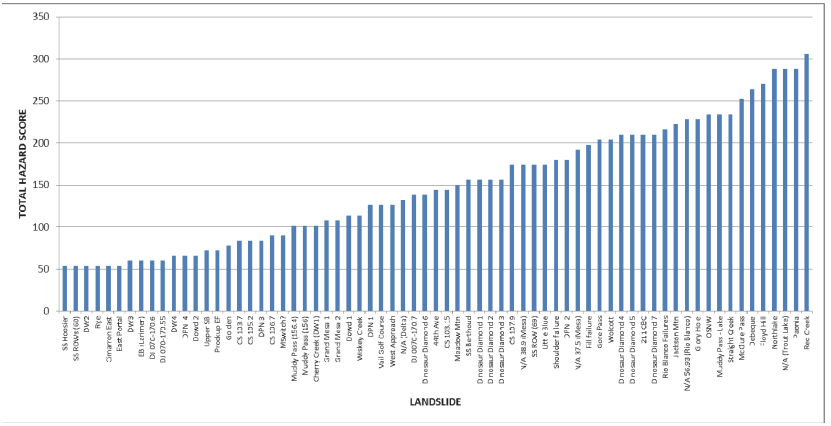

FIG. 4. Distribution of total hazard scores based on the six statistically-validated factors.

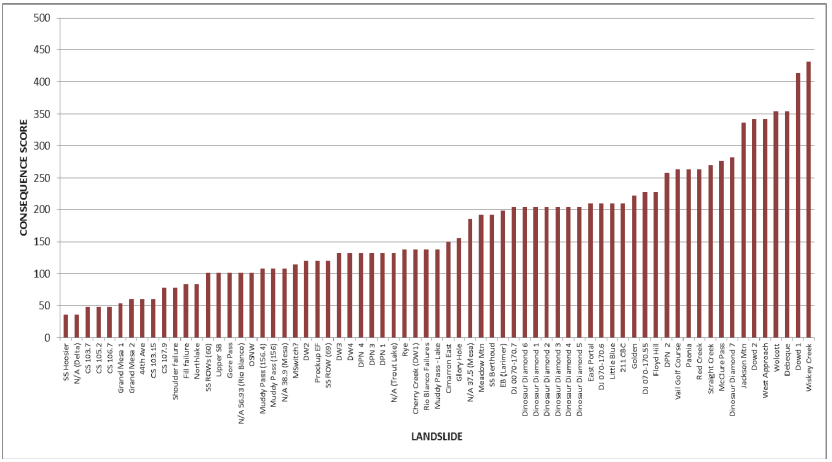

FIG. 5. Distribution of total consequence scores based on the six statistically-validated factors

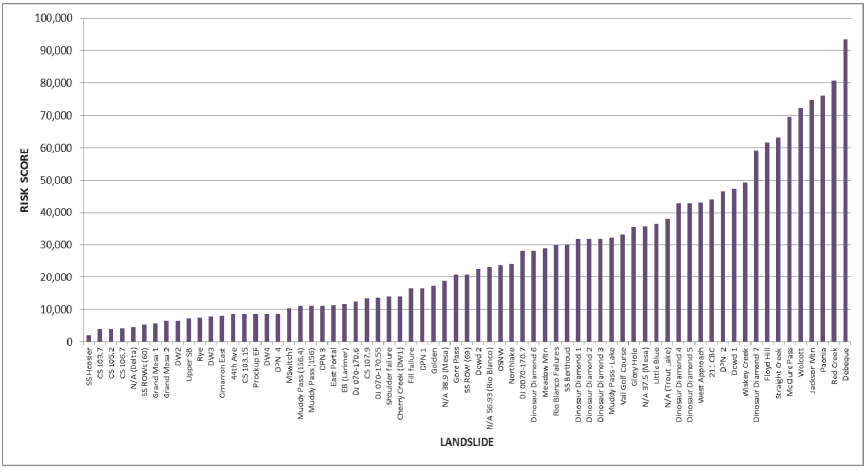

FIG. 6. Distribution of total risk scores based on the twelve statistically-validated factors.

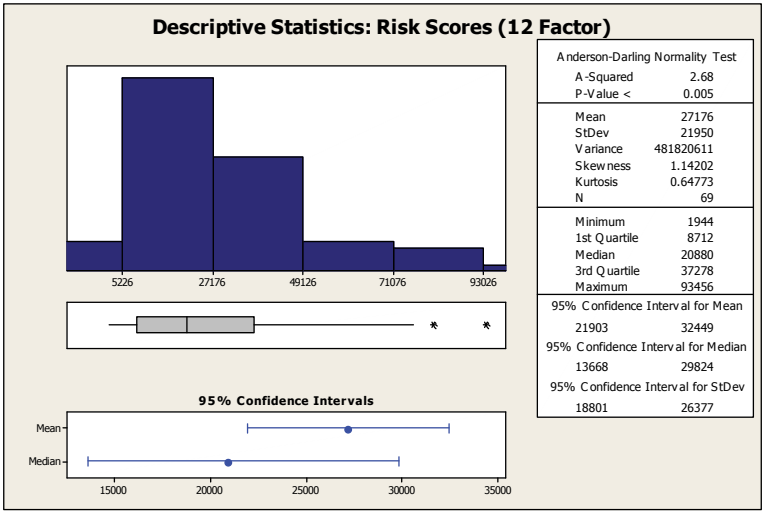

FIG. 7. Graphical summary of descriptive statistics for total risk scores based on the twelve statistically-validated factors.

Table 3. Total Risk Score Severity Classes (12 Factors)

Risk Class	Risk Score Range	Severity Identifier
I	$R < 8{,}712$	Very Low
II	$8{,}712 \leq R \leq 20{,}880$	Low
III	$20{,}880 < R \leq 37{,}278$	Moderate
IV	$37{,}278 < R \leq 76{,}032$	High
V	$R > 76{,}032$	Severe

REFERENCES

Canadell, J., Jackson, R. B., Ehleringer, J. B., Mooney, H. A., Sala, O. E., Schulze, E. D., 1996. Maximum rooting depth of vegetation types at the global scale. Oecologia, 108(4), pp. 583-595.

Crow, P., 2005. The Influence of Soils and Species on Tree Root Depth. Information Note, Forestry Commission, Edinburgh, November 2005.

Dai, F.C., Lee, C.F., 2002. Landslide characteristics and slope instability modeling using GIS, Lantau Island, Hong Kong. Geomorphology, Volume 42, Issues 3–4, 15 January 2002, pp. 213-228.

Dalqamouni, A.Y., 2011. Development of a Landslide Hazard Rating System for Selected Counties in Northeastern Ohio, Doctoral Dissertation, Kent State University, Kent, Ohio, May 2011.

Eberhardt, E., Thuro, K., Luginbuehl, M., 2005. Slope Instability in dipping interbedded conglomerates and weathered marls – the 1999 Rufi landslide, Switzerland. Engineering Geology, No. 77, 2005, pp. 35-56.

Ecole Polytechnique Fédérale de Lausanne (EPFL), Laboratory for Rock Mechanics (LRM). Chapter 4 – Properties of Rock Materials. http://lmrwww.epfl.ch/en /ensei/Rock_Mechanics/ENS_080312_EN_JZ_Note_Chapter_4.pdf. Last accessed September 1, 2013.

Ercanoglu, M., Gokceoglu, C., 2002. Assessment of landslide susceptibility for a landslide-prone area (north of Yenice, NW Turkey) by fuzzy approach. Environmental Geology 41.6 (2002): pp. 720-730.

Ghestem, M., Sidle, R.C., Stokes, A., 2011. The Influence of plant root systems on subsurface flow: implications for slope stability. BioScience, 61, pp. 869-879.

Greenway, D.R., 1987, Vegetation and Slope Stability. In: Slope Stability: Geotechnical Engineering and Geomorphology, edited by Anderson, M.F. and Richards, K.S., John Wiley and Sons.

Gokceoglu, C., Aksoy, H., 1996. Landslide susceptibility mapping of the slopes in the residual soils of the Mengen region (Turkey) by deterministic stability analyses and image processing techniques. Eng Geol 44: pp.147-16.

Goudelis, G., Ganatsas, P.P., Spanos, I., Karpi, A., 2007. Effects of repeated fire on plant community recovery in Penteli, central Greece. In: Eco- and Ground Bio-Engineering: The Use of Vegetation to Improve Slope Stability, eds. A Stokes, I., Spanos, J.E. Norris, pp. 337-344. Proceedings of the First International Conference on Eco-Engineering, 13-17 September 2004. Dordrecht: Springer.

Huat, B.B.K., Ali, F.J.H., Low, T.H., 2006. Water infiltration characteristics of unsaturated soil slope and its effect on suction and stability. Geotechnical & Geological Engineering 24.5: pp. 1293-1306.

Iwahashi, J., Watanabe, S., Furuya, T., 2003. Mean slope-angle frequency distribution and size frequency distribution of landslide masses in Higashikubiki area, Japan. Geomorphology 50: pp. 349-364.

Jibson, R.W., Harp, E.L., 2011. Field Reconnaissance Report of Landslides Triggered by the January 12, 2010, Haiti Earthquake. USGS Open File Report 2011-1023.

Liang, R., Geiger, G., Beach, K., Pensomboon, G., 2006. Landslide Hazard Rating System in Ohio DOT. Proceedings of GeoCongress 2006: Geotechnical Engineering in the Information Technology Age. ASCE Conf. Proc. doi:10.1061/40803(187)124

Lowell, S., Morin, P., 2000. Unstable Slope Management: Washington State, *TR News*, No. 207, March-April 2000.

Maharaj, R., 1993. Landslide processes and landslide susceptibility analysis from an upland watershed: a case study from St. Andrew, Jamaica, West Indies. Eng Geol 34:53-79

McGuffey, V.C., 1991. Clues to Landslide Identification and Investigation. In Geologic Complexities in the Highway Environment (R.H. Ficies, ed.), Proc., 42nd Annual Highway Geology Symposium, Albany, New York, New York State Department of Transportation, Albany, pp. 187-192.

Morgan, R.P.C., 2007. Vegetative-based technologies for erosion control. In Eco- and Ground Bio-Engineering: The Use of Vegetation to Improve Slope Stability, eds. A. Stokes, I. Spanos & J.E. Norris, pp. 337-344. Proceedings of the First International Conference on Eco-Engineering, 13-17 September 2004. Dordrecht: Springer.

Nott, J., 2006. Extreme Events: A Physical Reconstruction and Risk Assessment. Cambridge: Cambridge University Press.

Norrish, N.I., Wyllie, D.C., 1996. Rock Slope Stability Analysis. In: Landslides: Investigation and Mitigation, Special Report 247, Transportation Research Board, National Research Council, (eds, A. Keith Turner and Robert L. Schuster) National Academy Press, Washington, D.C.

Oregon Department of Transportation, 2001. Oregon DOT landslide and rockfall pilot study (Final Report): Oregon DOT Geo-Hydro Section, HQ Geo-Hydro Unit, 2001.

Pierson, L.A., 1991. The Rockfall Hazard Rating System, Oregon Department of Transportation, Final Report FHWA-OR-GT-92-05

Pratt, D., 2014, A Landslide Hazard Rating System for Colorado Highways, unpublished MS thesis, Colorado School of Mines, 109 p.

Regmi, R. K., Lee, G., Jung, K., 2013. Analysis on failure of slope and landslide dam. *KSCE Journal of Civil Engineering*, *17*(5), pp. 1166-1178.

Saldivar-Sali, A., Einstein, H.H., 2007. A Landslide Risk Rating System for Baguio, Philippines, Engineering Geology, Vol. 97, pp. 85-99.

Santi, P.M., 2006. Field methods for characterizing weak rock for engineering. Environmental and Engineering Geoscience 12, pp. 1-11.

Santi, P.M., Russell, C.P., Higgins, J.D., Spriet, J.I., 2009. Modification and tatistical analysis of the Colorado Rockfall Hazard Rating System, Engineering Geology, Vol. 104, No. 1-2, Feb. 2009 pp. 55-65.

Sidle, R.C., Ochiai, H., 2006. Landslides: Processes, Prediction, and Land Use. Water Resources Monograph, volume 18. Washington, D.C.: American Geophysical Union.

Stokes, A., Atger, C., Bengough, A.G., Fourcaud, T., Sidle, R.C., 2009. Desirable plant root traits for protecting natural and engineered slopes against landslides. Plant and Soil, 324, 1-30.

United States Department of Agriculture (USDA), Natural Resources Conservation Service (NRCS), 1998. Soil Quality Resource Concerns: Available Water Capacity, Soil Quality Information Sheet, January, 1998.

United States Geological Survey (USGS), 2012. Colorado Seismic Hazard Map, Earthquake Hazards Program,http://earthquake.usgs.gov/earthquakes/states/colorado/hazards.php. Last modified: November 1, 2012. Last accessed: January 6, 2014.

Walker, S.R., Santi, P.M., 2004. Influence of the Blue Mesa Reservoir on the Red Creek Landslide, Colorado. Environmental & Engineering Geoscience,Vol. 10, No. 1, pp. 13-26.

Wieczorek, G.F., Mandrone, G., DeCola, L., 1997. The influence of hillslope shape on debris-flow initiation. In: Chen, C.L. (Ed.), Debris-flow hazards mitigation: mechanics, prediction, and assessment. American Society of Civil Engineers, New York, pp. 21 – 31. In: F.C Dai, C.F Lee, Landslide characteristics and slope instability modeling using GIS, Lantau Island, Hong Kong, Geomorphology, Volume 42, Issues 3–4, 15 January 2002, Pages 213-228,

Wieczorek, G.F., 1996. Rock Slope Stability Analysis. In: Landslides: Investigation and Mitigation, Special Report 247, Transportation Research Board, National Research Council, (eds, A. Keith Turner and Robert L. Schuster) National Academy Press, Washington, D.C.

An Innovative Case Study on the Use of Launched Nails for Landslide Repair

Matt Birchmier, P.E.[1], Cameron Lobato, P.E.[2]

[1]Chief Engineer, GeoStabilization International, P.O. Box 4709 Grand Junction, CO 81502; PH (970)812-6675; email: matt@gsi.us
[2]Director of Western Operations, GeoStabilization International, P.O. Box 4709 Grand Junction, CO 81502; PH (970)985-1066; email: cameron@gsi.us

ABSTRACT: A record snowfall during the winter of 2010/2011 throughout the Rocky Mountains combined with torrential spring rainfall led to infrastructure damage throughout Montana, Wyoming, and North Dakota. Many roadways were closed due to flooding and landslides. Interstate 90, between Hardin, MT and Buffalo, WY experienced multiple deep-seated landslides and several shallow slips. One of the landslides occurred at MM 16.3 on the westbound onramp, a critical access point to I-90 due to the vicinity of the Wyoming Port of Entry. A 3 m to 4 m (10 ft to 12 ft) scarp near the guardrail led the Wyoming Department of Transportation (WYDOT) to look for innovative techniques to quickly stabilize the ramp to permit safe traffic flow. Safety and right of way concerns also complicated the design and construction of any earthwork structures. WYDOT chose launched (ballistic) soil nails faced with reinforced shotcrete to provide temporary stabilization of the near-vertical scarp. The temporary stabilization allowed for stability of the roadway platform and also permitted construction of a large earthen buttress. Due to the time and safety constraints involved, as well as the innovative technology selected, unique approaches in the slope stability modeling, onsite design, and construction planning were required.

INTRODUCTION

Following the winter of 2010 and the spring rains of 2011, Wyoming DOT was faced with multiple slope stability concerns throughout the northern I-90 corridor. GeoStabilization International (GSI) was contacted to provide design recommendations and temporary support of multiple head scarps to permit construction of toe buttresses to mitigate the landslides. The slide at MM-16.3 off of I-90 posed risk to an onramp providing access to I-90 for the Wyoming Port of Entry. Launched nails were chosen due to their economical and quick installation. The native soils in the region, silty to sandy clays also permit high nail penetrations, which greatly enhance stability. When used effectively, launched soil nails can

provide a repair solution that is both economical and quick; the rapid installation allows for instant stability improvement, even before the use of pressure grouting.

These kinds of emergency landslides served as the driving force behind the development of the first soil nail launcher, which was constructed in the 1980s from a compressed air cannon originally developed and manufactured by the British military to launch Thermos®-sized chemical weapon canisters up to 11.3 km (7 miles) on enemy targets. Powered by air at pressures up to 20.7 MPa (3,000 psi), the cannon typically fires a 6.1 m (20 ft) long, 38 mm (1.5 in) diameter bar or tube into the ground in a single shot at velocities exceeding 100 m/s (200 mph) in order to help stabilize shallow landslides. These rods reinforce an unstable or potentially unstable soil mass by transferring the nail's tensile and shear resistance into the sliding soil. When perforated, the tubes can also serve as horizontal drains or as conduits for pressure grouting. Production rates approaching 250 nails per day make the technology viable for landslide repairs where rapid construction is critical.

LAUNCHED SOIL NAIL DESIGN METHODOLOGY

Basic design methodology for launched soil nails is outlined in the joint U.S. Forest Service (EM-7170-12A) and U.S. Federal Highway Administration (FHWA-FPL-93-003) publication "Application Guide for Launched Soil Nails, Volume 1." Originally published in 1994, this guide provides a relatively simplistic approach to shallow landslide repair, modeling shallow landslides and embankment failures as a planer-sliding wedge.

In the 20 years since the first use of ballistic soil nails in the United States, uses for these inclusions have increased alongside the availability and capability of PC-based limited equilibrium slope stability programs. Using nail input parameters from the USFS Manual, Excel spreadsheets, and commercially available slope stability evaluation programs, designers can effectively model slide surfaces of any shape, add multiple types of materials and water tables, and choose their desired factor of safety. However, this process requires multiple iterations and can be time-consuming.

SHEAR STRENGTH CALCULATIONS FOR LAUNCHED SOIL NAILS

Unlike traditional drilled and grouted soil nails, launched soil nails have a high shear capacity to axial capacity ratio. Shear capacities of up to 20 percent or more of axial pullout capacity have been observed (compared with typical values well below 5 percent for traditional drilled and grouted nails (Jewell and Pedley 1992)). Because of this divergence, the shear component of a launched soil nail is not ignored as it would be in traditional soil nail design using grouted soil nails.

It is important to note that the ultimate shear resistance of the nail is not assumed to be controlled by the shear strength of the nail material, but by the ultimate bearing capacity of the soil in a localized area near the active failure surface. This localized bearing failure develops over a length of nail L_o (typically 1 m (3 ft)) or less for launched soil nails. Typical shear values generally range from 1.3 to 5.3 kN (300 to 1200 lbs). The general assumptions for the stress condition are:

- Normal stress on the nail is a function of soil properties and the vertical depth at sliding surfaces
- The total shear force applied on each nail is the bearing capacity of the soil along the effective length of the nail, L_o
- Transient surcharge loads do not increase the shear resistance of the nail

For a nail of diameter of d, the ultimate shear resistance S_u:

$$S_u = q_u L_o d \tag{1}$$

where q_u – ultimate bearing capacity of the soil in the effective length of L_o
L_o – effective length of the nail over which q_u is developed

The ultimate bearing capacity of the soil is calculated by:

$$q_u = \sigma_n N'_q \tag{2}$$

where σ_n – normal pressure on the nail at the intersection of the nail and the failure surface
N'_q – Terzaghi bearing capacity factor

The ultimate shear resistance and bearing capacity of a nail installed into a slope is depicted in Fig. 1.

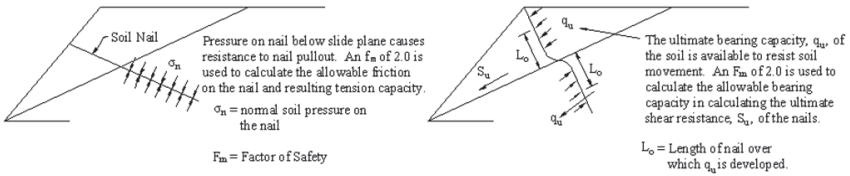

FIG. 1. Tensile and shear resistance of nail.

The effective length of the nail is a function of the ultimate moment of resistance of the nail in bending and calculated by:

$$L_o = \sqrt{\frac{2M_u}{q_u d}} \tag{3}$$

and

$$M_u = \frac{If_y}{d/2} \tag{4}$$

where M_u– ultimate moment of resistance
I – moment of inertia of the nail

f_y – yield strength of the nail

The allowable shear resistance can be calculated by:

$$S_{allowable} = \alpha_s S_u \quad (5)$$

where α_s – shear resistance factor (typically 0.5 for launched soil nails)

SITE DESIGN

A 3.05 m (10 ft) head scarp approximately 0.6 m (2 ft) off the guardrail on the north-bound on-ramp posed significant risk to the critical on-ramp. Upon discovery, WYDOT mobilized their surveying and geotechnical forces to map and explore the site. The borings generally encountered saturated, medium stiff clay to loose clayey sand (fill) for depths up to 7.6 m (25 ft). These materials were underlain by native, medium dense clayey sands to silts with shale bedrock at approximately 12.2 m (40 ft).

GSI acquired this information from WYDOT subsurface investigations and began to analyze the slope using RocScience Slide 6.0, a limited equilibrium program. The layering described above was input into the cross section and a back analysis was performed on the existing slope to obtain design parameters, shown in Fig. 2.

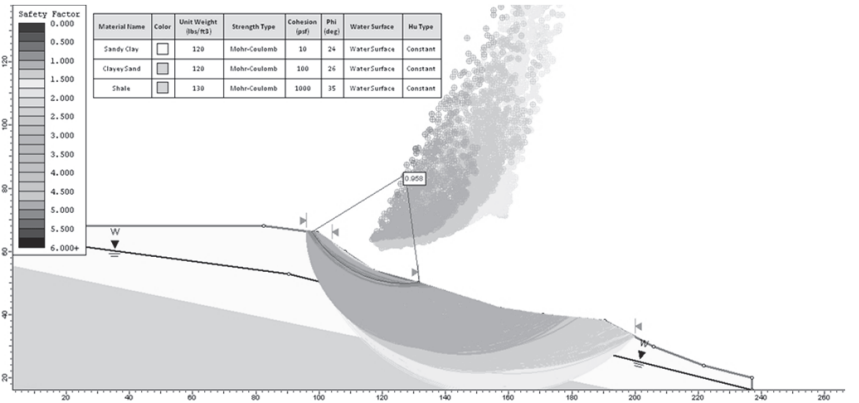

FIG. 2. Back-analysis of MM 16.3 slope

Discussions with WYDOT followed the back-analysis to understand the construction methodology of the toe buttress. Significant excavation of the slide mass was required, which exacerbated the temporary stability of the slope by removing resisting forces. WYDOT and GSI decided on a wall height of about 4.6 m to 6.1 m (15 ft to 20 ft) to bench the excavation for the buttress at an approximate slope of 2.5:1 (horizontal:vertical). GSI's preliminary design confirmed a FS greater than 1.2

(Fig. 3) and a FS of 1.5 (Fig. 4) for the temporary and permanent cases, respectively. The design consisted of five rows of launched nails with penetrations up to 5.8 m (19 ft) in length on a 0.91 m (3 ft) horizontal by 0.91 m (3 ft) vertical pattern. A pullout strength of 340 N/m (250 lb/ft) and shear strength of 678 N/m (500 lb/ft) were used in the analyses.

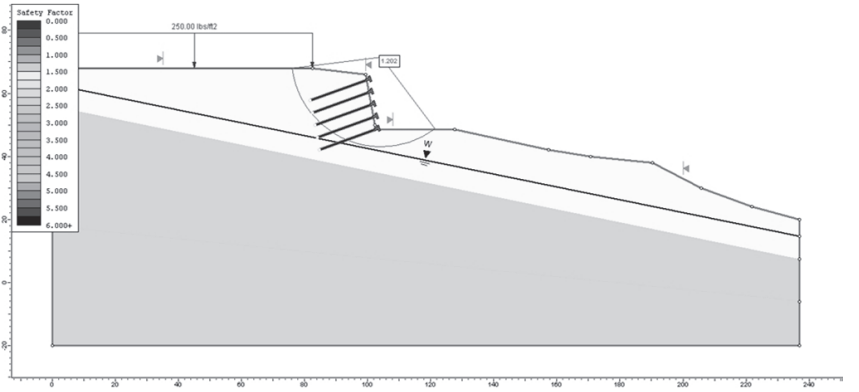

FIG. 3. Temporary Case of MM 16.3 slope

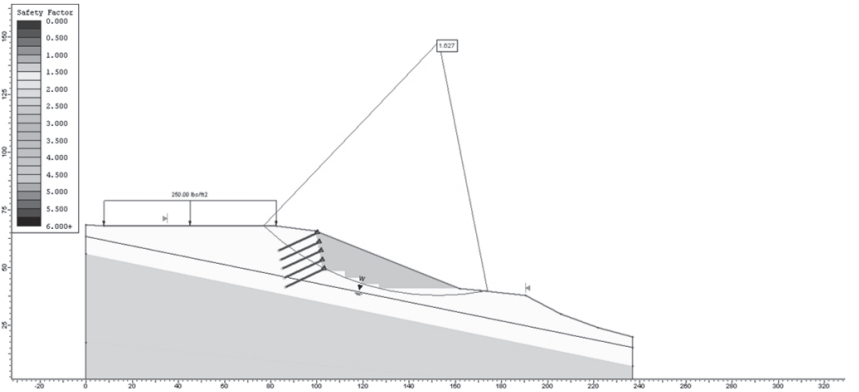

FIG. 4. Permanent Case of MM 16.3 slope

CONSTRUCTION

With WYDOT providing assistance for excavation and traffic control, GSI was able to focus on the head scarp stabilization to prevent further migration into the travel lanes. Benches were initially constructed to provide access to the upper nails. Care

was taken not to place excessive driving forces on the already unstable mass during this process.

Photograph 1. Bench Placement

Installation began with top-down construction. Launched nails were installed on a 0.91 m (3 ft) horizontal by 0.91 m (3 ft) vertical pattern at a rate of about 100 nails/work day. Once finished with an area, nails were pressure grouted to provide additional pullout resistance. Near the head scarp area, penetration depths exceeded 4.6 m (15 ft); on areas near the flanks, penetration was less than 3 m (10 ft), in areas. For these cases, GSI performed sensitivity analysis of the slope to ensure acceptable stability. Nails with penetration less than 2.7 m (9 ft) were reinstalled. The variation in the fill material is shown in the fill color difference in Photograph 1 and the nail penetration depth in Photograph 2.

At the bottom of the proposed five rows, significant water and weak soils were encountered. Launched drains (ungrouted perforated launched nail) were installed on a 1.8 m (6 ft) horizontal spacing to reduce hydrostatic pressure in Photograph 3. GSI prepared the slope, installed drain strip and welded wire fabric, and waler bars and was prepared to shoot shotcrete per the original design.

Collectively, WYDOT and GSI decided additional material needed to be removed and shored to permit proper sloping and construction of the eventual structural toe buttress. GSI confirmed, through observation at the site and real-time on-site modeling, the temporary stability of the slope prior to construction. The slope was excavated at an approximate slope of 1:1 below the fifth row to prevent excessive undermining of the upper material. Two additional rows of launched nails were

Photograph 2. Launched Nail Installation

Photograph 3. Horizontal Drain Placement

installed below the original five rows. Photograph 4 shows the installation of the last two rows of nails. Bearing plates were welded onto the nails and shotcrete was placed over the majority of the slope, depicted in Photograph 5. Portions of the flanks received only a flexural facing. The amount of water associated with the northern end is also shown Photograph 5. GSI demobilized from the site and WYDOT excavation contractors re-established the slope and constructed the prescribed earthen buttress.

Photograph 4. Final row installation

Photograph 5. Removing Shotcrete Blankets

CONCLUSIONS

Innovative design, new technology, and design/build construction concepts came together to create an efficient, cost effective repair at this site. Ballistically launched soil nails were rapidly installed to prevent regression of the slide into the driving

lanes while providing temporary shoring suitable to allow removal of weak and saturated soils prior to replacement with and engineered earthen buttress.

ACKNOWLEDGMENTS

The authors appreciate and would like to recognize the efforts and support of WYDOT.

REFERENCES

Barrett, C.E., and Devin, S.C. (2011). "Shallow Landslide Repair Analysis using Ballistic Soil Nails: Translating Simple Sliding Wedge Analyses into PC-Based Limit Equilibrium Models." *Geo-Frontiers 2011* (CD-ROM), ASCE, Reston, VA.

Duncan, J. Michael, and Wright Stephen G., "Soil Strength and Slope Stability." John Wiley & Sons, Inc. 2005.

Elias, V. and Juran, I. (1988). "Manual of Practice for Soil Nailing. Contract DTFH-61-85-C-00142." Federal Highway Administration, Washington, D.C.

Federal Highway Administration and USDA Forest Service (1994). "Application Guide for Launched Soil Nails, Volumes 1 and 2 (Forest Service EM7170-12A and Federal Highway Administration FHWA-FPL-93-003)."

Jewell, R.A., and Pedley, M.J. (1992). "Analysis for Soil Reinforcement with Bending Stiffness." *J. Geotechnical Engrg.* 118 (10): 1505-1528.

Lazarte, C.A., Elias, V., Espinoza, R.D., and Sabatini, P.J. (2003). "Geotechnical Circular No. 7 – Soil Nail Walls." FHWA0-IF-03-017. Federal Highway Administration, Washington, D.C.

Manual for Design & Construction Monitoring Of Soil Nail Walls. U.S. Department of Transportation Federal Highway Administration, Publication No. FHWA-SA-96-069R, 1996.

Full Scale Testing of Rockfall Barrier and Post Foundation Systems

Ben Arndt[1], M. ASCE, P.E., P.G., Ty Ortiz[2], P.E., and Bob Group[3]

[1]Principal, Yeh and Associates, Inc., 2000 Clay Street, Ste 200, Denver, CO 80211, barndt@yeh-eng.com
[2]Geotechnical Program Manager, Colorado Department of Transportation, 4670 Holly Street, Unit A Denver, CO 80216, ty.ortiz@state.co.us
[3]Rockfall Program Manager, Colorado Department of Transportation, 4670 Holly Street, Unit A Denver, CO 80216, robert.group@state.co.us

ABSTRACT: The use of rockfall barrier systems is common in the United States in mountainous areas. Many of these rockfall systems are placed along the shoulder of roadways to stay within the right of way owned by the various transportation agencies. Many issues have arisen with the design, certification, testing, and application of barrier and post systems as most of the rockfall barrier systems marketed in the United States are tested and approved in Europe.

The rockfall barrier testing guidelines generally follow the Guideline for European Technical Approval of Falling Rock Protection Kits otherwise known as ETAG 027. This guideline provides a basis for documenting full scale testing of rockfall barrier systems for energies ranging from 100 kJ to 4,500 kJ. When specifying and/or designing post foundation systems for transportation agencies, two major limitations become apparent using ETAG 027; 1) no specified limit for outward panel deflection resulting from a rockfall event, and 2) no protocols or guidance for post foundation testing or design.

This paper provides observations, results, and summaries of the seventeen vertical-drop tests in which concrete "boulders" were dropped into various barrier fence systems for energies up to 1,000 kJ, and separately twenty nine post and post foundation direct impact tests that were conducted for energies up to 220 kJ.

INTRODUCTION

Rockfall barrier systems have been widely used in the United States, but the majority of the large manufacturers of these systems are based in Europe. Many of the rockfall systems are designed, manufactured, and tested in Europe using European guidelines and standards. The main European guideline for rockfall testing presently is known as ETAG 027 (2008). This guideline is intended to provide criteria for testing rockfall barrier systems. One major limitation in the European guideline is the exclusion of the design of the post foundation systems, leaving many professional

engineers and designers at a loss as to a practical manner in which to design these foundation systems.

ETAG 027

The European Organization for Technical Approvals created the Guideline for European Technical Approval of Falling Rock Protection Kits otherwise known as ETAG 027. This 2008 guideline outlines testing procedures for rockfall barrier systems to be used throughout Europe. The guideline document replaced previous guidelines that had been developed by the Swiss and other countries in an attempt to provide a baseline in much the same way as ASTM is used to test multiple material or engineered systems in the United States. Central elements of the ETAG 027 guidelines that are typically notable for rockfall barrier designers in the United States are the following:

- Service Energy Level (SEL)
- Maximum Energy Level (MEL)
- Residual height categories
- Outward deflection of barrier panels
- Exclusion of post foundation guidelines

The SEL is defined as the kinetic energy of a regular block impacting the barrier system. The MEL is defined as the kinetic energy of a regular block impacting the barrier system at an energy level that is 300 percent of the SEL. In effect, the MEL is an energy factor 3 times greater than the SEL. The various energy level categories for ETAG 027 are as follows in Table 1.

Table 1. ETAG 027 Energy Level with SEL and MEL

Energy Level	0	1	2	3	4	5	6	7	8
SEL (kJ)	n/a	85	170	330	500	660	1000	1500	>1500
MEL (kJ)	100	250	500	1000	1500	2000	3000	4500	>4500

Two SEL tests are called out in the ETAG guideline. The testing of two SEL tests is considered passing if the following are met:

First SEL Test:

- The block is stopped by the barrier.
- No ruptures in the connection components (which remain connected to foundations), posts, and ropes. The rupture of a connection component is defined as the complete separation of the component itself into two distinct parts. The opening of the mesh of the net shall not be two times bigger than the initial size of the mesh.

- The residual height of the barrier system after the test (without removing the block) is higher or equal to 70 percent of the nominal height. The measured value has to be documented.
- The block has not touched the ground until the kit has reached the maximum elongation during the test.

Second SEL Test:

- The block is stopped by the net panel.
- The block has not touched the ground until the kit has reached the maximum elongation during the test.
- No maintenance is allowed between the first and the second launch at SEL.
- The maximal elongation of the net panel during the SEL test shall be measured and provided in the test report.

One MEL test is called out in the ETAG guideline. The MEL can be performed before or after the SEL testing. The one MEL test is considered passing if the following are met:

Single MEL Test:

- The net fence has stopped the block.
- The block has not touched the ground until the kit has reached the maximum elongation during the test.
- The maximal elongation of the net panel during the MEL test shall be measured and declared.
- The residual height of the net panel after the impact shall be measured and declared.

The residual system height resulting from a test as described and defined in ETAG 027 is illustrated in Fig. 1 and Fig. 2. Categories are based on comparing nominal (pre-test) and residual (post-test heights).

- Category A: Residual height is less than or equal to 50 percent nominal height
- Category B: Residual height is greater than 30 percent nominal height but less than 50 percent nominal height
- Category C: Residual Height is less than or equal to 30 percent nominal height

ETAG 027 also describes other testing results that include measurements of the outward deflection of the barrier and is outlined by the following:

- The maximal elongation (Fig. 3) of the net panel during the MEL and SEL tests shall be measured.
- The maximal elongation of the net panel during the MEL and SEL tests shall be declared.
- No limitations on outward deflection are described.

The post foundation is excluded as described in ETAG 027 as follows:

- The foundation is not considered part of the system. The design of the post foundation is the responsibility of the designer, taking account of special provisions.
- The “force” shall be measured during all the time of impact.
- The peak force shall be declared and the time-force diagrams shall be provided. The measured values shall be declared.

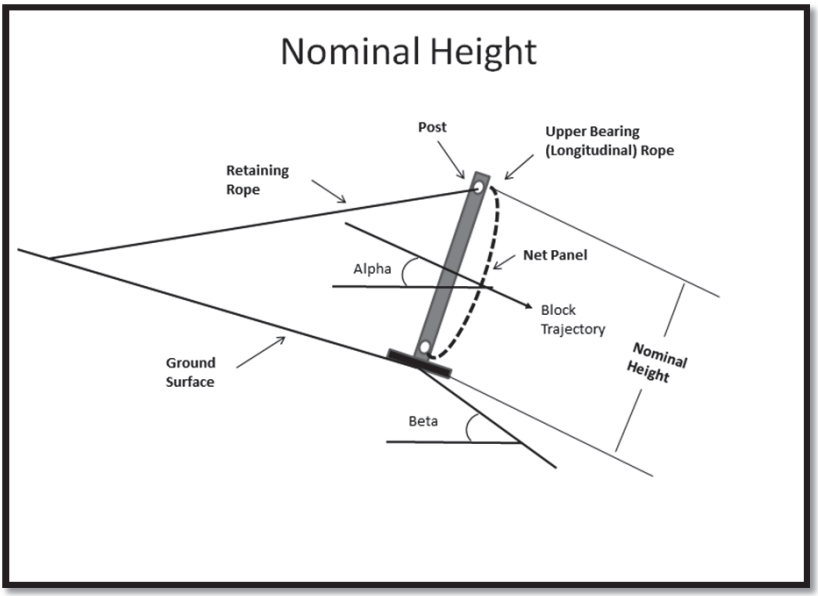

FIG. 1. Nominal Height Representation of Rockfall Barrier System.

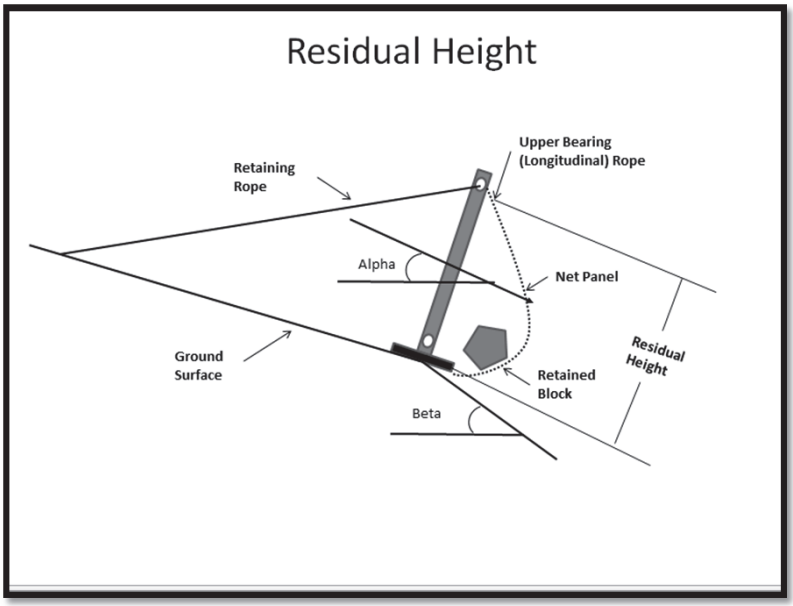

FIG. 2. Residual Height Representation of Rockfall Barrier System.

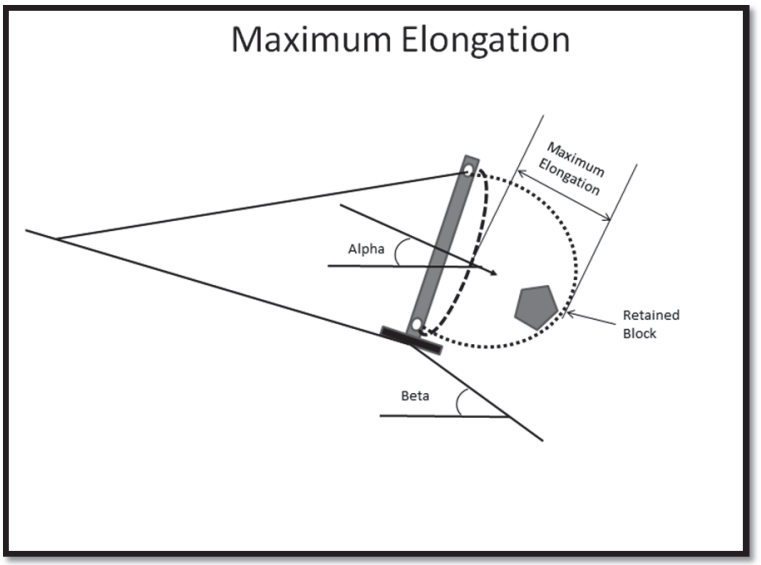

FIG. 3. Maximum Elongation Representation of Rockfall Barrier System.

- The type of force and/or direction and/or magnitude to be measured is not defined creating further ambiguity in what the manufacturer is measuring or what is supposed to be measured.

The preceding is a brief summary of the notable ETAG 027 guidelines for professionals either providing plans and specials for projects or attempting to design the post foundations.

Full Scale Barrier Testing in Colorado

Based on a review of ETAG 027, a full-scale barrier test system was constructed with the ETAG 027 concept in mind, in an attempt to test different panel systems to limit outward deflection for barrier applications placed next to the roadway travel lane. The reported outward barrier deflections for many ETAG 027 tested systems can range from 3 m to 8.5 m for energies ranging from 500 kJ to 2,000 kJ. Outward deflections of this magnitude if a rockfall barrier system is placed along the shoulder of the roadway would place the deformed panel and rock in the travel lanes.

Part of the reason that rockfall barrier systems deflect so much is they have various proprietary braking elements developed by the manufacturers that are incorporated into the various retaining and support wire ropes that stretch and elongate during a rockfall impact. It was hypothesized that a method to limit outward deflection of a net panel during the test program would be to eliminate the braking elements to evaluate what energies the rockfall barrier system could absorb. It was believed for energies greater than 1,000 kJ, it would be necessary to have a braking device for proper

performance of a barrier system, but for energies less than 1,000 kJ, it was believed that braking elements were not necessary.

During April and May of 2010, a vertical test facility was constructed near Georgetown, Colorado. Two separate barrier systems were constructed: 1) a two-post system with a single net panel, and 2) a four-post system with multiple attached net panels. The two-post system was mainly to begin a testing effort and determine which components would function better.

Two- and Four-Post Test System Setups

The test systems consisted of constructing two and four posts that were anchored to a near-vertical rock face. The test systems consisted of (Fig. 4 through Fig. 6 and Photographs 1 and 2):

- W10x60 posts that were 4.5 m high (panel height) and spaced 9.1 m apart.
- Posts welded to steel base plates that were 610 mm by 610 mm by 25 mm thick.
- Pinned post connection systems were not evaluated.
- Two uphill 25 mm diameter wire ropes on each post.
- One to two 25 mm diameter wire rope anchors drilled and grouted approximately 1.5 m into hard metamorphic rock.
- Two upper and two lower 25 mm diameter bearing wire ropes that the net panel was shackled to.
- One lateral 25 mm diameter wire rope on each post.
- Net panels consisted of either Ring Nets or 12 mm Cable Nets.
- Foundations of posts consisted of 25 mm all-thread bar that was drilled approximately 1.5 m into hard metamorphic rock.
- Square concrete pads were constructed to support the post base plate.
- Circular load cells were placed around the 25 mm all-thread bar between an outer nut and the base plate to record compression within the load cell (i.e. tension of the bar) (Photograph 3).
- Circular link cells were attached to the two upper and two lower bearing ropes and uphill and lateral retaining ropes (Photograph 4).
- Vertically dropping a 1,551 kg block from either 18.3 m or 36.6 m to generate 278 kJ or 578 kJ of energy, respectively.
- For the four-post system, a 2,177 kg block was dropped from 42.7 m to generate 911 kJ of force.

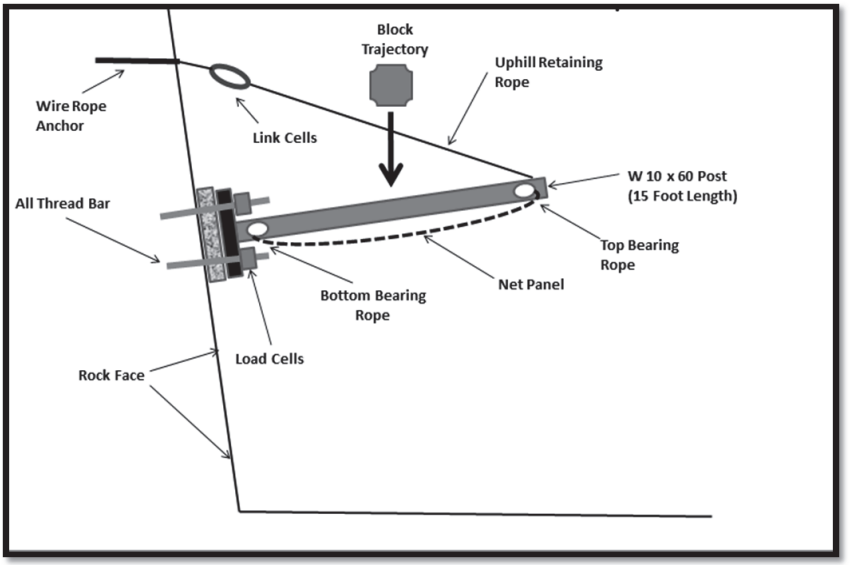

FIG. 4. Side View of Post and Barrier Test System.

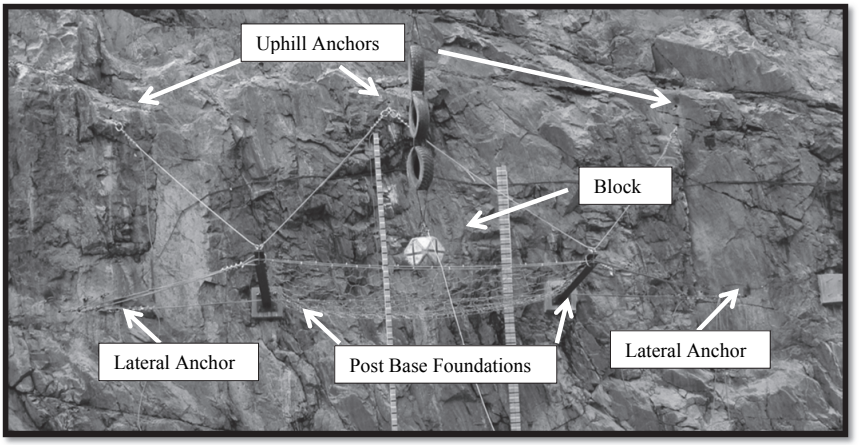

Photograph 1. Elevation View of Two Post and Barrier Test System.

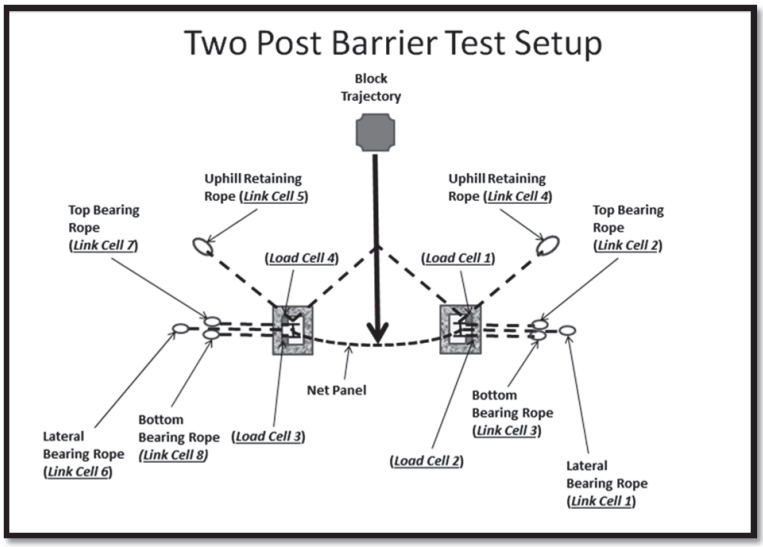

FIG. 5. Elevation View of Typical Setup for Two Post and Barrier System.

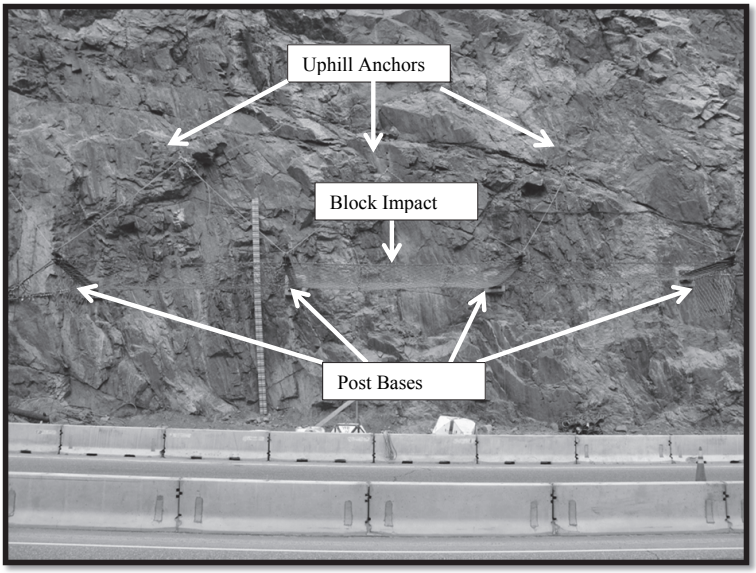

Photograph 2. Elevation View of Four Post and Barrier Test System.

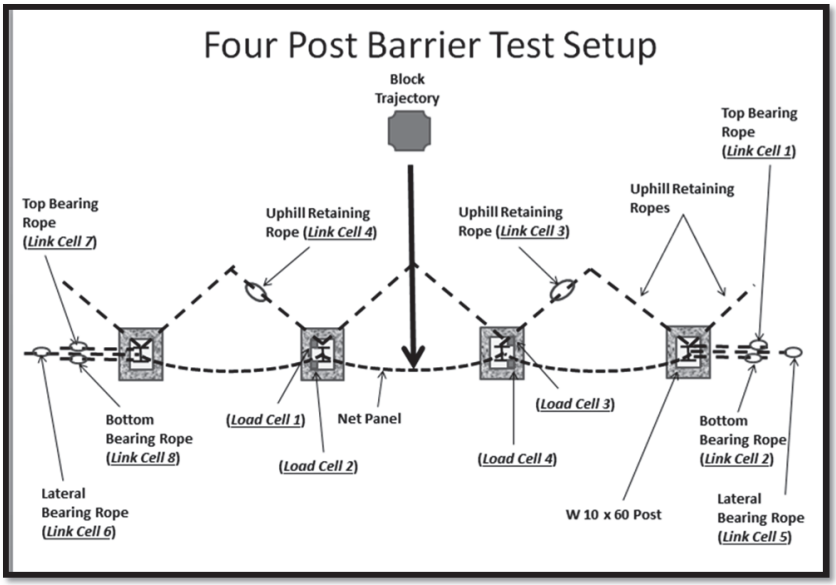

FIG. 6. Elevation View of Typical Four Post and Barrier Test System.

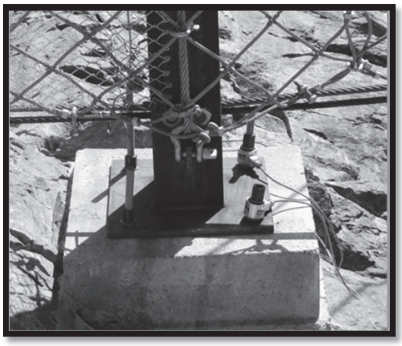

Photograph 3. Right side of Photograph Shows Load Cells for Measuring Tensile Loads in Foundation Bars.

Photograph 4. Center of Photograph Shows Link Cell for Measuring Tensile Loads in Wire Ropes.

RESULTS OF TESTING

The results of the testing are presented in Table 2. The following observations of the data show various loading conditions for the tests conducted at the Georgetown Site. The following should be noted:

- As with all testing, the instrumentation data can be evaluated by many different methods that can provide various results within a given framework. The maximum and minimum loads were evaluated for this publication.
- Load cells were placed to measure the tension in the grouted 25 mm foundation bars (Fig. 4 and Photograph 3). Link cells were placed to measure the tension in the wire rope systems (Fig. 4 and Photograph 4).
- Refer to Fig. 5 (Two Post System) and Fig. 6 (Four Post System) for locations of load cells on the post foundations and link cells in the wire rope supports.
- Axial loading of the post foundations were inferred from the load cell data. Shear and axial loading conditions were not specifically evaluated.
- The post system foundation was fixed and mounted on a rigid concrete base.
- For the testing, both cable net panel and ring net and systems were used. Cable net panels consisted of 12-mm diameter wire rope with 205 mm by 205 mm diagonal weave openings. Ring nets consisted of seven wire loops that were 3-mm in diameter with 300 mm openings.
- There did not appear to be a significant advantage or disadvantage between cable nets and ring nets for the four-post system tests. Cable nets were used throughout since CDOT had more supply available during testing.
- To achieve the final 911 kJ test, it was necessary to use a braking system to dissipate the energy of the rockfall impact. The simple brake system used is shown in Photograph 7 (slack brake). The slack brake is comprised of two overlapping wire ropes with loosened wire rope clamps that slide in opposite directions up to 0.3 m when dynamically loaded.

Two-Post Systems

The following observations were based on the data.

Post Load Cells (depicted in Fig. 5):

- The top and bottom wire support bearing ropes carry the majority of force of the impact applied to the net panel.
- No lateral or uphill anchors failed during the testing.
- The most of the loading on the post foundation 25 mm bar was in tension. The upper grouted bars were subjected to greater tension, but the lower bars were also in tension, indicating the entire post base was in tension for the geometry of the test setup.
- The range of loading on the foundation bars varied significantly from test to test even for seemly duplicate tests.

Wire Rope Link Cells (depicted in Fig. 5):

- The bottom bearing ropes were subjected to the highest tensile loading conditions.
- The range of loading on the wire rope anchor systems varied significantly from test to test even for seemly duplicate tests.
- The wires ropes did not have a significantly greater load when comparing the 278 kJ and 577 kJ testing. The 278 kJ testing showed many of the bearing ropes had loads in excess of 300 kN.

Table 2. Results of the Rockfall Barrier System Testing.

No. Posts	Test	Net Type	Energy (kJ)	Peak Force Load Cells (kN) (Fig. 5)				Peak Force Link Cells (kN) (Fig. 5)								Panel Deflection (m)	Comments
				LC1	LC2	LC3	LC4	LN1	LN2	LN3	LN4	LN5	LN6	LN7	LN8		
2	A	Ring Net	557	117	55	17	239	92	241	263	74	151	94	253	241	NA	1st Test - No Failure in Wire Ropes or Posts
	B	Cable Net	278	123	111	16	154	121	219	355	78	135	109	252	308	NA	2nd Test - No Failure in Wire Ropes or Posts
	C	Cable Net	557	131	106	58	280	108	173	376	77	154	110	254	281	NA	3rd Test - Failure of One Top and Both Bottom Bearing Ropes
	D	Cable Net	557	62	191	19	57	117	195	364	73	79	79	176	276	NA	1st Test - No Failure in Wire Ropes or Posts
	E	Ring Net	278	45	49	17	111	96	179	277	38	114	82	182	225	NA	1st Test - No Failure in Wire Ropes or Posts
	F	Cable Net	557	34	1	1	94	131	268	371	79	185	129	249	311	NA	2nd Test - Failure of Both Bottom Wire Bearing Ropes
4	G	Cable Net	278	110	42	152	2	157	170	104	37	26	99	176	210	1.4	1st Test - No Failure in Wire Ropes or Posts
	H	Cable Net	278	137	65	150	8	188	193	123	48	33	113	215	232	0.3	2nd Test - No Failure in Wire Ropes or Posts
	I	Cable Net	557	214	95	378	32	233	239	136	55	48	144	231	296	5.2	3rd Test - Failure Both Bottom Bearing Ropes and Post Base
	J	Cable Net	557	233	53	92	175	229	259	116	65	51	150	272	303	2.0	1st Test - No Failure in Wire Ropes or Posts
	K	Cable Net	557	251	167	107	12	255	164	145	46	53	166	322	243	Failed	2nd Test - Failure Both Top Bearing Ropes
	L	Cable Net	911	209	245	114	14	117	109	124	70	120	90	173	144	4.2	1st Test - No Failure in Wire Ropes. Minor Post Damage. Slake Brakes Used

Four Post Systems

The following observations were based on the data.

Post Load Cells (depicted in Fig. 6):

- The data indicated the foundation bar elements were in tension (pullout) for the test setup.

Wire Rope Link Cells (depicted in Fig. 6):

- The bottom bearing ropes were subjected to the highest tensile loading conditions.
- The range of loading on the wire rope anchor systems appeared to be more repeatable from test to test when compared to the two post system.
- During Test I, the foundation post broke at the weld in overturning and not in shear at the base (Photograph 5).
- Deflection was limited to 4.2 m for the 911 kJ tested system but it was necessary to use slack braking systems (Photographs 6 and 7).

Photograph 5. Broken Post Resulting from Test I. (Per ETAG 27 this could be considered a Category A test since it stopped the rock and the residual height would be greater than 50 percent).

SUMMARY BARRIER TESTING

Based on the rockfall barrier system testing conducted the following general observations were made:

- It was possible to achieve multiple passing tests in excess of 557 kJ without any braking elements.
- It was not possible to achieve a 911 kJ non-failing test without utilizing some sort of simple braking device “slack brake” (Photograph 7).
- The data indicated the foundation 25 mm bar elements were in tension and were susceptible to failure in pullout (overturning of the post) rather than shear for a fixed welded base on a concrete pad.

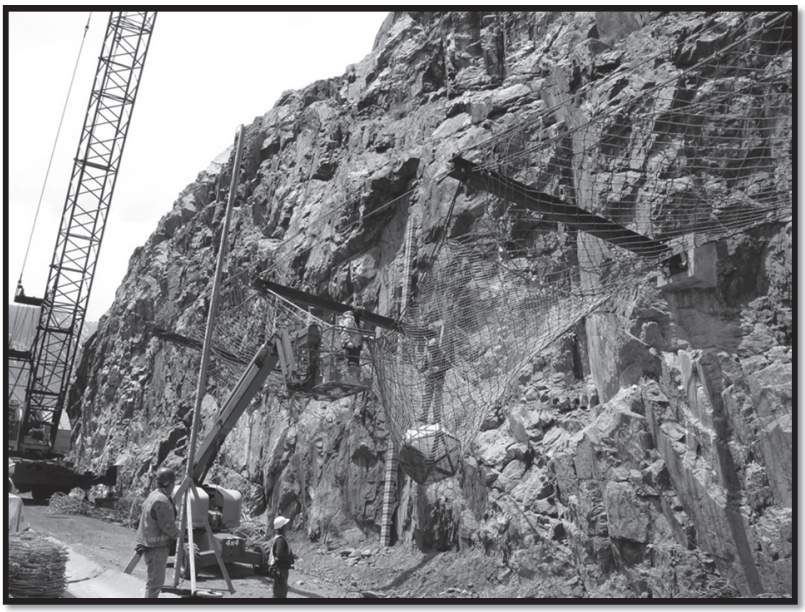

Photograph 6. Side View of Actual Post and Barrier Test System for Four Posts for Test L – 911 kJ test.

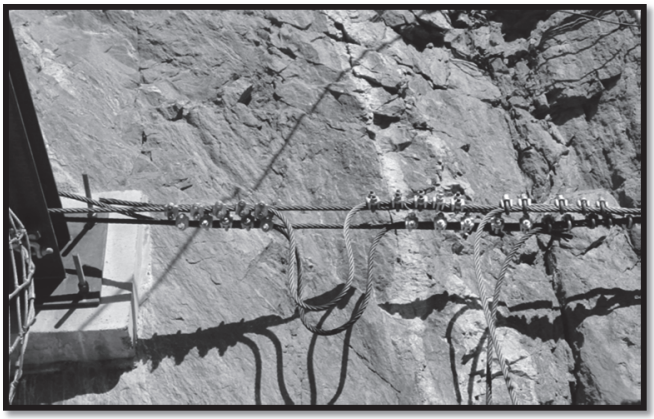

Photograph 7. Dissipation slack in bottom bearing ropes (Slake Brake) Test L. Wire rope clamps are allowed to slip slightly allowing the "U" shaped section of the wire rope to lengthen during a dynamic impact.

- Significant axially loading along the post normal to the concrete pad was not observed, however this was not specifically instrumented.

- The data indicated that the four-post testing system provided more consistent data of foundation bar and wire rope loadings when comparing similar tests for the two-post testing system.
- For the test in which the post foundation broke at the weld (Photograph 5), the residual height of the overall system was still greater than 90 percent. ETAG provides for a Category A rating for a residual height greater than 50 percent, however this rockfall barrier system was severely compromised and would likely need to be replaced when considering long-term maintenance.
- Overall outward panel deflections of the testing were as follows (approximately):
    - 1.4 m for 278 kJ (no braking system)
    - 2.0 m for 557 kJ (no braking system)
    - 4.2 m for 1,000 kJ (using slack braking system)

POST BASE TESTING IN COLORADO

In addition to rockfall barrier system testing, it became apparent during other full-scale testing of rockfall systems that the major function of a rockfall barrier post is to support the net panel components. When a rockfall event occurs, if the post system can support and hold a net panel in a functioning state for even a few seconds during a rockfall event, it may mean the difference between having rocks contained in the net panel system or having rocks rolling through a failed system and reaching the roadway. CDOT's primary goal is to keep rockfall from reaching the roadway. Net panel systems that have residual heights that are 30 percent to 50 percent of the nominal height will likely not be effective at keeping rock off the roadway.

Assuming the goal is to keep rock off the roadway and maintain a rockfall system in a functioning state as long as practical, one of the perceived shortcomings of the current ETAG 027 guideline is that it does not address direct rockfall impacts to a post or post foundation systems. The guideline allows for impacts to the center of the net panel system, but not to a post system. Many designers exclude a post impact from design calculations and emphasis has been to market and design more easily replaced pinned type post systems that breakaway if impacted during a significant rockfall. However, these systems require more maintenance and may result in more rock on the roadway.

Due to lack of guidelines for post foundation systems for rockfall barrier systems, testing was conducted on different types of post systems. A total of twenty nine direct post impacts were conducted for energies up to 220 kJ. The post bases were either fixed or "floating" on the ground surface. Pinned type post base systems were not evaluated. A selection of specific series of post testing is presented in this publication.

Manufacturers in many instances may provide the results from instrumentation data obtained from secondary loadings on the post systems resulting from direct net panel impacts but do not necessarily have data for direct post impacts. Typical design issues for provided post foundation test results are as follows:

- ETAG 027 has no established protocols for the type of data provided. For example, some manufacturers provide shear and vertical loading on the posts, but these may not be the critical loading conditions on the post systems as

overturning may control.

- Depending on the foundation type, the loading conditions may or may not be comparable to what is constructed at a given site. For example, a rigid post foundation anchored into solid bedrock will likely perform quite differently than a foundation system that is allowed to deflect and rotate.
- Static and dynamic loading conditions are generally not comparable. Designing a foundation for static loads acting on a foundation over long time periods may not be equivalent to a dynamic impulse momentum force that acts over a fraction of a second.

With these limitations in mind, the post foundation testing program was designed to evaluate the design of post foundations for further use in:

- Overall design options for post foundations.
- Comparison of static versus dynamic loading conditions of foundation systems.
- Maintaining a functioning post system during multiple impacts.

Based on the testing conducted, the following five post foundation testing series are presented in this paper:

- A Series - Post base consisting of a concrete leveling pad with grouted bar foundation elements. No uphill wire rope support anchors.
- B and C Series - Post bases consisting of a precast circular concrete shaft embedded 1 m and 2 m in the ground. No uphill wire rope support anchors.
- D and E Series - Post bases consisting of a concrete leveling pad with grouted bar foundation elements. Comparison of only top wire rope support anchors and both top and bottom uphill wire support ropes.
- F and G Series - Post base consisting of only a steel footing plate that was free to deflect (float). Post supported with top and bottom wire rope anchors.

Pendulum Site Testing Setup

The general testing of the posts consisted of creating a pendulum system capable of swinging various concrete boulders into various posts and post foundation systems. Various elements of the testing were as follows:

- A pendulum type system was erected to swing preformed cuboctahedron concrete blocks that ranged from 1,475 kg to 3,628 kg into a post system.
- The vertical pendulum drop height of the system was limited to 6.1 m, which corresponded to maximum generated energies up to 220 kJ with the blocks used.
- Two types of posts were used, a W8x48 for the smaller and grouted bar foundation systems and a W10x60 for the deeper circular shaft type foundations.
- Post foundations were rigid, no pinned base posts were tested.
- The post base plates allowed for four all-thread 25 mm bar to be tightened to the base plates with nuts and washers.
- The same load cells that were used in the fence barrier testing were placed on all the 25 mm all-thread bars to provide compression change values.

- The nuts and washers on the bar/load cell system were tightened as much as possible prior to the testing so a load loss could be recorded in the data. It appeared that up to 60 kN could be pre-loaded on the foundation bars by tightening the nuts prior to testing.
- The link cells that were used in the net panel barrier testing were also attached to either the top or bottom uphill wire retaining anchors to provide tensile readings in the system.
- The top and bottom uphill wire retaining ropes were connected to a stack of concrete guard rail barriers to approximate an anchor system. The stacked concrete barrier could be readjusted after each test so that potential replacement of anchor systems if they were pulled out of the ground did not affect the testing schedule.

Fig. 7 depicts the plan view of the anchor test site setup with the load and link cell designations. Photographs 8 and 9 show a side view and elevation (front) view of the testing setup. Photograph 10 shows the location and tightening of load cells. Photograph 11 shows the link cell anchored to the concrete barrier system.

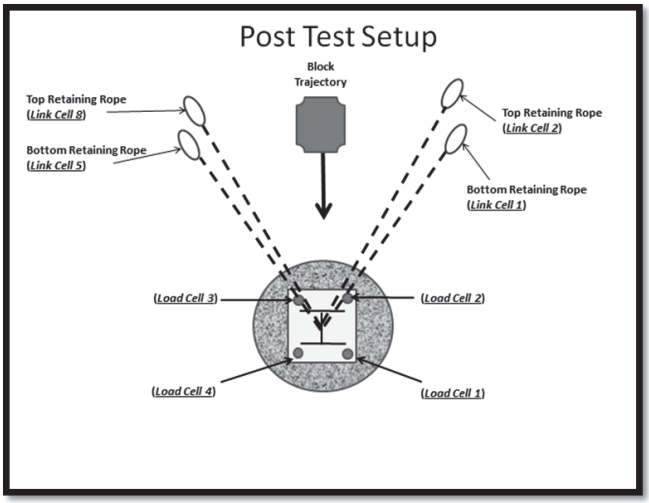

FIG. 7. Anchor test site plan view of set up with load and link cell designations.

Photograph 8. Side view of the test site setup. Rock is released and swings to right side of photograph.

Photograph 9. Front view of the test site setup. Rock is directly behind test post prior to raising it.

OUTLINE OF TESTING SERIES

A Series.

Post base consisting of a concrete leveling pad with grouted bar foundation elements (Photograph 11). No uphill wire rope support anchors.

This test series consisted of:

- W8x48 posts that were 4.5 m high with 508 mm by 508 mm by 25 mm base plate.
- Base plate allowed for four 25 mm all-thread bars that were tightened to approximately 60 kN with nuts and washers.

Photograph 10. Location and tightening of load cells prior to testing.

Photograph 11. Link cell of uphill wire rope anchors attached to the concrete barrier system.

- Base plate of post founded on concrete base pad 150 mm thick and 0.9 m in diameter with one No. 4 horizontal rebar stirrup reinforcement.
- All thread bar 25 mm bars installed and grouted approximately 1.5 m in the ground in an approximate 50 mm predrilled hole.
- No uphill or downhill wire rope anchors.

Photograph 12 shows pouring concrete base pad. Fig. 8 depicts the typical cross section of the system.

B and C Series.

Post bases consisting of a circular concrete shaft embedded approximately 0.91 m (B series) and 1.82 m (C series) in ground. Foundations were backfilled with well graded material that was compacted. No uphill wire rope support anchors (Photograph 13 and Fig. 9).

This test series consisted of:

- W10x60 posts that were 4.5 m high with 610 mm by 610 mm by 25 mm base plate.
- Base plate allowed for four 25 mm all-thread bars that were then tightened to approximately 60 kN with nuts and washers.
- Base plate of post founded on two types of concrete shafts that were 0.9 m in diameter with #4 horizontal rebar stirrup reinforcement on 300 mm centers. The first test the concrete shaft was 0.91 m deep and the other test was 1.82 m deep.
- All-thread bar 25 mm bars installed into concrete shaft full length of shaft.
- No uphill or downhill wire rope anchors.

Photograph 12. Pouring the concrete foundation pad around the grouted bar elements.

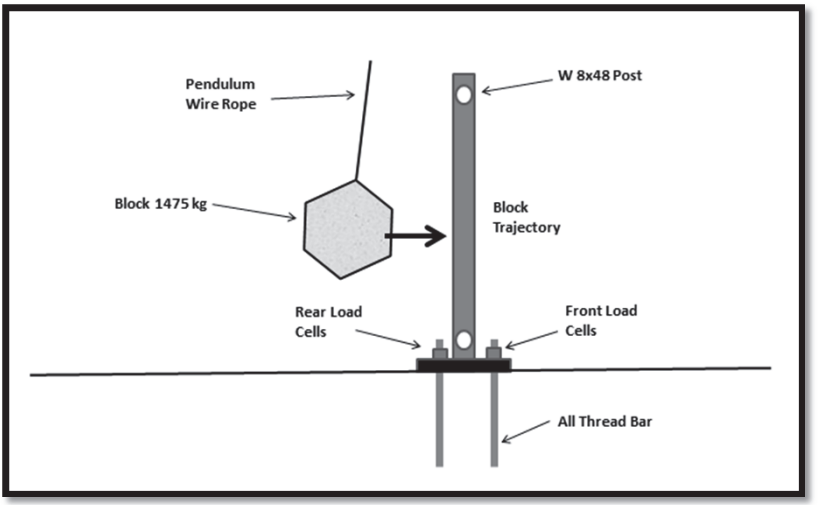

FIG. 8. Typical section of A series test setup.

Photograph 13shows construction of the circular concrete shafts. Fig. 9 depicts the typical cross section of the system.

Photograph 13. Installation of circular concrete shaft post foundation systems with completed system compacted in place.

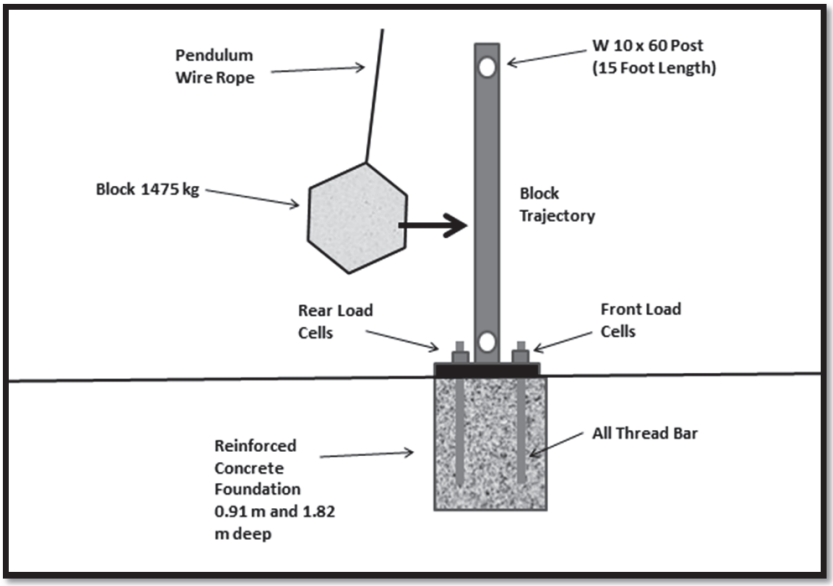

FIG. 9. Typical section of B and C series test setup.

D and E Series.

Post bases consisting of a concrete leveling pad with grouted bar foundation elements. Comparison of uphill only top wire rope support anchors (D series) and both top and bottom uphill wire rope support anchors (E series).

This test series consisted of:

- W8x48 posts that were 4.5 m high with 508 mm by 508 mm by 25 mm thick base plate.
- Base plate allowed for four 25 mm all-thread bars that were tightened to approximately 60 kN with nuts and washers.
- Base plate of post founded on concrete base pad 150 mm thick and 0.9 m in diameter with one No. 4 horizontal rebar stirrup reinforcement.
- All-thread bar 25 mm bars installed and grouted approximately 1.5 m in the ground in an approximate 50 mm predrilled hole.
- First series of tests with top uphill wire rope anchor
- Second series of tests with both top and bottom uphill anchors.

Figs. 10 and 11 depict typical cross section of the test setup.

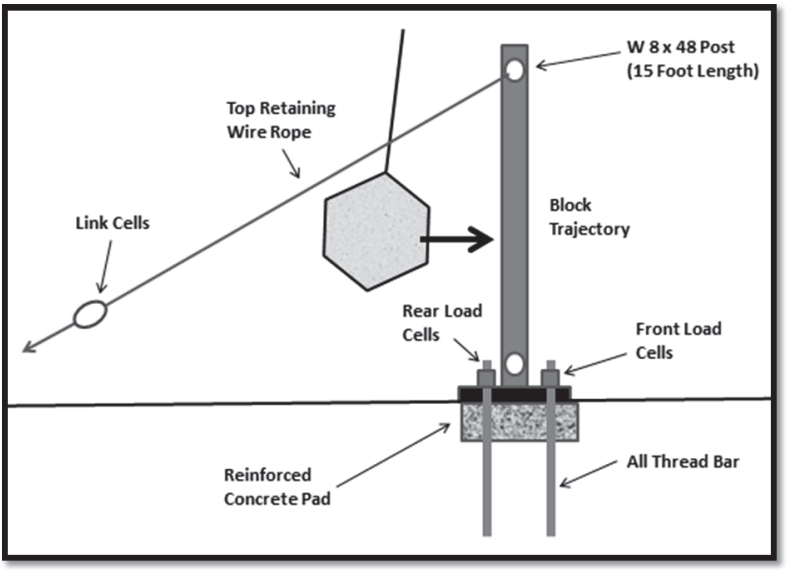

FIG. 10. Typical section of D series test setup.

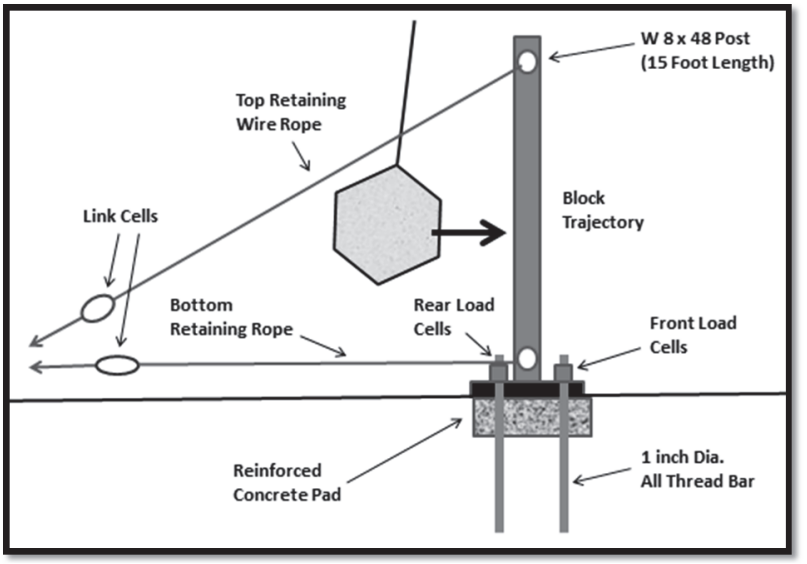

FIG. 11. Typical section of E series test setup.

F and G Series.

Post bases consisting of a steel plate in contact with the ground. Plate is free to move within the constraints of the top and bottom uphill anchors.

This test series consisted of:

- F-series was W8x48 post that was 4.5 m high with square 508 mm by 508 mm by 25 mm thick base plate in contact with the ground. (Photograph 14)
- G-series was W8x48 post that was 4.5 meters high with circular 457 mm diameter by 25 mm thick base plate in contact with ground. Base had wire rope protective sleeves for bottom wire rope anchor. Post was also set on approximate 20 degree angle to approximate placement on a slope. (Photograph 15). Fig. 12 depicts the typical setup.

RESULTS OF POST BASE TESTING

The results of the post base testing are presented in Table 3. The following observations of the data show various loading conditions for the tests conducted. The following should be noted:

- As with all testing, the instrumentation data can be evaluated by many different methods that can provide various results within a given framework. The maximum change in loading was evaluated for this publication.
- Load cells were placed to measure the tension in the grouted 25 mm foundation bars (Fig. 7 and Photograph 10). Link cells were placed to measure the tension in the wire rope systems (Fig. 7 and Photograph 11).

Photograph 14. Typical setup for F series test.

Photograph 15. Typical setup for G series test.

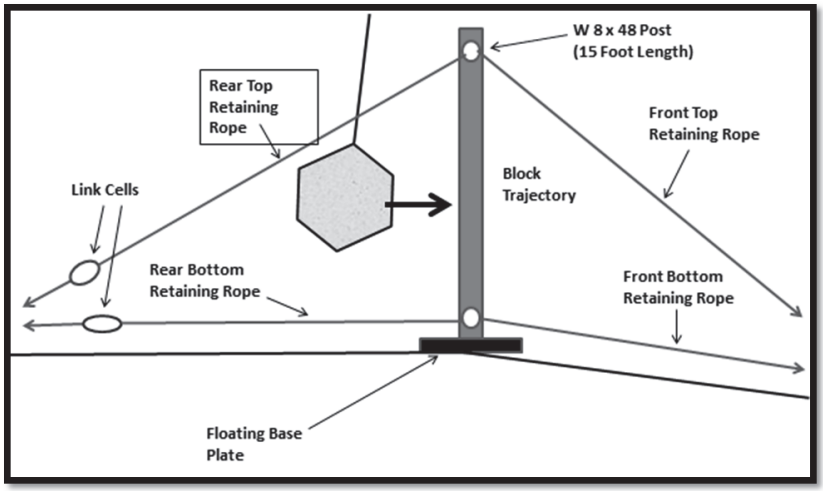

FIG. 12. Typical section of F and G series test setup.

- Refer to Fig. 7 for locations of load cells on the post foundations and link cells in the wire rope supports.
- Axial loading of the post foundations were inferred from the load cell data. Shear and axial loading conditions were not specifically evaluated.
- Many test results indicated the load cells on the post foundation anchors lost load resulting from the post impacts. The peak load on the foundation bar elements and link cells resulting from the impacts are reported in the tables.

- Most of the loads recorded in the load cells on the foundation elements indicated tension in the bar elements. Greater tension (load) was typical for the rear or impact side of the tests (Load Cell 2 and Load Cell 3).
- The test data are provided per A, B, C, D, E, F, and G to show the similarities and differences between the post systems.
- Potential energy was calculated from the vertical drop of the pendulum system.
- The calculated horizontal force was based on impulse-moment using:

$$\mathbf{F = ma = m(dv/dt)}$$

where: F = Force
m = mass
a = acceleration or dv/dt where change of velocity over change in time

- Based on the data, it appeared that most of the impacts occurred over a time interval between 0.12 second to 0.15 second. For the purposes of comparison a time interval of 0.15 second was used.
- Most of the block impacts where at or just below the midpoint of the post (i.e. 2.1m to 2.2 m above base plate of post). The test Series G block hit the post as low as possible to maximize the potential energy.

SUMMARY OF POST BARRIER TESTING

Based on the post and post foundation testing conducted, the following general observations were made.

A Series.

- At 19.7 kJ of energy (50.8 kN of horizontal force), the entire post system rotated in a moment failure.
- Virtually no damage to post, concrete, or foundation elements. Uphill bar elements pulled out of ground.
- Both rear and front foundation bar elements were in tension.

Photograph 16 shows the results of the 19.7 kJ test with no uphill anchors on grouted bar foundation system.

Table 3. Results of the Post Base Testing

Series	Swing	Test	Post	Potential Energy (kJ)	Impulse Momentum Horizontal Force (kN)	Peak Force Load Cells (kN) (Fig. 7 and Photograph 10)				Peak Force Link Cells (kN) (Fig. 7 and Photograph 10)				Comments
						LC1	LC2	LC3	LC4	LN1	LN2	LN5	LN8	
A	16	A-2	W8x48	19.7	50.8	5.2	76.2	71.9	19.7	-	-	-	-	At 19.7 kJ the entire test post foundation bar system pulled out of ground.
B	42	B-1	W10x60	8.9	34.1	1.9	65.1	58.2	4.0	-	-	-	-	1st Test. Negligible post and foundation damage.
	43	B-2	W10x60	19.7	50.8	71.5	145.5	102.1	42.6	-	-	-	-	2nd Test. Soil/ground failure surrounding concrete. Minimal post damage but rotated outward.
C	39	C-1	W10x60	8.9	34.1	0.5	180.4	164.9	19.3	-	-	-	-	1st Test. Negligible post and foundation damage.
	40	C-2	W10x60	19.7	50.8	0.3	283.2	287.0	17.7	-	-	-	-	2nd Test. Base plate damage to post. Still functional
	41	C-3	W10x60	67.8	94.3	118.8	272.9	335.4	94.3	-	-	-	-	3rd Test. Complete base plate failure to post. Not functional.
D	17	D-1	W8x48	8.5	33.4	0.6	95.6	82.2	0.2	-	6.7	-	10.1	1st Test. Negligible post and foundation damage.
	18	D-2	W8x48	19.7	50.8	3.1	82.2	84.6	0.2	-	19.3	-	18.1	2nd Test. No damage to post. Cracking in concrete base
	19	D-3	W8x48	64.8	92.1	9.4	117.7	93.1	33.7	-	55.2	-	64.6	3rd Test. Post bent slightly. Concrete foundation cracked significantly revealing stirrup bars
	25	D-4	W8x48	113.1	144.8	0.5	0.5	108.8	44.5	-	48.0	-	78.5	4th Test. Post bent slightly. Foundation bar elements visibly bent. Concrete foundation cracked further.
	26	D-5	W8x48	116.1	146.7	72.2	101.1	113.1	108.4	-	59.4	-	83.9	5th Test. Post bent slightly. Foundation bar elements visibly bent. Concrete foundation cracked further.
E	20	E-1	W8x48	8.9	34.1	1.4	83.2	50.6	1.3	4.0	10.1	7.9	9.4	1st Test. No visible post and foundation damage.
	21	E-2	W8x48	19.7	50.8	2.0	94.9	9.7	8.7	14.1	28.7	1.2	19.3	2nd Test. Minor bending in post. Initial cracking in concrete base
	22	E-3	W8x48	E	96.0	39.3	165.0	72.5	42.9	7.2	78.7	2.7	52.0	3rd Test. Post bent slightly. Concrete foundation cracked further

Table 3. Results of the Post Base Testing (continued).

Series	Swing	Test	Post	Potential Energy (kJ)	Impulse Momentum Horizontal Force (kN)	Peak Force Load Cells (kN) (Fig. 7 and Photograph 10)				Peak Force Link Cells (kN) (Fig. 7 and Photograph 10)				Comments
						LC1	LC2	LC3	LC4	LN1	LN2	LN5	LN8	
E	23	E-4	W8x48	110.8	143.3	107.3	95.9	69.3	90.5	30.7	82.6	10.1	58.7	4th Test. Post bent slightly. Foundation bar elements visibly bent. Concrete foundation cracked further.
	24	E-5	W8x48	112.8	144.6	56.6	83.8	64.5	111.1	49.2	68.5	17.3	35.9	5th Test. Post bent slightly. Foundation bar elements visibly bent. Concrete foundation cracked further.
F	37	F-1	W8x48	95.8	133.3	-	-	-	-	34.6	50.8	87.4	98.5	1st Test. Bent post slightly
	38	F-2	W8x48	95.8	133.3	-	-	-	-	18.8	13.3	60.1	89.8	2nd Test. Bent not secure, fell over after test.
G	60	G-1	W8x48	217.5	264.9	-	-	-	-	91.3	21.5	124.0	60.1	1st Test. Bent post slightly.
	61	G-2	W8x48	217.5	264.9	-	-	-	-	160.6	60.9	176.0	50.8	2nd Test. Bent post significantly


Photograph 16. Results of 19.7 kJ test for A series test.

B Series.

- At 19.7 kJ of energy (50.8 kN of horizontal force), the entire post foundation that was embedded 0.9 m in ground rotated outward in moment failure of confinement of the surrounding soil.
- Virtually no damage to post, concrete, or foundation concrete.
- Both rear and front foundation bar elements were in tension but at approximately 50 percent loads of the A series tests.
- Summing moments around the post base using the horizontal impulse moment versus the passive resistance indicates the 0.9 m embedment is insufficient to withstand the post rotation, which is illustrated in the soil failure condition depicted in the photos.

Photograph 17 shows the results of the 19.7 kJ test with no uphill anchors on 0.9 m deep foundation system.

C Series.

- At 19.7 kJ of energy (50.8 kN of horizontal force), minor damage was observed to post foundation that was embedded 1.8 m (6 feet) in the ground.
- At 67.8 kJ of energy (94.3 kN of horizontal force) significant damage was observed to post foundation plate. No damage to circular shaft foundation embedded 1.8 m (6 feet) in the ground.
- Both rear and front foundation bar elements were in tension at loads similar to A series tests.

Photograph 17. Results of 19.7 kJ test for B series test.

- Summing moments around the post base using the horizontal impulse moment versus the passive resistance indicates the 1.8 m embedment is sufficient to withstand the post rotation at impacts up to 19.7 kJ, but is insufficient to withstand the post rotation at impacts up to 67.8 kJ. Since this is a rigid system, the post base was the weakest link and failed.

Photograph 18 shows the results of the 67.8 kJ test with no uphill anchors on a 1.8 m deep foundation system.

D Series.

- A series of five successive tests was conducted on this system ranging in energy from 8.5 to 116.1 kJ.
- Post system had only top uphill wire rope anchors on grouted bar foundation system.
- At 116.1 kJ of energy (146.7 kN of horizontal force), significant damage was observed to post bar and concrete foundation system. Post was also bent but system was still functioning overall.
- Even though impact energy was much higher than Tests A, B, and C, the overall tension to the bar foundation elements was much less since the foundation pad broke away.

Photograph 18. Results of 67.8 kJ test for C series test.

Photograph 19 shows the results of the 116.1 kJ test with only top uphill anchors on grouted bar foundation system.

Photograph 19. Results of 116.1 kJ test for D series test.

E Series.

- A series of five successive tests was conducted on this system ranging in energy from 8.9 to 112.8 kJ.
- Post system had both top and bottom uphill wire rope anchors on grouted bar foundation system.
- At 112.8 kJ of energy (144.6 kN of horizontal force), much less damage was observed to post bar and concrete foundation system as compared to D series

of tests likely due to the bottom uphill wire rope anchor. The post was also bent but the system was still functioning overall.

- The overall tension to the bar foundation elements was similar to D series tests.

Photograph 20 shows the results of the 112.8 kJ test with both top and bottom uphill anchors on grouted bar foundation system.

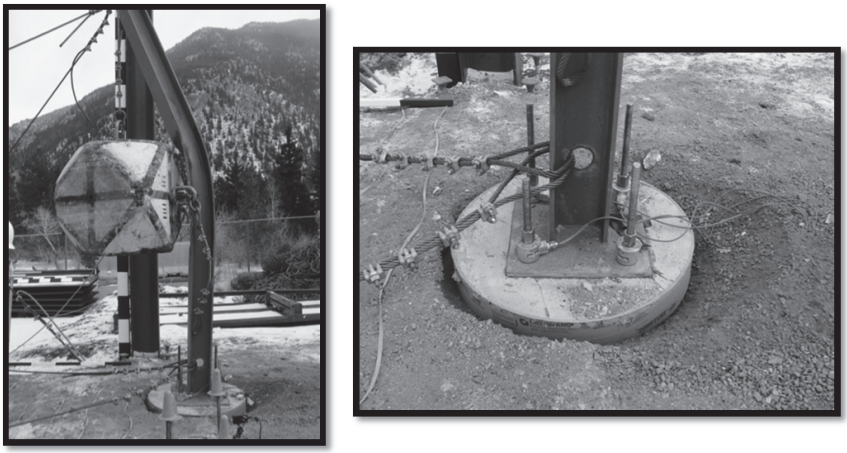

Photograph 20. Results of 112.8 kJ test for E series test.

F Series.

- A series of two successive tests was conducted on this system at 95.8 kJ.
- Post system had both top and bottom uphill wire rope anchors on a floating steel base foundation system.
- At 95.8 kJ of energy (133.3 kN of horizontal force), slight post damage. The post was bent but the system was still functioning overall.
- The overall loads in the wire rope anchors were higher than other tests, but still well within capacities for reasonable anchor pullout and wire rope strength.

Photograph 21shows the results of the 95.8 kJ test with top and bottom uphill anchors on a floating steel plate foundation.

G Series.

- A series of two successive tests was conducted on this system at 264.9 kJ.
- Post system had both top and bottom uphill wire rope anchors on a circular floating steel base foundation system that was inclined approximately 20 degrees.
- At 217.5 kJ of energy (264.9 kN of horizontal force), the post was bent but the system was still functioning overall.

Photograph 21. Results of 95.8 kJ test for F series test.

- The overall loads in the wire rope anchors were higher than other tests, but still well within capacities for reasonable anchor pullout and wire rope strength for 25 mm (1 in) diameter.

Photograph 22 shows the results of the 217.5 kJ test with top and bottom uphill anchors on a circular floating steel plate foundation.

Photograph 22. Results of 217.5 kJ test for G series test.

SUMMARY OF POST AND POST FOUNDATION TESTING

Based on the post foundation testing conducted, the following general observations were made:

- Overall the most flexible post foundation systems were best at absorbing impact energy with the least amount of damage (test series F and G).

- The flexible floating base foundations could absorb more than 3 times the impact energy than fixed-rigid-base systems.
- Using both top and bottom uphill wire rope anchors lessened damage to the stiffer foundation systems (comparing test series D to E).
- The stiffer the post foundation system, the more damage that was concentrated with respect to the structural elements (test series C).
- The posts were impacted with a horizontal force (normal to the post); significant axial loading along the post into the foundation was not observed.

CONCLUSIONS

The testing of rockfall barrier systems and post foundation systems illustrated that European barrier guidelines (ETAG 027) may be a way to compare various rockfall systems, but for a design engineer, the protocols outlined in those guidelines may not be appropriate for the design intent. Specifically, the tested systems may have residual post impact heights at 50 percent to 30 percent of the original (nominal) barrier system height and still be considered a successful test. In reality, if a rockfall barrier system is 50 percent of the nominal height, it will require extensive repair and/or replacement, which is be counterproductive for DOTs trying to reduce maintenance costs and maintain barrier systems by keeping rock off the roadway.

The post foundation testing illustrated that a flexible foundation (floating) steel base plate system offers the greatest potential to absorb multiple rockfall impacts at higher energies and still maintain the original (nominal) height of the post system. Flexible floating foundations absorbed more than three times the impact energy than rigid structural foundations and testing indicated that uphill anchor systems are much better designed to absorb dynamic impacts than rigid structural foundations. Rigid concrete and steel systems tend to concentrate the energy of the rockfall impact into the structural elements, creating more localized foundation failures. Additionally, the static evaluation for overturning and pullout of the foundation elements should be considered rather than evaluating only shear at the base of the post.

When designing a floating base post system, the designer should be aware that the base plate system may present certain construction challenges since the post would need to be braced until the retaining anchors are attached on all sides. Also, depending on the impact type and impact orientation there may be axial loading on the post system, but based on other observed rockfall system case histories Giacchetti et al. (2014), the axial loads may be relatively small for grouted foundation bar systems similar to the E Series system.

Overall, the most flexible “floating” base offered the most flexibility and energy capacity for impacts normal to the post and rockfall system. If axial loading along the post was deemed to be a concern then an E Series system may offer a constructability and flexibility balanced option.

ACKNOWLEDGMENTS

The authors would like to acknowledge the support of CDOT Region 1, Russel Cox and James Van Dyne for their efforts and support in the project. The authors would also like to acknowledge Midwest Rockfall and especially Doug Fetzer for their

contributions and efforts in providing services for the successful test programs. The authors would like to also acknowledge Brett Arpin for his review assistance.

REFERENCES

Arndt, B., Ortiz, T., Group, R., (2013). "*Testing of Rockfall Post Foundations in Colorado*", 64th Highway Geology Symposium, September 9-12, 2013.

Arndt, B., Ortiz, T., Turner, K., (2009). "*Colorado's Full-Scale Field Testing of Rockfall Attenuator Systems*", Transportation Research Circular E-C141, October 2009.

European Organization for Technical Approvals, (2008). "ETAG 027 Guideline for European Technical Approval of Falling Rock Protection Kits", 2008-02-01.

Giacchetti, G., Brunet, G., Grimod, A., (2014) "Case Histories on Light Anchor Post System for Flexible Barriers", 65th Highway Geology Symposium, July 7-10, 2014

Turner, R., Duffy, J., Turner, J., (2009). "*Post Foundations for Flexible Rockfall Fences*", 60th Highway Geology Symposium, September 29-October 2, 2009.

William F. Kane, W. and Shevlin, T., (2012) "*Rockfall and Debris Flow Barrier Post Foundation Design*", 63rd Highway Geology Symposium, May 7-10, 2012.